ISTITUTO ITALIANO DI TECNOLOGIA
AND
UNIVERSITY OF GENOA

PHD PROGRAM IN BIOENGINEERING AND ROBOTICS
CURRICULUM: ADVANCED AND HUMANOID ROBOTICS

# Design and Development of a Robotic System for Pediatric Neurosurgery

by

**Nabeel Kamal**

Thesis submitted for the degree of *Doctor of Philosophy* ($33^{rd}$ cycle)

June 2021

| | |
|---|---|
| Dr. Leonardo S. Mattos | Supervisor |
| Prof. Darwin G. Caldwell | Supervisor |
| Prof. Giorgio Cannata | Head of the PhD program |

***Thesis Jury:***

| | |
|---|---|
| Prof. Brian Davies, *Imperial College, London* | External Examiner |
| Prof. Edward Grant, *University of North Carolina* | External Examiner |
| Dr. Sajid Nisar, *Kyoto University of Advanced Science* | External Examiner |

Department of Advanced Robotics
and
Department of Informatics, Bioengineering, Robotics and Systems Engineering

# Abstract

The advent of Minimal Invasive Surgery (MIS), a relatively modern method for performing surgeries, laid the grounds for robotic assistance in surgical procedures. Unlike conventional or open surgery, MIS uses long and slender surgical tools passed into the human body through small openings called incision points. The surgeons operate these tools from outside of the patient's body by viewing the video feedback of an endoscopic camera inserted into the patient's body.

The most evident benefits of the MIS are reduced blood loss, lessened postoperative morbidity, shorter hospital stay, and slashed cost of healthcare. It is common to use MIS for various surgical procedures such as Laparoscopy, Nephrectomy, Orthopedics, Cardiology and Thoracic, and Neurosurgical procedures. In some procedures, such as Cholecystectomy, laparoscopy is considered the gold standard.

The first robotic surgery was recorded more than three decades ago, and meanwhile, there was tremendous growth in surgical robotics in general. Surprisingly, neurosurgical robots developed at a slower pace. One reason behind this is the complex and delicate structure of the brain compared to other anatomical regions of human body which demands more sophisticated and miniaturized robotic tools. However, research on neurosurgical robots has gained pace during the last decade, and newly developed systems have started establishing their versatility, stability, dexterity, and potential to provide haptic feedback. Current neurosurgical robotic systems have contributed to enhancement of the quality of the surgery by minimizing registration errors and to acquiring spatial information. Nevertheless, all this advancement did not address the delicacy of neurosurgery in neonatal and infants.

This thesis addresses the research gap mentioned above by developing a new neurosurgical robotic system for newborns and infants. Due to the absence of such a robotic system, surgeons have to perform these complex, delicate and time- consuming procedures manually. The challenges in performing these procedures include the requirement of multiple hands (to perform the surgery) in a confined space, inefficient sleeve holder, and the need for fine motor skills to perform delicate motions.

To address these challenges, we have developed a robotic system that can assist surgeons in performing neonatal neurosurgeries. In this study, we presented a novel surgical robotic platform to assist surgeons in neuroendoscopy in infants. The design requirements of the robotic system were primarily obtained from observing the neuroendoscopic procedures. Subsequently, the acquired requirements were discussed with the team of neurosurgeons. Consequently, we agreed upon set of the requirements that the robotic system has to fulfil. The requirements were; establishing the remote center of motion (RCM) at the point of intervention and motorized manipulation (orientation, insertion, and inter-operative adjustment) of the end effector. The ranges of design requirement parameters were calculated using the real-life MRI of a baby. The MRI was later converted to a CAD model. The CAD model helped us in deriving the kinematic structure of the robotic system. We have realized that we needed a cartesian coordinate motion system to fix the RCM on a given point. However, a spherical motion system is required to cater to a (quasi) spherical workspace. We have used servo motors for the actuation of the joints and to have the required accuracy and repeatability.

The actuated six degrees of freedom (DOFs) of the system replaced multiple hands in the workspace with a rigid support and a fine positioning system. The new robotic system can orient, insert, and hold the surgical sleeve at any point assigned by the surgeon. The robotic system has been designed to work seamlessly with intra-operative neuronavigation as required during the surgery. All system requirements have been tested through simulation and physical experiments. Kinematic analysis was performed to ensure that the robotic system meets the workspace and surgical tool's reachability requirements. In addition, dynamic analysis was carried out to ensure the remote center of motion (RCM), decoupling of all the DOFs. These requirements were also validated through experiments with the new robotic system.

After the developing of the robotic system, rigorous experiments were performed under the guidelines for determining the accuracy and repeatability of numerically controlled axes. The spherical motion system achieved the repeatability of 0.47°, 0.141°, and $405\mu$ for yaw, pitch, and translation respectively.

In the future, the robotic system can be modified for haptic and force feedback. In addition, new control strategies could be developed to calculate and simulate the tool trajectory using the data from pre-operative MRI.

# Acknowledgements

This thesis would not have been possible without the support of numerous colleagues and friends.
First of all, I want to express my profound gratitude to my supervisor Dr Leonardo S. Mattos for giving me the opportunity. I am thankful to him for believing in me and not giving up on me until the last moment. This project would not have been possible without his continuous support. I would also like to thank our collaborators from Istituto Gianina Gaslini, Genoa, especially Dr Armando Cama and Dr Alfredo Consales, for providing effective feedback on the design and usability of the robotic system. I also want to extend my appreciation to Prof. Brian L. Davies, Prof. Edward Grant, and Prof. Sajid Nisar for assessing my thesis and shaping it better. Towards the realization of the robotic system, I would like to thank our "all-purpose" technician Andrea Maria Santangelo. He was a great help in the darkest hours. I am proud to work alongside such a competent engineer. I think without him, I could not have made the robotic system into a functional prototype. He was not only technical help, he also listened to all my ranting patiently. I would also like to mention Phil Edward Hudson to make the system alive by designing the control system.
It is tough to name everyone connected to this thesis, but I want to thank Roodra, Ali Ahmad, Siddharth, and Brendan to take the time out of their busy schedules to improve the thesis tremendously.
Several people are not directly related to the thesis, but they made my time in Genoa an experience of a lifetime. I want to mention my best friend, Vaibhav Bansal, who supports me technically and emotionally. He reviewed my manuscripts countless times at the nick of the time. He is the key reason that I survived the pandemic along with the doctorate. Apart from academics, I learned a great deal from him. I also want to thank Waseem, Shafique, and Usman for their continuous support during the write-up of the dissertation. Their matchless hospitality, along with delicious food, made that difficult time more manageable.
In the start, I was an alien in Italy. But then comes Tommaso Poliero. He taught me the language (not just the foul words), the Italian food and culture, invite me to his home, and made my stay in Italy way more convenient. He gave me precious advice regarding my career in Italy. I can proudly say he is my confidant. I also want to mention Andrea Cimolato for his share of my Italian experience. His "risotto al salmone" is still matchless. He was a great friend in need.
I feel so blessed to meet wonderful people in IIT from all over the world. I think I have a

deep imprint of those people on my personality. I feel obligated to thank my friends and colleagues Andre Geraldes, Anna Alves, Fanny Lahradet, Ammara, Erfan Shujaei, Taimoor Masood, Umair Gulzar, Matteo Sposito, Abu Bakar, Zahid, Pierre Ceysens, Yonas Tefaro, Nerea Itturioz, Olmo Alonso, Maria Lazzaroni, Joao Bimbo, Alperin Acemoglu, Wiebke Hinterlang, Enrico Turco, Valerio Bo (Cacao), Arya Akhavan, and Marzieh Armin, for sharing laughter, drinks, food, hikes, kayaking, and skiing.

I would like to thank my parents Talat and Zameer, and my siblings Hiba, Noor, and Baqir for not bothering me at all. In the end, I have to mention my beautiful wife, Iffat. Otherwise, she will be angry.

# Dedication

To,
all my fellow researchers,
pushing the boundaries of science and technology, day in day out!

# Contents

# List of Figures

# List of Tables

*Chapter 1*

# Introduction

**Summary**
The discussion in this chapter covers the introduction of neuroendoscopic procedures along with the brief history and different methods of performing neuroendoscopy. Later sections explains the motivation for the proposed research and the problems in the current neuroendoscopic procedures.

## 1.1 Background

Minimal Invasive Surgery (MIS) is a relatively modern method for performing surgeries. Unlike conventional or open surgery, MIS uses long and slender tools passed into the human body through small openings called incision points [17]. These openings could be natural orifices or the incisions made by surgeons. These surgical tools can be of numerous types, from graspers to cutters to 3D cameras and aspirators. The most evident benefits of the MIS are reduced blood loss, reduced postoperative morbidity, shorter hospital stay, and overall cost benefits of the health care. Currently, surgeons are using MIS techniques for various surgical procedures such as Laparoscopy [18], Nephrectomy [19], Orthopedics [20], Cardiology, Thoracic [20][21], and Neurosurgical procedures [22]. MIS techniques greatly enhance the quality of the health care. In some procedures, such as Cholecystectomy, laparoscopy is considered the gold standard [23].

## 1.2 Neuroendoscopy

Neuroendoscopy is a type of MIS. It uses specialized endoscopes to perform surgical procedures in deeper parts of the brain. Human brain is the most complex and delicate organ in our bodies. Unlike the other organs, deep parts of the brain are difficult to access with open surgery. The reason for this is the anatomy of the human brain. It consists of a cavity enclosed in a solid skull. This cavity is filled mostly by the cerebral tissues. These tissues are very sensitive to any retraction and/or displacement [24]. These reasons make open surgery to deeper parts of the brain nearly impossible without the risk of damaging critical structures. Thus Neuroendoscopy is the most effective way to perform surgeries at those deep

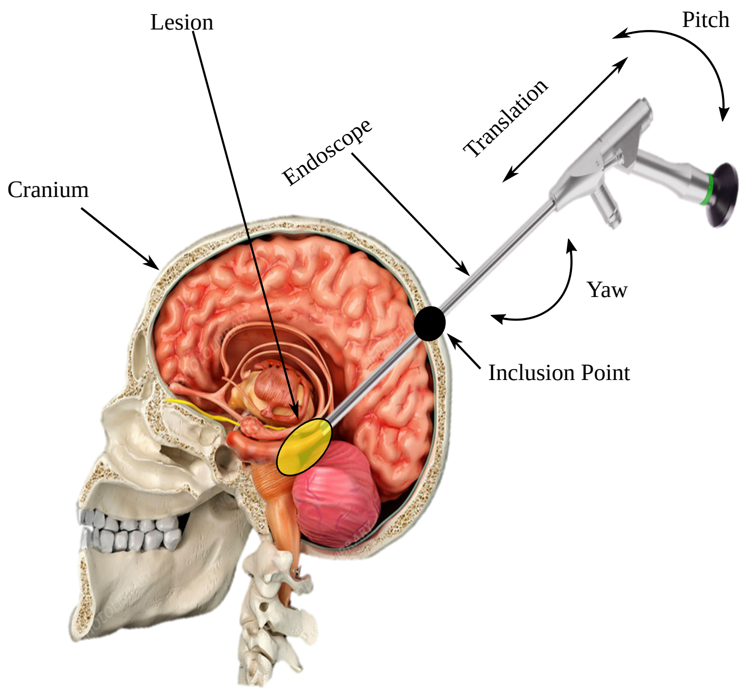


Figure 1.1: A simple schematic of a neuroendoscopic procedure

anatomical landmarks.

Neuroendoscopy is a minimally invasive interventional technique for neurosurgical procedures. It uses a long and narrow endoscope, which is passed through a small drilled hole on the skull made by the surgeon. This small opening is also known as burr-hole. Normally, the endoscope has a light source for illumination, a cutting or ablation tool, and an irrigation channel to suck up the blood and saline solution. Before the invention of neuronavigation systems based on Computerized Tomography (CT) scans or Magnetic Resonance Imagining (MRI), neurosurgeons used stereotactic clamps and brain atlases to navigate the endoscope inside the cranium. The navigation systems for neuroendoscopy will be discussed in later sections. A simple schematic of neuroendoscopy is shown in figure 1.1.

### 1.2.1 Brief History

Evidence of neurosurgical procedures dates back to as far as 800 B.C., based on the archaeological discovery of an operated skull found in Iran during an excavation campaign [25]. In modern world, the first recorded neuroendoscopy was performed by L'Espinass in 1910 [26, 27] at Northwestern University in Chicago. But this event went unnoticed. Later in 1922, Walter Dandy tried an endoscopic choroid plexectomy but the procedure was not successful [28]. He improved upon the procedure and reported the same procedure again in 1932 but it was marginally successful as compared to the open surgery [29]. At that time in history, neuroendoscopy was not gaining pace because of absence of the sophisticated endoscopes, and navigation technology. It was not until mid 1960s, when Hopkins invented a rigid endoscope with cold light and lens with smaller diameter and wide view angles [30]. He laid the foundation for modern day endoscopes. After this invention, not only neuroendoscopy but also other MIS techniques developed at a rapid pace. Over time, these procedures improved significantly with the development of the sister technologies such as enhanced endoscopes with a built-in camera, neuronavigation, computer tomography, and real-time intraoperative MRI. These minimal invasive techniques helped the use of robots in surgeries in the coming decades.

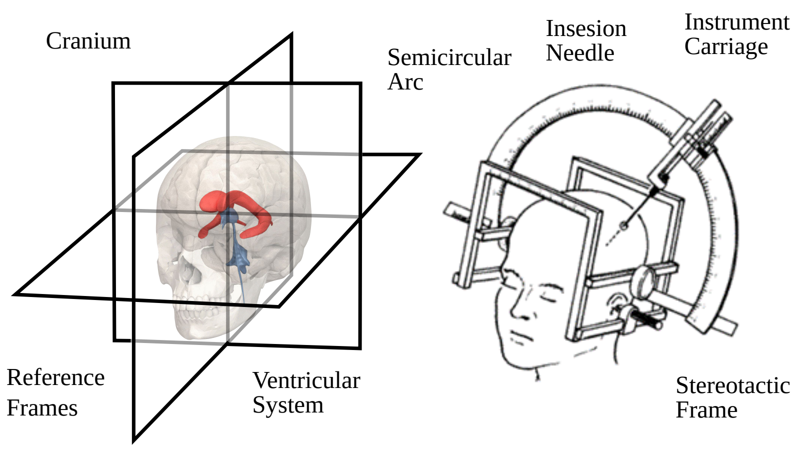


Figure 1.2: a) Cartesian coordinate system related to the Third Ventricle of the Brain. b) Stereotactic frame with inserting needle.

### 1.2.2 Different Methods of Neuroendoscopy

#### Frame based Stereotactic Neuroendoscopy

The surgical technique to access deeper parts of the brain is known as Stereotaxy. The word stereotaxy is originated from two Greek words "stereos" means solid and "takse" means touch. This terminology was used to "indicate the area of interest" in the neurology [31]. Such focused surgical intervention is called stereotactic surgery. Although animal trials for the stereotactic surgery were started in the early 20th century, the first reported human

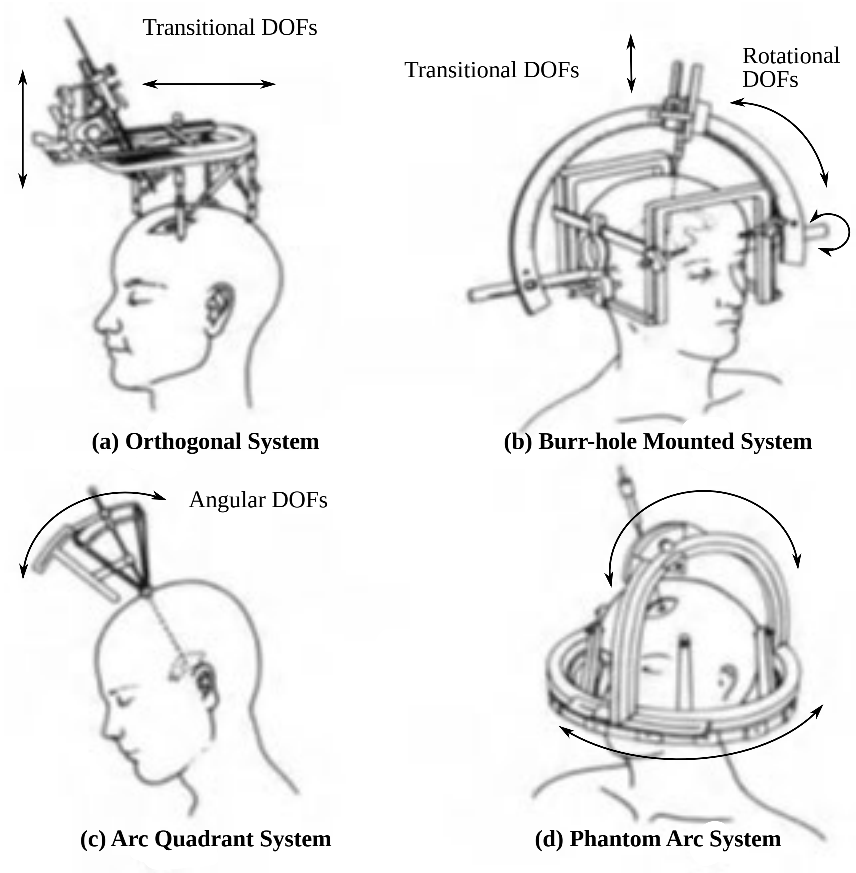


**(a) Orthogonal System** **(b) Burr-hole Mounted System**

**(c) Arc Quadrant System** **(d) Phantom Arc System**

Figure 1.3: Four basic types of stereotactic frames; (a) Simple orthogonal system, (b) Burr-Hole mounted system (c) Arc type (d) Interlocking arc or phantom arc system

stereotactic procedure was in 1947 with the stereotactic frame invented by Horsley and Clark [32] in London. Stereotactic neuroendoscopy is performed by inserting long slender tools into the brain and localization is done using a stereotactic frame as shown in figure 1.2. Compared to open surgery, stereotactic surgery causes minimal damage to brain tissues.

There are four basic types of stereotactic frames as shown in figure 1.3.
(a) The simple orthogonal system holds the probe/endoscope carrier perpendicular and has two translational Degrees of Freedom (DOFs).
(b)The burr-hole mounted stereotactic frame has two angular, and a translational DOF. The two angular DOFs are from the horizontal, and vertical planes respectively. The translational DOF is for the depth adjustment.
(c)Arc-Quadrant systems are more accurate and simpler in operation. In these systems, the probe is mounted on a circular carrier so that the probe is always directed towards the center of the arc. In this manner, the probe can have angular motion about the horizontal and vertical axes. In this configuration, the probe always passes through the center of the


Figure 1.4: Surgeons performing neuroendoscopy using intra-operative neuronavigation

arc, providing a pivot point at the entry, which is also known as Remote Center of Motion (RCM).
(d)In Phantom Arc Systems, an aiming bow is attached to the head ring, that is fixed on the patient skull. The aiming bow simulate the position of the target in x, y, and z coordinates. These coordinates are then transfered to the probe holder [33].
Some major disadvantages of these frames are that they are bulky in size and cause discomfort to the patients. They also obstruct the surgeon's field of view and restrict access to patient (e.g., for the anesthesiologist). Some studies have reported large accuracy errors, because of their mechanical design [34].

**Frameless Stereotactic Neuroendoscopy**

Until 1980, stereotactic neuroendoscopy was the standard procedure for minimally invasive neurosurgeries. The reason was the absence of reliable navigation technologies such as those based on CT-scan and Magnetic Resonance Imagining (MRI) [35].

The concept behind frameless neuroendoscopy involves the localization of three points in the pre-operative images, which are used as a reference to define a volume in a three dimensional space. Then, these points are projected on the patient using fiducials/markers or anatomical landmark. Surgeons can then plan the probe trajectories using these points. During surgery, they can also track the probe insertion using an intra-operative electromagnetic

(EM) tracking systems, ultrasound, CT-scan, or MRI.

The process of localizing the target on the image scan and project it on to the patient is called registration. Once this is completed, surgeons follow the surgical plan to prepare the incision point, and perform the intracranial insertion of the probe. This process is performed under navigation, shown in figure 1.4. For this, surgeons use intra-operative EM tracking, MRI, or ultrasound, to track the probe's tip position in real time.

### 1.2.3 Tools used in Neuroendoscopy

Neurosurgeons use variety of tools for the interventions, depending upon the nature of the disease. Needles are mostly used for electrical stimulation and biopsies, while specialized surgical sleeves and endoscopes are used for shunting, resection of tumor and piercing of intraventricular membranes [36].

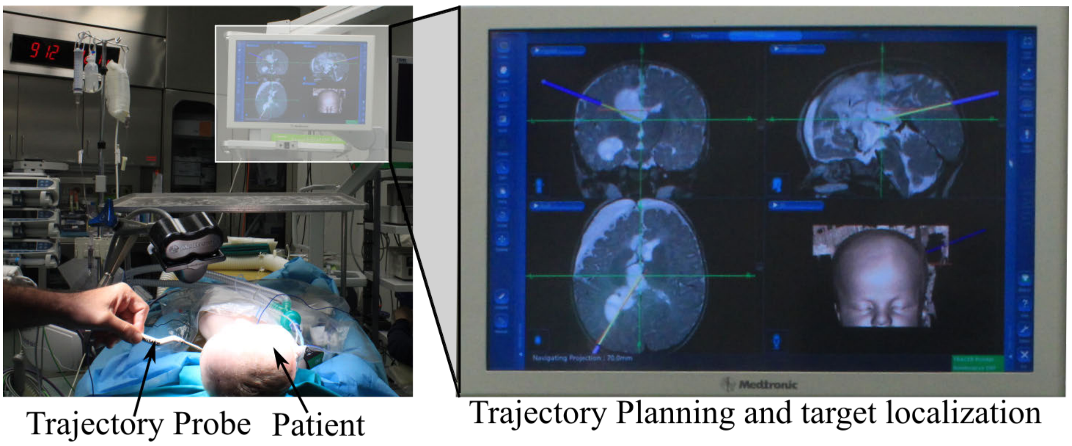


Figure 1.5: Surgical planning for neuroendoscopy

### 1.2.4 Types of Neuroendoscopy

**Deep Brain Stimulation (DBS)**
Deep Brain Stimulation (DBS) is a procedure to cure conditions such as essential tremor (ET) and Parkinson Disease (PD). This is done by inserting high-frequency electrodes to stimulate deep parts of the brain [37]. These areas are very difficult to reach by open surgery. The first case of DBS was reported in 1874 [38].In recent years, DBS was greatly enhanced by real-time neuronavigation. A schematic of DBS is shown in figure 1.6.

**Neuro Biopsy** Neuro biopsy is the resection of a sample of a brain tumor or a brain tissue for analysis. It is a minimally invasive procedure and can take out samples even from the deepest parts of the brain with minimal damage. During the insertion, surgeons also keep track of the biopsy tool using intraoperative tracking [39].

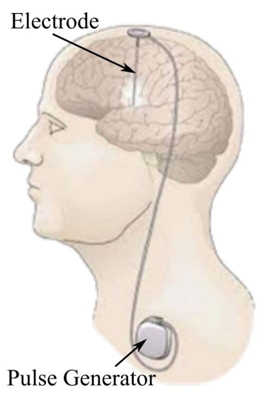


Figure 1.6: Deep Brain Stimulation (DBS)

**Electroencephalography (EEG)**
EEG based stimulation is a method to acquire encephalographic signals and send stimulus to control seizures [40]. EEG is also used in neural data acquisition and stimulus reconstruction [41]. Stereoelectroencephalography (sEEG) was invented in the 1950s by J.Talairach and J.Bancaud in France [42], and is currently considered as the most effective sensing technology to assist in the diagnosis and treatment of epilepsy [43].

**Endoscopic Third Ventriculostomy (ETV)**
ETV is performed by inserting an endoscope into the patient's skull to reach the third ventricle of the brain. It is a century-old neuro endoscopic procedure for the management of obstructive hydrocephalus. Surprisingly, the first ETV was performed by a urologist, William Mixter in 1923. He used an urethroscope as an endoscope to perform the ETV on a child with obstructive hydrocephalus [44]. The endoscope with special tools enables the creation of a bypass to release cerebrospinal fluid (CSF) pressure. figure 1.7 shows the basic concept of ETV.

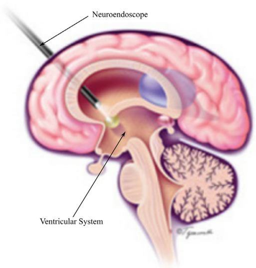


Figure 1.7: Endoscopic Third Ventriculostomy (ETV)

## 1.3 Motivation

Hydrocephalus is the excess production of the cerebrospinal fluid than needed. So it starts to accumulate in the third ventrical of the brain. It causes pain and abnormal growth of the head. Over 70,000 surgeries are performed annually for treating Hydrocephalus in United States. Four out of one thousand children are born with Hydrocephalus, and their treatment costs around 100 million US dollar per year [45]. Apart from this, 40% of the patients who suffered from Hydrocephalus had behavioral issues, while 20% of them suffered from autism in later stages of life [46]. Also, in 45% of the cases, patients had to undergo repetitive surgeries[47].
Pediatric neuroendoscopy is an optimal way to perform these surgeries. Surgeons perform these procedures manually and in a very careful way, because of the fragility and small size of the baby's head (10-12 cm). There are various evident problems in performing these procedures, including narrow workspace, delicate cerebral tissues, and long operating hours [48]. This leads to ample chances of human errors caused by fatigue, tremors and difficulties in maintaining the precision of surgical actions over extended periods of time. These challenges take their toll on the quality of the surgery and overall patient's well being and quality of life.

The motivation for this research project is to mitigate these issues by developing a robotic system dedicated for pediatric neuroendoscopy. This system should enable unprecedented levels of precision and safety during neuroendoscopy, facilitating and enhancing these delicate procedures by providing a highly precise and stable support for the surgical tools.

## 1.4 Problem Statement

We are living in an era of rapidly emerging robotic technologies. Robots are assisting surgeons all over the globe from Laparoscopy to Neurosurgery. Unfortunately there is no robotic system which address the issue of neuroendoscopy in neonatal and infants.

Currently, the process of pediatric neuroendoscopy is completely manual. In many cases, surgeons cannot use head clamps, stereotactic frames, nor facial landmarks. The main reason for this is the partial calcification of baby's head. The cranial fissures are not filled completely. Thus, the usage of any fixture can cause damage or permanent deformations. As a result, the patient's head can not be completely immobilized.

The surgical procedure of pediatric neuroendoscopy, itself is very intricate and requires higher level of dexterity with sub millimeter accuracy and precision. A slight tremor in surgeon's hand can cause life-long disabilities on the child.

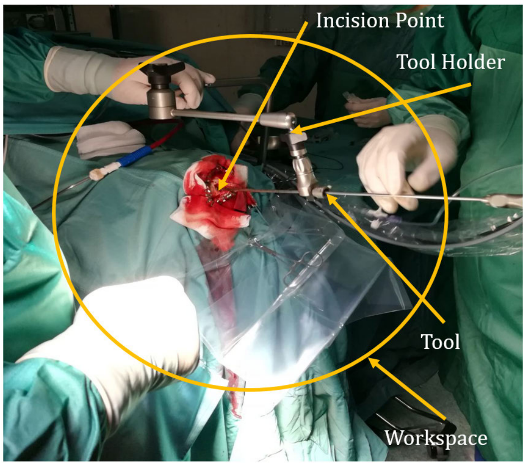


Figure 1.8: Team of surgeons performing manual neuroendoscopy using a mechanical tool holder. Multiple hands are required in a very small space for very long period of time.

In addition, because the available mechanical supports for pediatric neuroendoscopy are sub-optimal for this application, six hands are required to perform the procedures, which is complicated by the fact that the surgical workspace is very small. Figure 1.8 highlights the issues in manual neuroendoscopy.

## 1.5 Objectives

The objectives of this research are:

1. Study the utility of current robotic systems for pediatric neurosurgery.
2. Investigate potential robotic mechanisms for pediatric neuroendoscopy.
3. Design and develop a robotic system for pediatric neurosurgery.
4. Assess the robotic system performance experimentally.
5. Validate the new device through user trials.

## 1.6 Methodology

I started this research with a detailed literature review of neurosurgical robots. During this review, I categorized existing robots in three categories according to their kinematic structure, i.e., serial, parallel, and spherical. The purpose of the review was to get a deeper understanding of previous solutions proposed for this challenging problem. I also aimed to identify an p available neurosurgical robot that could be potentially used for, or customized to perform, pediatric neuroendoscopy.

After completing the literature review, we discussed possible scenarios with our clinical collaborators and arrived at the conclusion that there was a need to design a dedicated robotic system tailored to address the needs of both the surgeons and the patients. We closely collaborated with pediatric neurosurgeons to define the system requirements.

After having a clear understanding of the challenges and requirements, we started the mechanical design process following an iterative co-design approach with the surgeons. The first step was to convert the clinical requirements to engineering requirements for the robotic system.

Afterwards, we started the mechanical design of full scale robotic system using Computer Aided Design (CAD). The model of the robotic system was first verified through series of mechanism and kinematic simulations. Then, a scale down proof-of-concept prototype was created to verify the early design with the surgeons.

Based on the neurosurgeons feedback, the design was revised. Following the design revisions, the robotic system was manufactured and assembled. The system was tested on a 3D printed phantom head, using electro-magnetic tracking to access the system's motions. During the testing, we experimentally verified the physical system, the reach of the end-effector, and the robotic system accuracy. Figure 1.9 shows the methodology in detail.

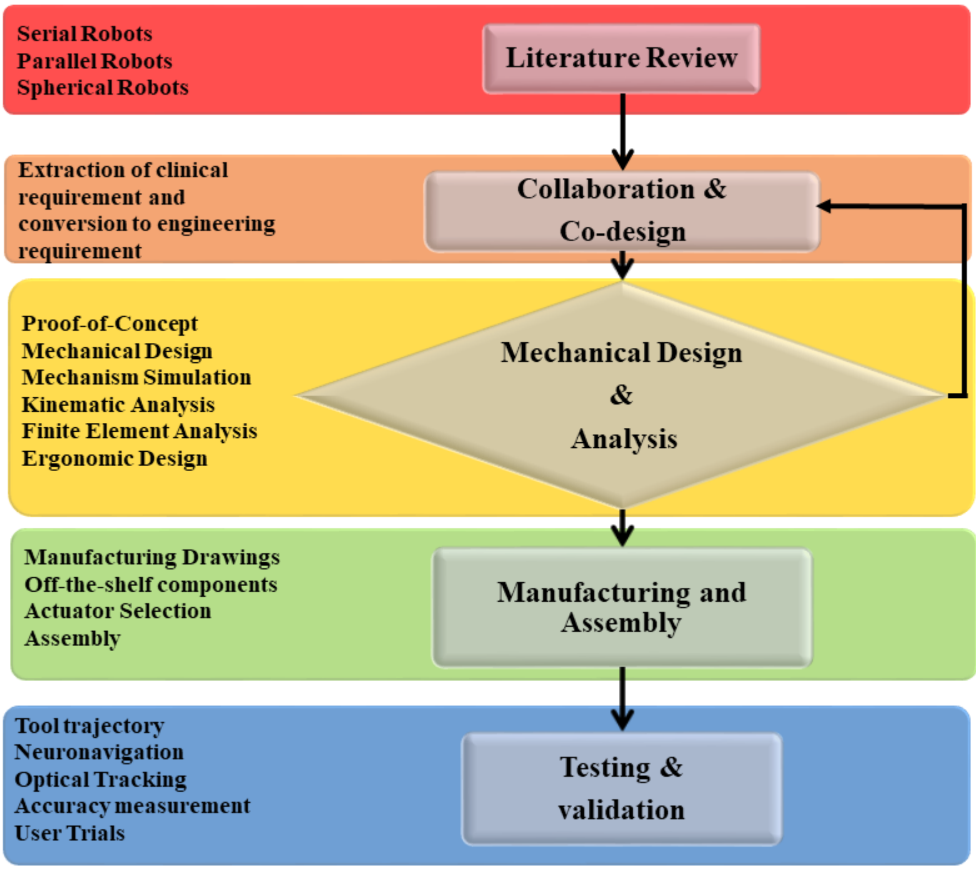


Figure 1.9: Methodology

*Chapter 2*

# Literature Review

**Summary**
In this chapter, we review the current robotic systems used for neurosurgical procedures. We classify the robotic systems according to their kinematic structure. A basic introduction of serial and parallel manipulators is also given to understand existing robotic systems better. In the end, a table is presented in which summarizes the presented robotic systems according to their chronological order.

## 2.1 Background

Robotic Surgery has seen its dawn with a neurological surgical procedure in 1985 [49]. Since then, surgical robotics has become a vast and rapidly growing field. Starting from neurobiopsy, the surgical robots now assist surgeons in other areas such as orthopaedics, laparoscopy, cardiology, neurology, and urology. It has been long since surgical robots have been commercially developed and clinically deployed. Neurological surgical robots, however, have seen a slow development compared to other types, possibly because of the complex nature of the procedures. These robots started as a tool to enable access to deep pathology and structures (such as the third ventricle) with less trauma and minimal invasiveness [50], since the robotic technology provides a steady and precise penetration of surgical/biopsy tools to the most complex parts of the brain. Despite the slow start, the development of neurological surgical robots gained pace towards the end of the 20th century, demonstrating their versatility, stability, dexterity, and potential to provide haptic feedback.Robotic systems also demonstrated to contribute to minimize registration errors and to acquire spatial information. This can be achieved by various means like fiducial markers, and laser scanning. This information handling/retrieving property of robotic systems enables the surgeon to concentrate on the surgical procedure.

There are numerous ways in which medical robots can be classified, such as surgical applications, level of autonomy, targeted anatomy, and targeted organ/part [9]. Considering the wide spectrum of disciplines involved in the development of surgical robotics, it is difficult to create a taxonomy for all kind of surgical robotics [51, 52]. Therefore, in this chapter we focus on neurosurgical robots. The proposed research is mainly focused on the mechanical design and development of a robotic system. So that we aim to analyze both commercial and research prototypes of robots for neurological procedures based on their mechanisms and kinematic structure. It is important to study the current mechanism and designs before designing our robotic system. That's why this study mainly focus on the design and mechanism part of the literature.

## 2.2 Classification of Neurosurgical Robots

Neurosurgical robots can be segregated in two major kinematic structure groups: Serial and Parallel robots. This classification has been used, for example, by Merlet et al. for the analysis of surgical robots available in 2005 [53]. Here, we start the analysis with a brief introduction to both serial and parallel mechanisms used in different neurosurgical robots.

## 2.3 Serial Robotic Manipulators

Serial robotic manipulators are the most widely used industrial manipulators. They consist of rigid links that are joined together either through revolute or prismatic joints in series. Usually, the first link of the manipulator is fixed and acts as the base. The distal end, or end effector, carries some tool or an object to position and orient [54]. This configuration makes an open-chain structure.

Most serial robots are anthropomorphic and have six degrees of freedom (DOF). These characteristics enable them to achieve any arbitrary position and orientation in a three-dimensional workspace [55]. The operator has to develop a common reference between the base and the end-effector before assigning a task to the robot. In some cases, joint angles of the manipulator are known, and the end-effector position has to be calculated. It is known as forward kinematics, and it is straightforward for serial manipulators. On the contrary, when the end effector's position is given, and the user has to calculate the joint angles of the manipulator, this is known as inverse kinematics. This is quite complex for serial manipulators [56]. The reason behind is, for each position and orientation of end-effector, there could be infinite number of joint motions. There are several methods to find these parameters, such as the geometric method, Denavit-Hartenberg method, etc. [57].

It is also important to note that most of the commercial serial manipulators have only revolute joints. This configuration provides a large and dexterous workspace and reduces the cost. However, all the joints are coupled [58]. Compared to parallel robots, serial robots are heavier in weight because the links need enough rigidity to be stable. Serial robotic manipulators tend to have lower accuracy because the successive link has to support all the preceding links and the load (if the end effector is attached). They also need stiffer links, which makes them heavier. Flexural deformation in the links can be a big problem, as the robot's internal sensors are often not able to detect them. This could also cause the error to magnify from the proximal to the distal end [59]. Moreover, they also have very low payload capacity as compared to their own loads. Nonetheless, the positive characteristics of serial manipulators make them an excellent choice for industrial and medical use.

## 2.4 Parallel Manipulators

Parallel manipulators are different from the far more traditional serial manipulators in their kinematic structure. Parallel manipulators employ multiple closed kinematic loops. Usually, these comprise multiple kinematic chains connecting a moving platform to the base. This type of configuration and the resulting kinematic structure enable a parallel manipulator to be driven by actuators that are located on or near the base of the manipulator. On the contrary, serial manipulators lack such a configuration of closed kinematic loops and are driven by actuators positioned at each joint along the serial linkage. This kind of actuator positioning causes a serial manipulator to experience heavy loading whereas the links in a parallel manipulator need not carry the actuator load. Consequently, the links in parallel manipulators can be designed much lighter in weight when compared to links in serial manipulators.

The number of actuators in a parallel manipulator exceeds the degrees of freedom (DOF) only when a repetitive DOF is required. Parallel robots strictly having an equal number of kinematic chains to the number of DOF are called fully-parallel manipulators. One of the first recorded usages of parallel robots was in the tire testing device known as the Gough-

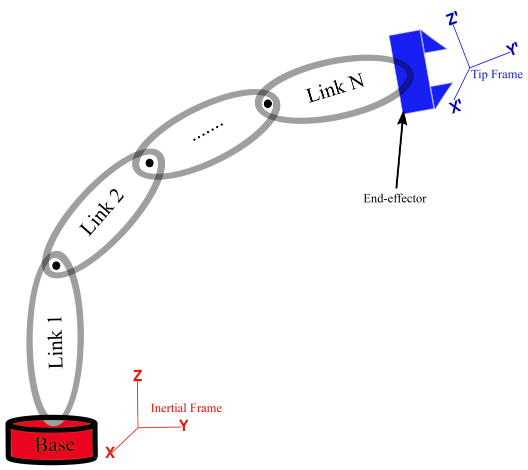


Figure 2.1: Serial manipulators: A class of robotic manipulator in which the successive link is attached serially to its predecessor.

Stewart platform [60]. Eventually, they found the use of the same mechanism in flight simulators which are also known as Stewart Platforms [61]. With the passing years, parallel robots have found many applications, such as high-speed manipulation, machine tools, material handling, and medical applications [60]. Usually, parallel manipulators have six DOFs but recently parallel robots with fewer DOFs have found their applications in different industries [62]. Unlike serial manipulators, parallel manipulators have very straightforward inverse kinematic, however, the forward kinematics can be complicated [63, 64, 65, 66]. There are several types of parallel robots according to their design topology and usage. The most noticeable advantage of parallel manipulators is that they have higher stiffness than serial manipulators. This makes parallel manipulators more accurate and enable them to handle heavy payloads as compared to their own weight. This allows them to have higher throughput movements and greater mechanical rigidity than serial manipulators. Parallel robots also attain higher accuracy than the serial robots because the parallel mechanism average the errors rather than adding them cumulatively. The parallel robots can be classified into symmetric, planar, spherical, and spatial categories. Industrial applications of parallel robots are mostly in the form of Hexapods, which are used in high accuracy and high payload applications and surgeries. Other applications include Delta Robots used in high-speed manipulations and cable-driven robots used in cargo handling.

## 2.5 Neurological Surgical Robots using Serial Mechanism

### 2.5.1 ROSA

ROSA system primarily consists of a 6 DOF rigid robotic arm. This robotic arm uses serial mechanism for the articulation and placement of the tool. The serial manipulator enables the surgeon to have a workspace also for himself to carry out the procedure [67]. This robotic manipulator is controlled by Rosana software which calculates the probe trajectory from pre-operative MRI images [68, 1]. The robotic arm is fixed with the skull clamp during the surgical procedure. It uses its laser system for indexing the patient head using MRI and CT scan images.

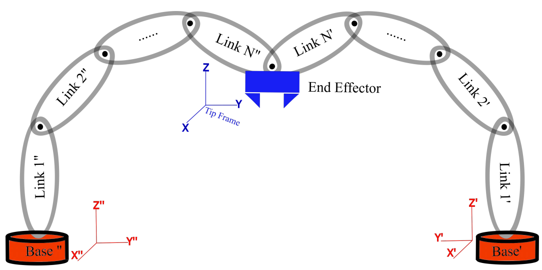


Figure 2.2: An example configuration of a parallel manipulator

Table 2.1: Robotic manipulators and their properties

| | | Type of manipulator | |
|---|---|---|---|
| | | **Serial Manipulator** | **Parallel Manipulator** |
| 1 | **Kinematic Structure** | Open Loop | Closed Loop |
| 2 | **Actuators** | On the joints | On the base |
| 3 | **Workspace** | Relatively large | Relatively small |
| 4 | **Stiffness** | Low | High |
| 5 | **Dexterity** | High | Low |
| 6 | **Forward Kinematics** | Straightforward and Unique | Difficult and Complex |
| 7 | **Inverse Kinematics** | Difficult and Complex | Straightforward and Unique |
| 8 | **Payload to Weight Ratio** | Low | High |
| 9 | **Application** | Material Handling, Inspection, | Precise Pick & Place |
| | | Medical | Machine tools, Medical |

When using ROSA, surgeons can choose the frameless or frame-based approach. The frameless approach uses fiducial markers. The frame-based approach uses a surface scanner. Frame-based registration has an accuracy of less than 1 mm, while frameless registration has an accuracy of 1.22 mm [69]. During the procedure, surgeon can also opt for the intraoperative MRI to visualize the actual position of the tooltip. The major benefit of ROSA are flexibility of use and the integration in the conventional workflow. Figure 2.3(a) shows ROSA surgical system.

### 2.5.2 Cyber Knife

CyberKnife is a Stereotactic Radiosurgery System (SRS) developed for frameless stereotactic procedures [70]. It is the combination of three neurological radioscopy techniques, namely 1) Stereotaxy, 2) Three Dimensional Target Localization, and 3) Radiating the target from multiple locations. CyberKnife is capable of delivering a high dose of radiation with sub-millimeter precision, producing minimal damage to proximal tissues [71]. The most recent version of CyberKnife uses a KUKA KR 240-2 robotic arm [72, 73]. This is a serial manipulator with six DOF rotary axes. Each of the joints mounted with high power motors. This configuration provides high payload with high precision. This robotic manipulator can achieve any point in the three-dimensional workspace through multiple configurations of the actuators[74]. Cyberknife radiation therapy is shown in figure 2.3.

### 2.5.3 Neuromate

Neuromate (Renishaw PLC) was developed on the basis of the works of Benabid et al. [75]. It is a stereotactic robotic system primarily developed at Grenoble University [76]. It was developed in 1992 by transforming a universal industrial robot into the hand of a neurosur-


(a)

(b)

Figure 2.3: (a) Medtec ROSA robotic system [1] (b) Cyberknife radiation therapy system [2].

geon. This a six DOF serial robotic arm. The angular joints were considered as shoulder, arm, elbow, forearm, wrist, and hand. Each of the degrees of freedom is equipped with a potentiometer as sensor to keep track of the angles. The data from these potentiometers are used in the registration and retrieval of robot coordinates during the surgery [77]. This was the first FDA approved and CE marked neurosurgical robots for the stereotactic neurosurgical procedure. It was approved in 1997. This image-guided robot has a technical positional accuracy of 0.7 mm and a precision of 0.15 mm [78]. It can also use conventional stereotactic frames.

The rationale for using Neuromate robot includes its mechanical stiffness, good accuracy and convenient workspace for cranial procedures [79]. While the robot was originally designed for positioning and orientating surgical tools, researchers have also experimented with it as a cooperatively controlled robot by attaching a six-DOF force sensor at the end-effector [2]. Neuromate stereotactic robotic system is shown figure 2.4.

### 2.5.4 Minerva

Minerva was one of the first neurosurgical robotic systems. It was developed in 1993 by EPFL, Switzerland [80]. Minerva can perform all the procedures from skin incision to dura perforation to probe manipulation by exchanging the tools. It was a custom-designed robot specifically to address the neurosurgical procedures. This robot has seven degrees of freedom with the serial type kinematic mechanism. It has three linear motion axes and three rotational axes completely independent from each other [3] shown in figure 2.5.

However, the end effector has only two degrees of freedom i.e rotation around its own axis and translation inside the brain. This gives a cylindrical workspace for the end effector. This

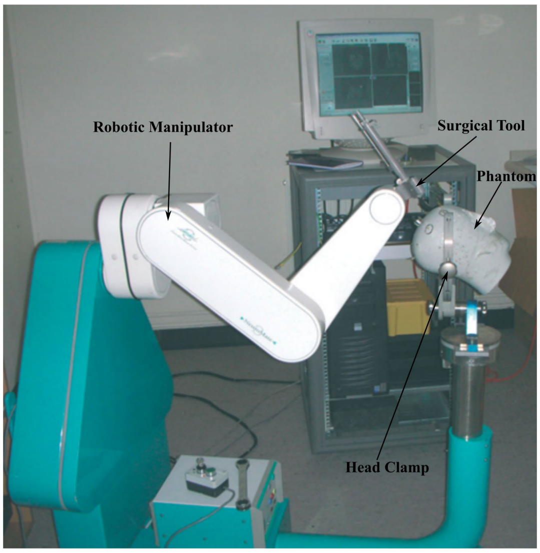


Figure 2.4: Neuromate stereotactic robotic system

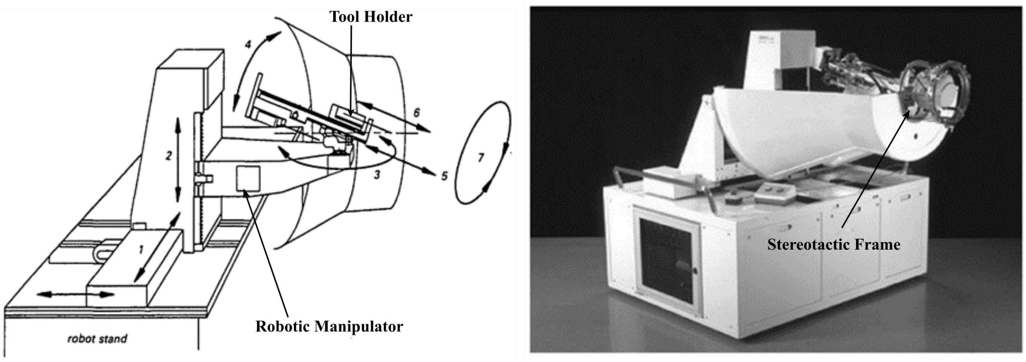


Figure 2.5: MINERVA robotic system [3, 4]

robotic system largely helps in reducing the operating time of the surgery to 30 minutes. The global accuracy of the robotic system is 1.3 mm for the whole operation [81]. The disadvantage of the Minerva system is the weight and the requirement to have a CT scanner in the operation room [82].

### 2.5.5 NeuroArm

NeuroArm was developed by a team of researchers at the University of Calgary, Canada, in 2002. It was the first MR-compatible robot to merge the precision and accuracy of the robotic systems with the intra-operative MR imaging [83, 84]. NeuroArm is capable of performing all the tasks involved in the neurosurgical procedures. The basic design of NeuroArm is an anthropomorphic seven DOF robotic arm that can hold a variety of surgical tools as an end-effector, shown in figure 2.6(a). Material selection for the robotic arm was one of the key

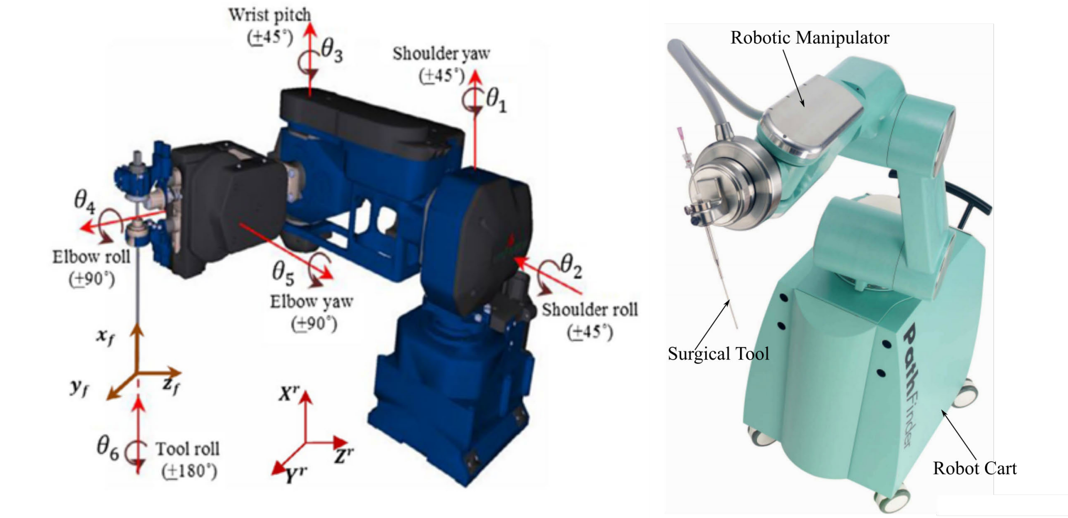


(a) (b)

Figure 2.6: (a)NeuroArm robotic system [5] (b) Pathfinder robotic system [6]

design parameters as it has to be MRI compatible. NeuroArm used ultrasonic piezoelectric actuators, which have self-braking capabilities in case of power failure. The major highlight of the NeuroArm was custom-made Titanium MRI-compatible 6 axis torque/force sensors to provide haptic feedback to the surgeons from the tool tip. The accuracy of the NeuroArm system is 4.35±1.68 mm [85].

### 2.5.6 Pathfinder

The Pathfinder Robot (by Prosurgics, UK) was developed to miniaturize the size of the surgical device and to surpass the skills of most experienced surgeons. It was mounted on a mobile platform that can be attached to the surgical bed and could detach easily [86]. It was a 6 DOF serial robotic arm with a tool holder on the distal end and a mobile platform at the proximal end [6]. In this system, fiducial markers were traced by the robotic arm in real-time. Pathfinder eliminated the problem of line of sight by triangulating the fiducial markers [87]. The reported accuracy of Pathfinder was 0.48 mm, which is considered better than most Image-Guided Surgery (IGS) systems [88]. The project was terminated in 2009 due to lack of funding and certification issues [9]. The manufacturing company of Pathfinder was acquired by FreeHand 2010 Ltd.[89]. The Pathfinder robotic system is shown in figure 2.6(b).

### 2.5.7 NeuRobot

NeuRobot was developed by Shinshu University, Japan in 2009. This robot actually consists of a micromanipulator which is mounted on a fully uncoupled six degrees of freedom serial manipulator [90], shown in figure 2.7. This serial manipulator is used to achieve the desired angle and position of the tooltip. However, the micromanipulator (the end-effector) has additional three degrees of freedom. It also has three surgical tools, which are inserted into the brain to perform the surgical actions. The motion of the surgical tools are independent of the serial manipulator [7]. The reported accuracy of the micromanipulator of the NeuRobot is 0.02 mm. However, the accuracy of the robotic arm, on which the micromanipulator is mounted, is 0.1 mm [91, 92].

### 2.5.8 MKM

Multi Coordinate Manipulator (Mehrkoordinaten Manipulator) or MKM is a neuronavigation system with a microscope and a tool holder for neurosurgical tools. It is a serial robotic manipulator with six degrees of freedom [8], as shown in figure 2.8. This robot achieve any point in a cartesian coordinate system. The claimed accuracy of this system was 20 µm by the manufacturer (Carl Zeiss). However, the studies indicated accuracies between 0.23 mm [93] and 0.36 mm [94]. MKM can carry out neuroendoscopic procedures with or without stereotactic frames, but higher accuracies were achieved with the stereotactic frame [95].

## 2.6 Neurological Surgical Robots using Parallel Mechanism

### 2.6.1 Renaissance

The Renaissance robotic system is comprised of MARS (Mazor Robotics Ltd. Israel) parallel robot with a commercial laser scanning system, a PC, a custom robotic base and target guiding/registration jig. MARS was actually developed for spine surgery. Due to its small size, it can be directly mounted over the patient at desired point. Later on, it was found useful also for minimally invasive neuroscopic procedures [96].

The Renaissance uses a parallel mechanism robot with six DOF and an accuracy of 1mm [97]. The major advantages of this system are reported as smaller size and better cost-

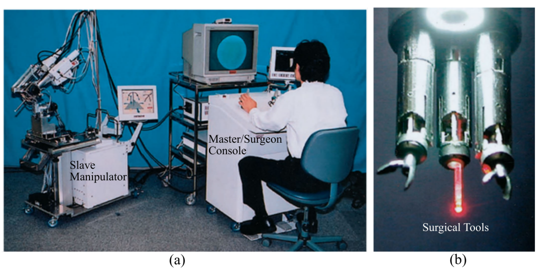


Figure 2.7: (a) Complete NeuRobot with master and slave manipulators. (b) Slave side: Closer view of micromanipulator with surgical tools [7]

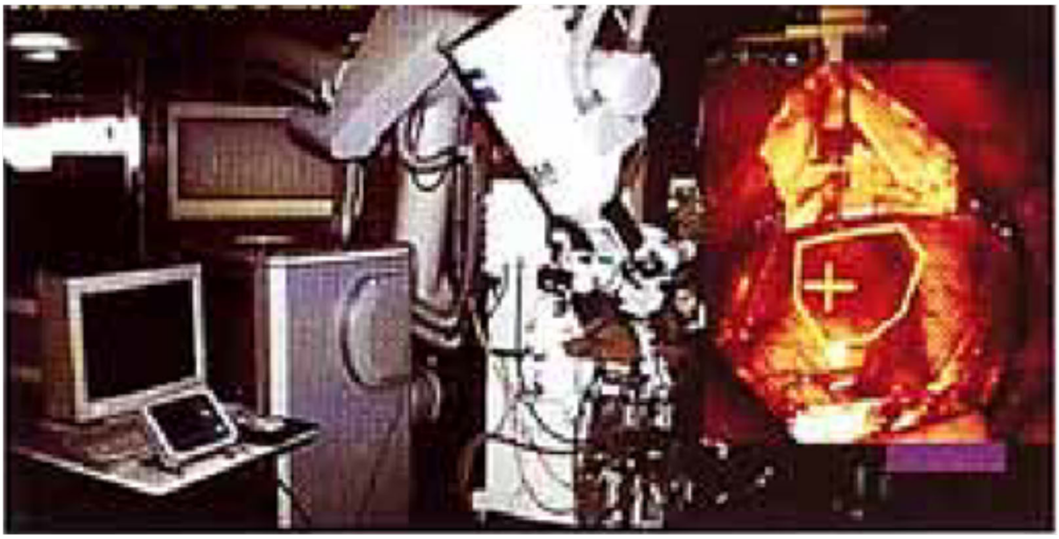

Figure 2.8: MKM system at Department of Neurosurgery in University of Vienna Medical School [8]

Figure 2.9: MARS robot used in Renaissance system [9]

effectiveness than other neurosurgical robotic systems. The Renaissance is a frameless and markerless system. Due to this characteristic, mobilization of head is not needed.

### 2.6.2 Robocast (ACTIVE)

The Robocast system was developed as a robotic system for minimally invasive surgical procedures. This robotic system is equipped with an Opto-electromagnetic system for tracking, the Pathfinder robotic system for coarse positioning and MARS for fine positioning. It is a multi kinematic chain robot comprised of both parallel and serial chains [10]. Robocast was further developed as the ACTIVE robot, which features two robotic manipulators. This solution proposed the integrated redundancy of 20 DOF in a single robotic platform. The accuracy of the ACTIVE robotic system is 0.3mm. [98].

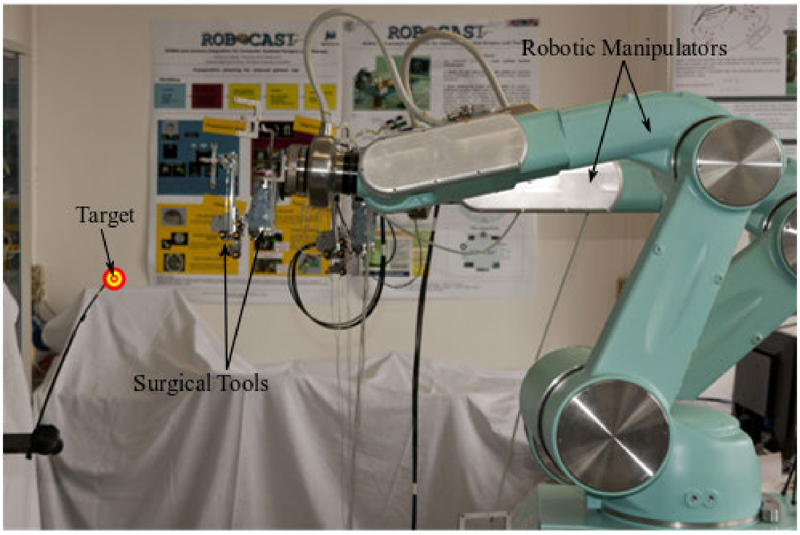


Figure 2.10: ROBOCAST: Serial and parallel manipulators. [10]

### 2.6.3 Evolution I

Evolution I was designed and developed by Universal Robot Systems, Germany in 2001. It is parallel hexapod robot with six degrees of freedom. There has been an alteration in design to make it work for the surgery. An additional seventh degree of freedom was added to hold the surgical instrument [11]. This additional degree of freedom is used to insert an endoscope through the sphenoidal bone. The intrinsic accuracy of the hexapod robot was 20µm with the minimum resolution of 10µm [99].

### 2.6.4 NeuRobot*

NeuRobot is basically a neuroendoscopic simulator to train the surgeons for robot-assisted neuroendoscopy. It was developed by the ROBOSCOPE consortium [12]. NeuRobot uses double-parallelogram mechanism to achieve a remote center of motion (RCM). The robot has four degrees of freedom at the incision point (pitch, yaw, roll, and translation) which are the fundamental requirements for any minimal invasive surgery [100].

*Note: This NeuRobot should not be confused with the NeuRobot developed by Shinshu University [7].

### 2.6.5 SurgiScope

SurgiScope (Intelligent Surgical Instruments and Systems, ISIS) is one of the first commercially developed robots for neurosurgical procedures. The development of this robotic system started in 1989 with the collaboration between University of Grenoble and AID [101].

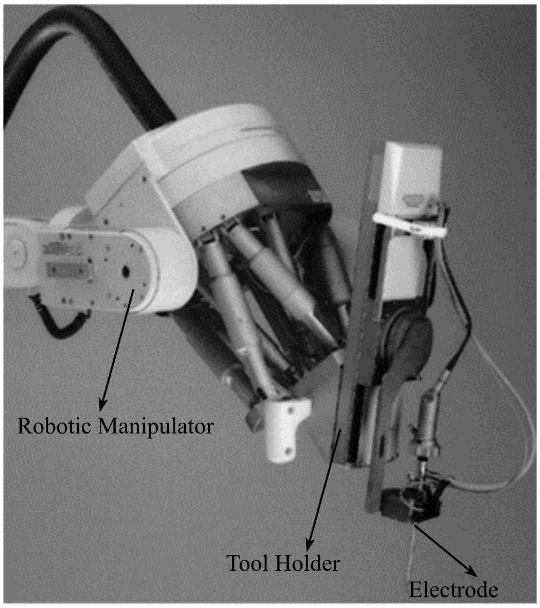


Figure 2.11: Evolution-I operating robot [11]

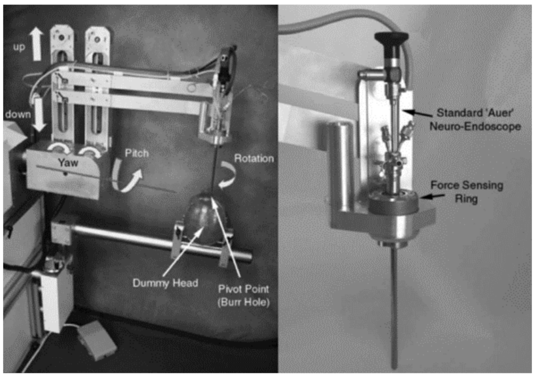


Figure 2.12: NeuRobot by ROBOSCOPE[12]

This robotic system is one the first robotic manipulators designed using parallel delta mechanism. It has seven degrees of freedom and the whole robotic system is mounted on the ceiling of the operating room [102]. Because of this, it has a large footprint (although mounted on the ceiling). This robotic system can hold a microscope and align its field of view with the surgical target [103]. In addition, a tool holder can also be attached to perform intracranial procedures. The reported accuracy of SurgiScope robotic system was 1.6 ± 0.3mm [104].

## 2.7 Conclusion

It is evident that surgical robotics can tremendously improve the healthcare scenario. It expands from neurology to obstetrics to orthopedics. But even after years of development,

Figure 2.13: ISIS SurgiScope robotic system[7]

there is still large space for improvements. Apart from facilitating and enhancing the quality of the surgery, surgical robots also have to satisfy other associated requirements to be clinically applicable and usable. This includes the robotic system size. The key parameter that determines the size of a surgical robot is the type of primary mechanism it uses.

A review of existing systems shows that most neurosurgical robots are based on serial mechanisms. The reason behind this is the basic properties of the serial robots. They have a higher level of decoupled motions, are easier to program, and provide a large workspace volume with very high dexterity. However, since the end-effector accumulates all errors of the previous links, their accuracy is limited. In addition, their payload capacity is typically low. However, in the case of surgical robotics, payload capacity is not much of a concern. With all the above mentioned benefits, a trade-off to be faced when designing serial robotic mechanisms for surgical applications regards the size and the weight of the robotic system.

Surgical robots based on parallel mechanisms provide better stability and higher stiffness at the end-effector. This factor leads to better accuracy and precision. Due to their configuration, they are smaller in size with a higher payload to weight ratio. Existing neurosurgical robots based on parallel mechanisms are mostly portable and don't occupy much space in the operation room. The inverse kinematics of parallel manipulators are easy to calculate. But the drawback of such mechanisms is their smaller workspace and low dexterity. It is also difficult to design uncoupled motions in the manipulator. All the reviewed neurosurgical robotic systems are tabulated in table 2.2.

Therefore, we can conclude that a single mechanism type cannot address all problems faced in neurosurgical applications. A combination of mechanisms has to be used, or one has to find satisfactory compromises in performance. Collaboration between engineers and doctors is required to tackle these challenges.

Table 2.2: Summary of the surgical robots reviewed in chronological order

| | Name | Year | Company | DOF | Primary Mechanism | Precision/ Accuracy (mm) | FDA Approval | Approval Year | Target Patients | Ref. |
|---|---|---|---|---|---|---|---|---|---|---|
| 1. | SurgiScope | 1989 | Uni. of Grenoble | 7 | Parallel Delta | 1.6±0.3 | Yes | | Adults | [99, 103] |
| 2. | MKM | 1990s | Carl Ziess | 6 | Serial | 0.23±0.14 | No | | | [94] |
| 3. | CyberKnife | 1994 | Stanford University | 6 | Serial | - | Yes | 1999 | Adults and Childern> 4y | [105, 106] |
| 4. | Neuromate | 1992 | Uni. of Grenoble | 6 | Serial | 0.7 | Yes | 1997 | Adults and Childern >7y | [107, 108] |
| 5. | MINERVA | 1993 | EPFL | 7 | Serial | 1.3 | - | - | - | [82] |
| 6. | Evolution I | 2001 | Universal Robot Systems, Germany | 6 | Parallel | 0.02 | No | | | [99] |
| 7. | NeuRobot | 2002 | Fokker Control Systems | 4 | Parallel/Planer | - | No | | | [91] |
| 8. | Pathfinder | 2003 | Prosurgics, UK | 6 | Serial | 0.48 | Yes | 2004 | - | [88] |
| 9. | ROSA Adults | 2006 | Med Tech, France | 6 | Serial | 1 | Yes | | Adults and Childern>11y | [69] |
| 10. | NeuRobot | 2006 | Shinshu University, Japan | 6+3 | Serial | 0.1 | No | | | [8] |
| 11. | NeuroArm | 2007 | University of Calgary | 7+1 | Serial | 4.35 | Yes* | 2015 | Adults | [5] |
| 12. | Renaissance | 2007 | Mazor Robotics Ltd. | 6 | Parallel | 1 | Yes | 2012 | Adults, Childern >13y | [10, 109], |
| 13. | Robocast | 2010 | Politecnico di Milano | 20 | Serial and Parallel | 0.3 | No | | | [98] |

*Chapter 3*

# Mechanical Design of the Robotic System

**Summary**
As concluded in chapter 2, there are no existing dedicated robotic systems for pediatric neurosurgery. We started this project by deriving the requirements and specifications for the developing of a dedicated robotic system for paediatric neurosurgery. This chapter explains the mechanical design of the system by segregating it into three sub-components. A comprehensive literature review was done before designing a sub-component, and the pros and cons of each type of mechanism are discussed in detail. The chapter concludes with the assembly of all sub-components into the complete robotic system.

## 3.1 Requirement and Specifications

It is important to lay down the requirements and specifications of any engineering design regardless of their size and complexity. A design requirement and specification document helps in all the stages of a project, i.e., from proof-of-concept (PoC) to finished product. A detailed document is also helpful in quantifying the project goals and objectives. It is essential if the project is inter-disciplinary, as is the case for this pediatric neurosurgery robot project.

### 3.1.1 Derivation of Requirements

The derivation of correct requirements is a critical foothold in any project. It saves time, effort, and budget assigned to the project. It should be derived with the mutual understanding of all the stake holders: creators and end-users.

In this research, we started this process by getting a high level understanding of brain anatomy, and of the steps involved in neuroendoscopy. The next step was to observe real surgeries in an operating room (OR). Our collaborators from Istituto Giannia Gaslini in Genoa, Italy allowed us to observe the neuroendoscopies in their OR. These procedures start with a pre-surgical MRI scan of the patient's head, usually twenty four hours before the surgery. Surgeons identify the problematic site using an MRI scan and plan the intracranial intervention. On the day of the surgery, surgeons register the pre-operative MRI to

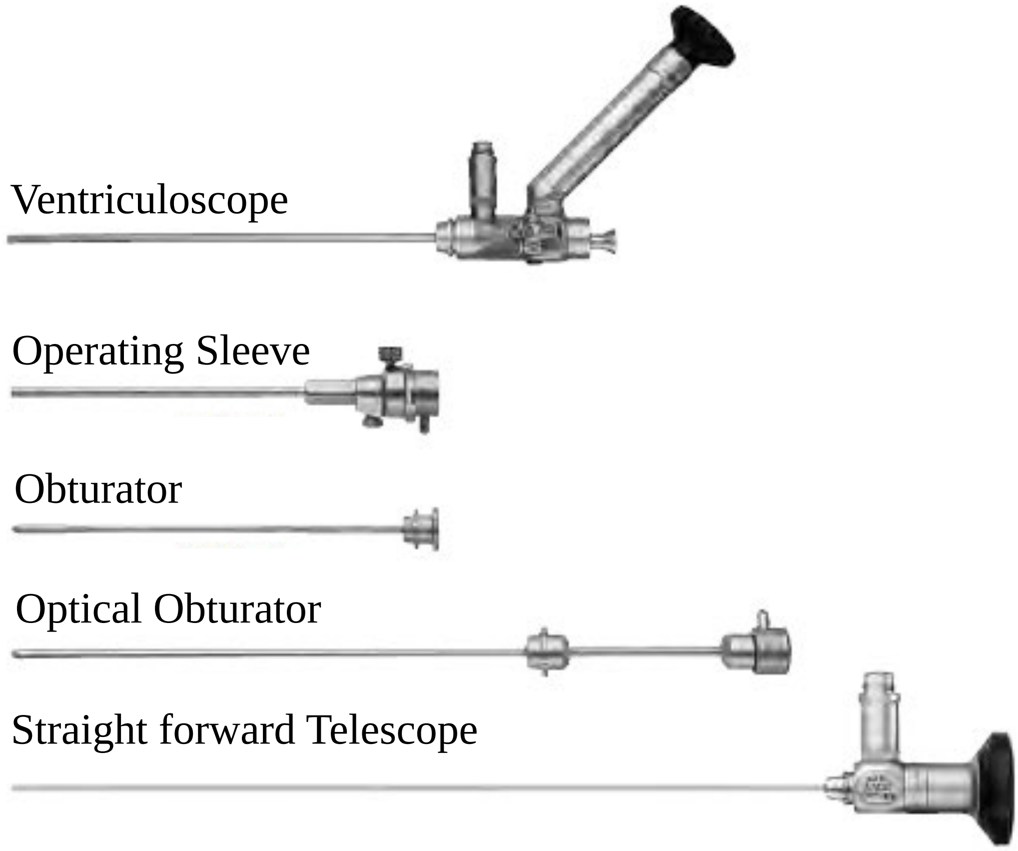


Figure 3.1: Set of neuroendoscopy tools. Courtesy of KARL STORZ. Gmbh

intra-operative neuronavigation and mark the incision point on the patient's skull. While selecting the incision point, the surgeon also projects the trajectory of the endoscope using pre-operative MRI, and intra-operative neuronavigation. Then, they remove the scalp and drill a small hole (burr-hole) of around 10 mm into the skull. This procedure can be categorized as a pre-surgical setup.

Continuing the procedure, the surgeon inserts a concentric endoscopic sleeve (as shown in figure 3.1) into the dura matter of the brain until it reaches the surgical site, while constantly monitoring the trajectory using the intra-operative neuronavigation. This is a very delicate procedure and requires high degrees of precision and steadiness. Once the sleeve reaches the target, the surgical assistant mounts a mechanical support arm to hold the sleeve in position (see figure 3.2). Then, the surgeon inserts a specialized endoscope through the surgical sleeve to carry out the desired procedure. Finally, once the intracranial procedure is finished, the surgeon carefully retracts the endoscope and the surgical sleeve, fills the burr-hole with bone dust and sews up the scalp.

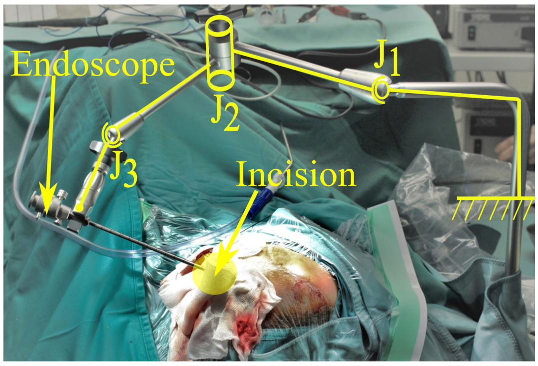


Figure 3.2: Mechanical tool holder for neuroendoscopic surgery

It was observed that even slight changes to the orientation of the endoscope during the intracranial procedure requires unlocking and manipulating the mechanical holder. These adjustments are inevitable but risky, especially due to the holder characteristics. This device becomes completely loose when unlocked, requiring the surgeon to support the entire system with both hands while the assistant unlocks and re-locks the holder. Observing the procedures, it also came to our attention that six hands are consistently required to execute these long surgical procedures.

It was evident from the observations and discussions with the surgeons that the most critical part of the surgery was the orientation, insertion, and intra-operative manipulation of the surgical sleeve. Hence, we decided to address these challenges with the design of a new robotic system. The goal of the new robot is to replace the currently used passive mechanical holder, providing a highly precise, stable and safe platform specifically designed for operations on neonates and infants.

### 3.1.2 Design Requirements

For defining the robotic system requirements, the first question to be answered was about the workspace and required range of motion. To calculate this, we used the MRI scan of a baby's head. This MRI was in the form of Digital Imaging and Communications in Medicine (DICOM) image. It was then converted to CAD readable curves. Then, the data was imported into a CAD platform (Creo Parametric) and converted to an actual size skull as shown in figure 3.3.

Another system requirement was the incision point on the skull. It was evident from our discussions with the surgeons that this point is patient-specific and depends on the type and location of the lesion to be treated. Therefore, the robotic system must be capable of inserting the endoscope from any orientation in space as shown in figure 3.4.

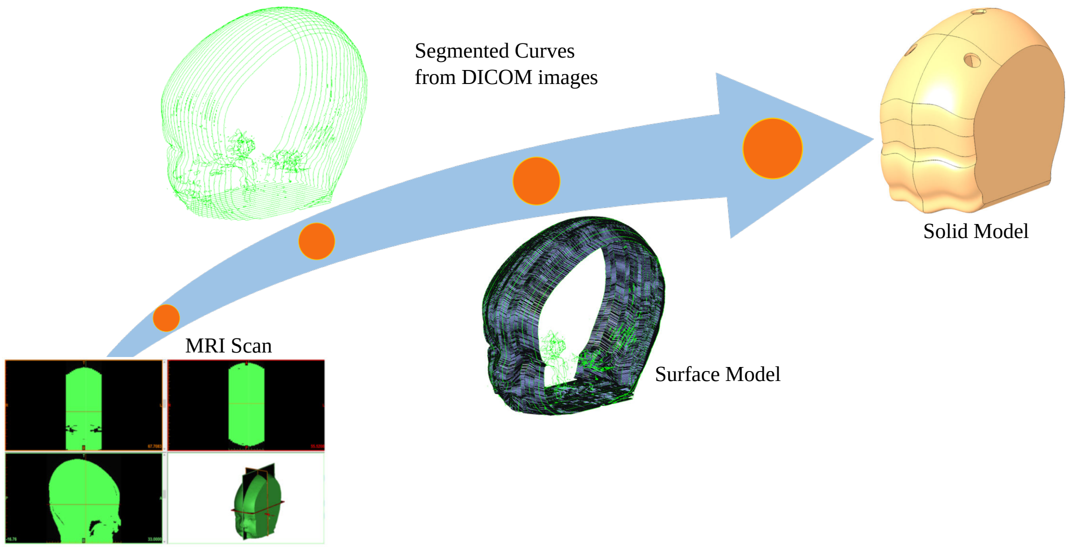


Figure 3.3: Conversion of MRI to solid CAD model

It became clear that the workspace should be spherical, with its remote center of motion (RCM) located at the incision point. The RCM is the term also used in surgical robotics to describe the pivot point for the surgical tool. The RCM restrict the tool to move linearly, though it can rotate around it. Once the RCM is established, three DOFs are required for anterior-posterior, lateral-medial and transcranial insertion. Figure 3.5 shows the medical terminologies of respective movements.

Figure 3.4: Estimated incision points

Since the RCM has to be moveable to cater for a variety of insertion points, a mechanism is required to achieve this. In this case, we opted to perform cartesian motions, which adds an additonal three DOFs to the system.

In some cases, surgeons are required to minutely change the position of the endoscope after the transcranial insertion. These adjustments requires the joints to be decoupled. The decoupled joints facilitate the motion control and the safety of the system.

The compactness of the robotic system is another key requirement. Currently, most of the

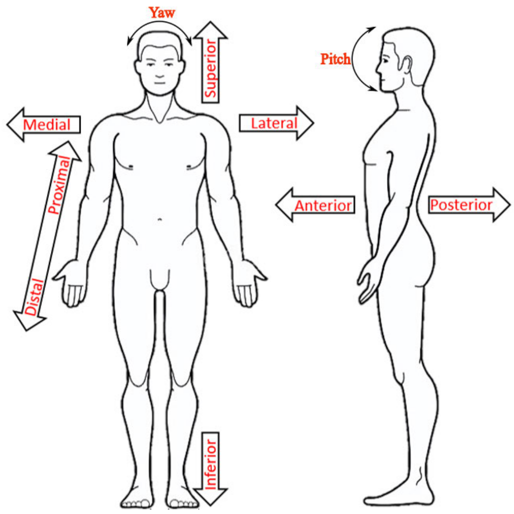


Figure 3.5: Motion reference system

Table 3.1: Design requirement for the robotic system

| **Name** | **Requirement** |
|---|---|
| DOFs | Three for the pre-surgical adjustments<br>Two for the orientation of the surgical tool<br>One for the insertion of the surgical tool |
| Remote Center of Motion | Yes |
| Entry port/position | Multiple |
| Robot Placement | Anchored on Surgical Table |
| Core Material | Non Magnetic |

commercially available robotic systems are large in size. They often occupy a huge space in an already crowded OR, hindering the work flow of the support staff. Therefore, a major requirement is to reduce the size of the robotic system. Ideally, the system will be mounted on the surgical bed. This will allow seamless integration with the OR environment and foster the adoption of the new system by the surgeon.

Finally, given the need for using electromagnetic navigation and localization during procedures, the robotic system must be carefully designed to minimize electromagnetic interference in the OR. Table 3.1 summarizes the design requirements for the robotic system.

### 3.1.3 Design Specifications

After careful consideration of the requirements, we were able to conclude the specifications of the system, including size, DOFs, range of motions, safety, precision, and required material properties.

Table 3.2: Desired specifications of the robotic system

| **Required Parameters** | **Value** |
|---|---|
| Max. Robot Size | 1000 x 500 x 200 mm |
| Motions | AP = -55° to 55°<br>LM = -60° to 60°<br>Depth = 130 mm<br>$\Delta$X >150 mm, $\Delta$Y >70 mm<br>$\Delta$Z >100 mm |
| Accuracy | 400 $\mu$m |
| Arbitrary RCM | Yes |

It is imperative to minimize the size of the robotic system, so we decided to utilize the space under the surgical bed. In this manner, the robotic system will not affect the surgical workflow. The volume of the whole system will kept under 1000 x 500 x 100 mm.

As above, the basic DOFs are designed to be two rotational degrees, pitch and yaw, for anterior-posterior and lateral-medial, respectively. An additional DOF is needed for the insertion of the endoscope.

Other design specifications include the use of non-magnetic materials for the construction of the robotic system to avoid errors in intra-operative neuronavigation. The accuracy of the robotic system was set at 200 $\mu$m, as a benchmark, which was defined heuristically considering the limited accuracy surgeons are able to achieve today with their bare hands. Finally, the specified range of motion for each DOF was obtained using the MRI scan of a baby's head. The complete set of specifications can also be seen in Table 3.2.

## 3.2 Design of the Robotic System

### 3.2.1 Conceptual Design

Since the required workspace is spherical, it was decided to use a circular track motion system that includes a translation mechanism mounted on a carriage platform. This whole mechanism must be stable, as the surgeon will apply forces directly on the carriage block while performing the procedure. Therefore, the whole motion must be stabilized by supporting the circular track (arc) from both ends.

A dedicated 3-DOF translation motion system was then designed to position the circular track and carriage platform in space. The design provides the required rigidity to the circular track and also enables the placement of the RCM at any point in the workspace, maximizing the surgical potential of the system. Therefore, this motion stage must allow motions in x, y, and z axes, i.e., superior-inferior, lateral-medial, and anterior-posterior, respectively. A free

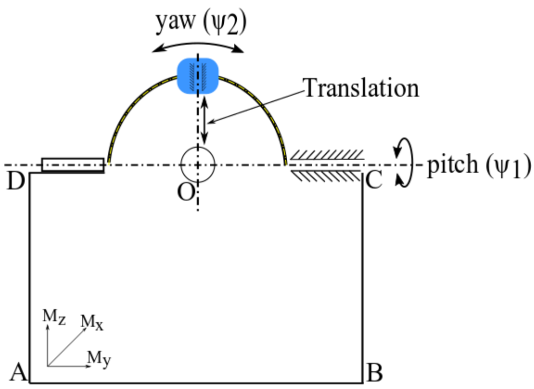

Figure 3.6: Free body diagram of the robotic system

body diagram (FBD) of the proposed robotic system is shown in figure 3.6.

Most commercially available robotic systems for neurosurgery use serial manipulators, whose safety are dependent on each actuator, because each successive link is dependent on the preceding link. Since safety is a critical aspect of the proposed robotic system, we have selected mechanisms that are stable, so that the safety of the system will be dependent on the least amount of components as possible. The safety of each mechanism is discussed in detail in their respective sections.

It is an essential design practice to develop a minimalistic proof-of-concept before designing the actual system. This approach helps to rectify major design problems at the initial design stages. The proof-of-concept also gives a physical prototype of the product, which helps to communicate the design to the non-technical stakeholders such as surgeons.

The proof-of-concept was completed at the beginning of this project by developing a scaled-down skeleton structure of the robotic system. The already selected mechanisms were incorporated (discussed in section 3.2.2.1 and 3.2.2.2) with the minimum details possible. These parts were designed and modeled such that they could fabricated on in-house 3D printers. Some off-the-shelf parts helped to achieve the minimum functionality needed. Later on, all these parts were assembled into a proof-of-concept, which can be seen in figure 3.7.

The proof-of-concept prototype proved very helpful in demonstrations to the surgeons. It also allowed them to give clear feedback about the system design, which guided the subsequent refinements. This prototype was also very useful from an engineering design perspective. The prototype verified the functionality, constraints, redundancies, relative motions, workspace, and structural stability. And a life size baby manikin was used to have better visualization of the appropriateness of the system design.

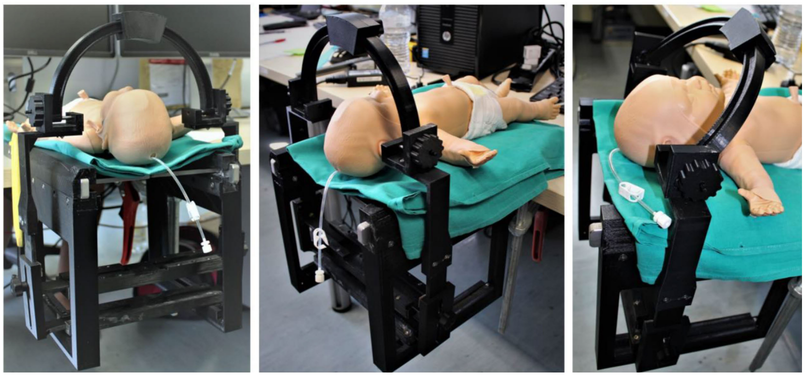

Figure 3.7: Scaled down model of the robotic system

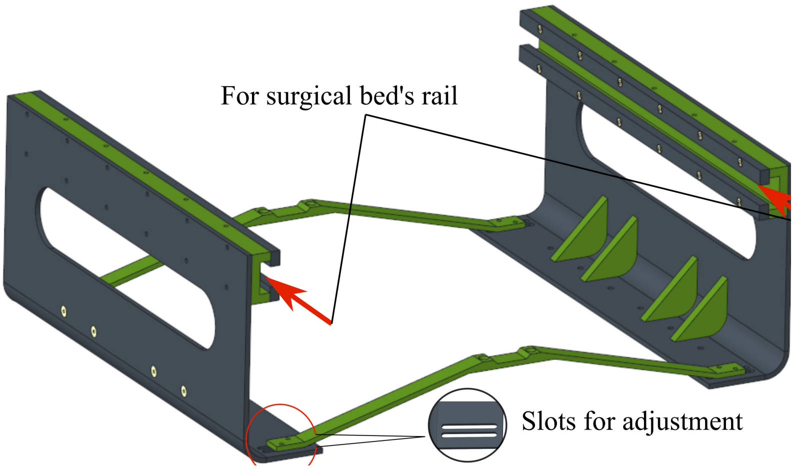


Figure 3.8: Anchoring system

### 3.2.2 Design of system sub-components

The design of the robotic system can be explained based on its sub-components and their primary functions.

**Anchoring**

The robot was designed to be anchored to the rails of the surgical bed. This is done by sliding the anchoring blocks onto the rails. This setup operation is done manually. Once the robot is at its designated position, the anchoring blocks are locked in place using fasteners. These fasteners constrain the motion in both the longitudinal and lateral directions. So the position of the robot is locked with respect to the surgical bed. The anchoring blocks provide a solid and stable support for the robot. This part can be designated as the grounded part of the robot. The anchoring blocks can be seen in figure 3.8.

#### 3.2.2.1 Cartesian Motion System

Initially, a Cartesian motion system was designed to place the RCM at a specific point. The basic requirements of the Cartesian motion system are:

1. The system will support the circular track from both ends.
2. All the motion axes will be decoupled from each other.
3. It will cover the required workspace.
4. Preferably the motion axes will be locked naturally while at rest.
5. It will not provide motion in steps such as gears and belts to allow automatic control with high accuracy and precision.
6. It will be relatively straight-forward in construction (for ease of assembly and disassembly).

The numerous mechanisms will provide all requirements, such as Cartesian parallel mechanisms, cable-driven mechanisms, and off-the-shelf precision linear actuators. Before designing the mechanism, The state-of-the-art validation of the candidacy of the above mentioned mechanisms has been carried out, and these will now be discussed in the following sections.

**Cable Driven parallel mechanisms**

Cable driven parallel mechanisms (CDPMs) are widely used for manipulation. The basic principle is to use motor driven tendons attached to a static base on one end, while the other end is attached to the end-effector. The relative motion of the tendons move the end-effector to the desired position and orientation [110]. CDPMs find their applications in various fields such as the movement of high payload in a large workspace [111], large radio telescopes [112], and material handling [113]. Medical applications of CDPMs are mostly in prosthesis [114] and rehabilitation equipment [115].
CDPMs are also used for Cartesian coordinate motions. A related study by Behzadipour et al. presented a design that satisfies the requirements of our application [13]. The system they describe is constructed using a hybrid of rigid links (connected prismatically) and a cable loop. It also features a special arrangements of cable routing to move the end-effector in a Cartesian motion. Cable and pulley arrangement can be seen in figure 3.9. However, this mechanism cannot be directly applied to our problem because it cannot support the circular track from both sides. Such an the arrangement will not allow motion in the Y-axis. In addition, the the motions of different axes are coupled in their mechanism [13].

Other types of CDPMs for Cartesian motion have been proposed by Metillon [116] and Tho [14]. The major limitations of these systems are related to their construction. The design in [14, 112] are not feasible for the surgical operation being considered in this research. These mechanism cannot support the circular track from both sides. Even the modifications in [14, 112] cannot support the mechanism shown in figure 3.6.

Another interesting type of cable-driven mechanism is the Large Cable Delta Robot (LCDR), which can provide Cartesian motions [117]. It has the same construction as a common delta robot but instead of rigid links, the end-effector is controlled by cables. Each cable link is supported with a winch and actuator. The motion is produced by varying the length of the cable. This mechanism has some limitations regarding our neurosurgery application. The motions of the end-effector are coupled and it is not optimal to mount the circular track on the end-effector.

**Rigid Link Parallel Mechanisms**

Rigid Link parallel mechanism address some of the short comings of cable driven/delta robots, such as coupled motions, limited workspace and complex kinematics. Kim et al. [118] presented a rigid link manipulator with 3-DOF Cartesian motion. This manipulator consists of a fixed base with 3 PRRR (one parallel and three rotational) links. It can provide completely decoupled motion and a large workspace. There are multiple variants of such Cartesian manipulators presented in other studies[15, 16]. These systems are shown in figure 3.10.

These mechanism seems to be the ideal choice but it is not possible to use them on an "as is" basis. The major problem is compensating for the motion along the Y-axis on both sides to keep the Z-axis in the center. However rigid link manipulators did provide a design idea for

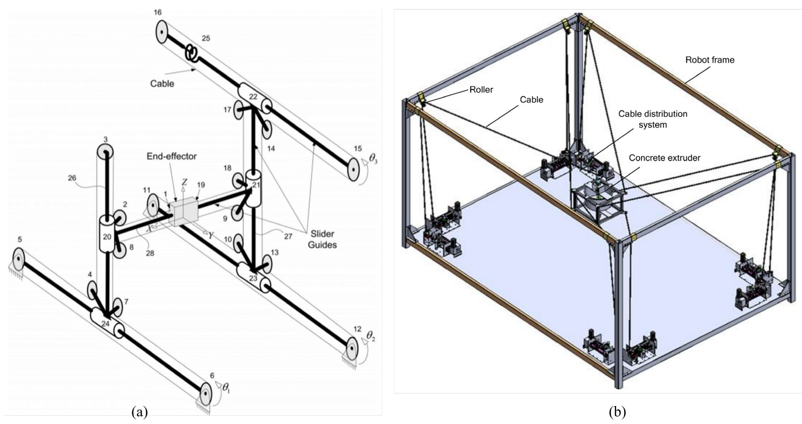


Figure 3.9: (a) Hybrid cable-driven cartesian mechanism [13] (b) Cable-driven parallel mechanism [14].

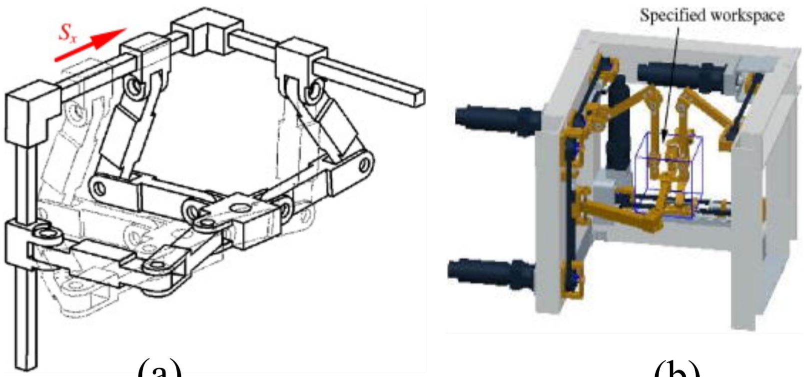


Figure 3.10: (a) Cartesian parallel manipulator [15] (b) 4-DOF Cartesian parallel manipulator [16]

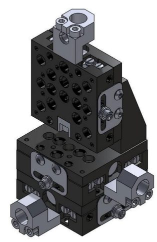

Figure 3.11: Cartesian positioning stage (Courtesy of Sisikiyo Co.)

further development of a custom mechanism.

**Positioning Stages**

There are several types of commercial precision Cartesian manipulators available in the form of positioning stages and linear actuators as shown in figure 3.8. They are available in various forms and configurations, but tend to be expensive and their use for our purposes would required significant customization. Moreover, they also are limited because they cannot constrain the Y-axis, which is required to support the circular track.

**Design of a Cartesian Motion System**

For simplicity, we divide the design into the three motion axes, i.e. X (Superior-Inferior), Y (Lateral-Medial), and Z (Anterior-Posterior). The motion of the X-axis is the backbone of the whole structure of the robotic system. For this axis, a commercial electric rodless actuator (SMC E-MY2B16-300WTPL-Q) was selected. This actuator has a stroke length of 270 mm with a nominal precision of 0.01mm. This actuator is rigidly attached to the fixed base of the robotic system with pre-stressed trusses. These supports are connected to the base through slotted holes. The slotted holes are used to adjust the straightness of the linear actuator and avoid parallelism errors during the assembly. This structure is shown in figure

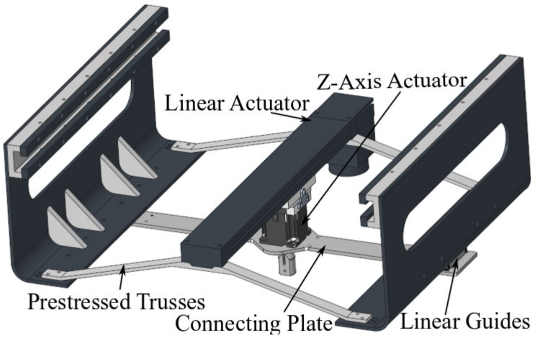


Figure 3.12: X-Axis

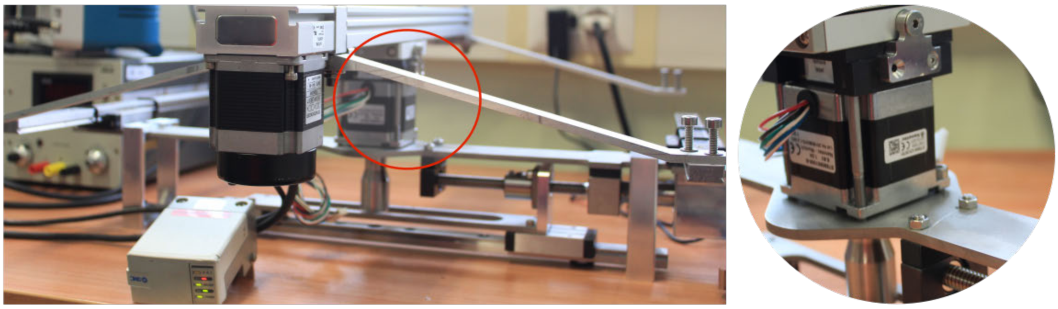

Figure 3.13: X-Axis during assembly

3.13 and 3.12.

The linear actuator's carriage supports the mechanisms for the Y and Z axes. It is also stabilized by two additional linear guides on either side and a plate connecting them. The mechanism for this motion can be seen in figure 3.9. The X-axis's movement is parallel to the ground. It is safe even in case of mechanical or electrical failure.

The actuator of the Z-axis (Stepper motor ST5909) is mounted on the carriage of the X-axis linear actuator as shown in figure 3.9. The Z-axis actuator provides motion using a lead screw, which passes through the top linear guide and is fixed (in translation) on the carriage of the bottom linear guide. A bearing supports the distal end of the lead screw to allow the rotation of the lead screw. The lead nut is fixed on the mid linear guide.

To clarify how the mechanism works, consider a rectangular frame A (A1, A2, A3, and A4) shown in red in the figure 3.14 and 3.15. Frame A slides in Frame B (B1, B2, B3, and B4), shown in orange under the action of the lead screw powered by the Z-axis actuator. Frame A has two open ends on top where we mount the circular track system (discussed in later sections). The Z-axis has a stroke length of 150 mm.

The mechanism for motion in Y-axis is relatively complex. The Y-axis actuator (as shown in

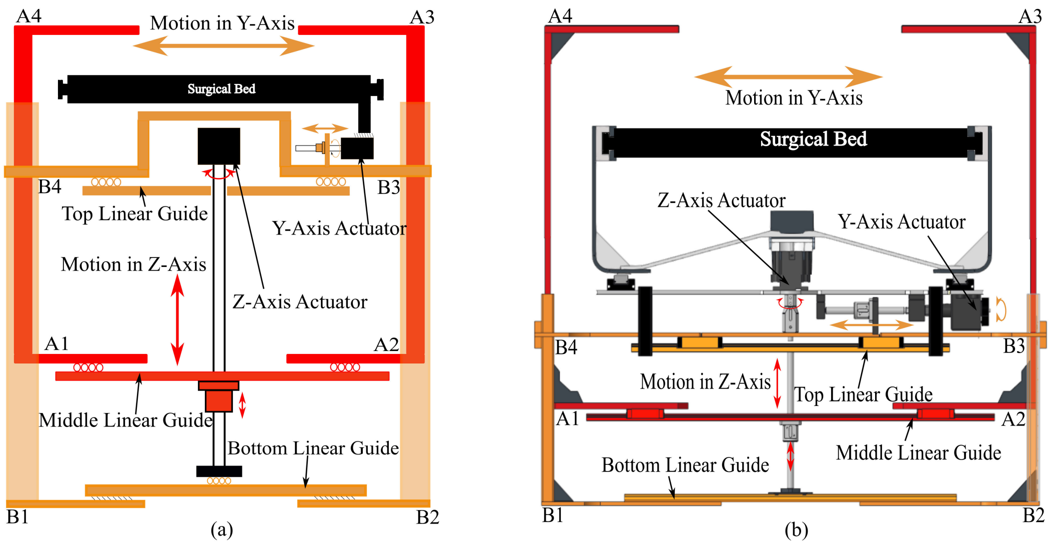


Figure 3.14: Cartesian motion system

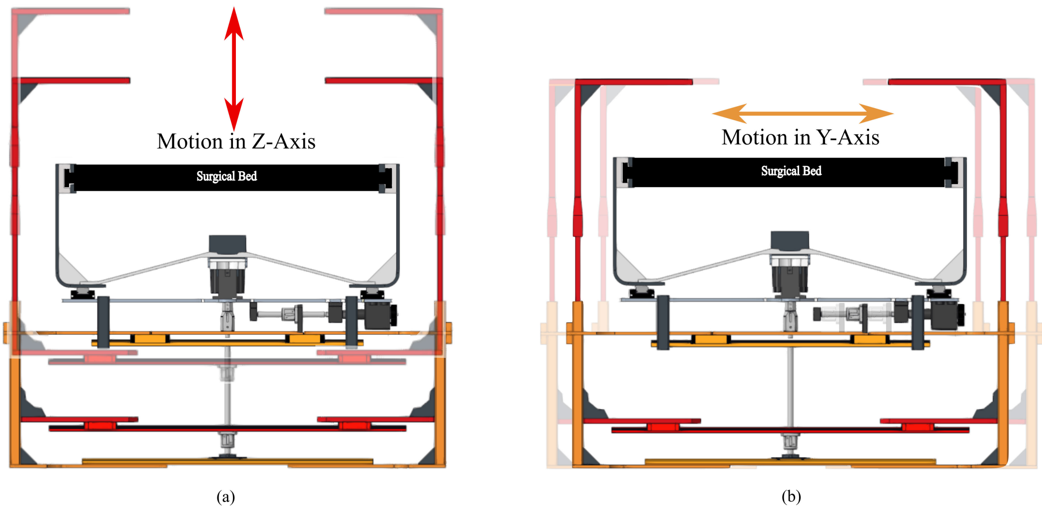


Figure 3.15: (a) Motion in Z-axis (b) Motion in Y-axis

the figure 3.15) moves frame B (in orange) normal to Z-axis by using the nut of the Y-axis lead screw (Y-axis Motor Model). As a result, the upper part of frame B (B3 & B4) will slide over the top guide, while the bottom guide slide relative to its carriage keeping the carriage in the center. Since frame A is already inserted in frame B, it also moves in the y-direction. The lower part of frame A (A1 & A2) slides over the carriages of the middle guide to it compensates for the relative motion in the y-direction. Motion in both Z-axis and Y-axis are shown in 3.11. The advantages of this cartesian mechanism are decoupled motions on each axis, structural integrity because of rigid links, straight-forward kinematics, and support for the circular track above it. From the safety perspective, the motion is dependent on the lead

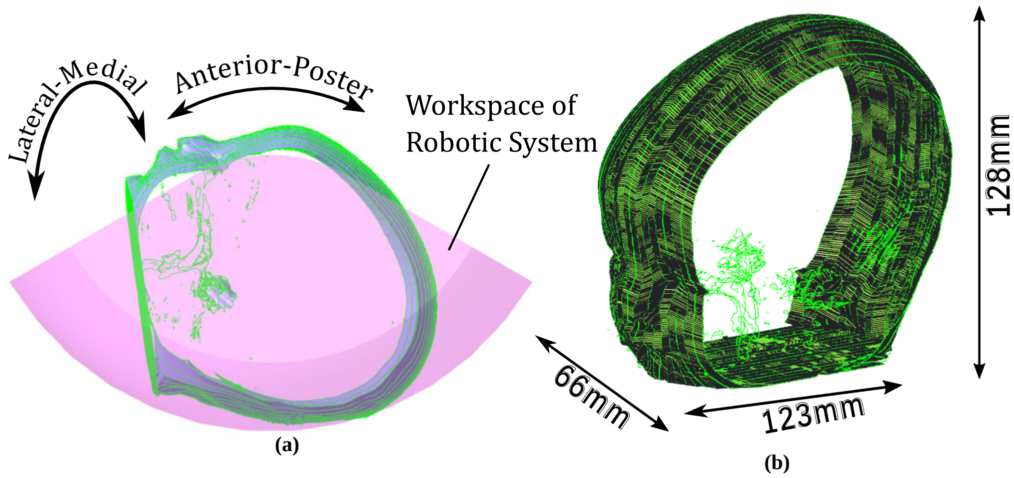


Figure 3.16: (a) Required kinematic workspace (b) Real MRI of a baby's head converted to a CAD model.

screws, so it is inherently safe in the case of any failure.

#### 3.2.2.2 Circular Motion System

It was observed in the surgeries, that one fixed entry point into the skull was used, through which a rigid surgical endoscope is inserted. The endoscope orientation is established before entry, based on a pre-operative plan and using intraoperative electromagnetic navigation. The references are Anterior-Posterior and Lateral-Medial angles. This is also shown in figure 3.16.

The endoscope is inserted by a very slow translation motion, which is constantly checked using the navigation system (see section 3.1.1). When the treatment area is reached, the endoscope is locked in place and the surgeon operates through the endoscope working channels. In this section, the focus is on studying and designing a new mechanism to enable precise orientation and delicate translational insertion of the endoscope towards the surgical area, while also providing a rigid and stable support for the subsequent manual surgical actions.

From the descriptions above, it is clear that achieving proper endoscope orientation and insertion actions require at least three DOFs to enable two rotations and one translation. Based on the system requirements and specifications, the robotic system should allow -55° to 55° in AP, -60° to 60° in LM and at least 130 mm of depth motion. In addition, also in this case it is required to avoid interference with the neuro-navigation system.

**State-of-the-art**

In the past three decades, numerous mechanisms were devised for robotic neuroendoscopic procedures. Among them, serial mechanisms are the most popular. Several commercially available neurosurgical robots use serial manipulators such as Medtech ROSA [1] and Renishaw Neuromate [79] . Although serial manipulators offer various advantages such as simple construction and large workspace, but summed up inertia at the end-effector due to the consecutive links makes them bulky. These manipulators tend to block the vision window of the surgeon. Their massive size also disrupts the workflow in the surgical room.

Spherical mechanisms are also widely used in neurosurgical applications. These seem as a logical choice, as a spherical workspace is required with a RCM at the incision point. Essomba et al. [119] developed a spherical mechanism for the neuroendoscopy. They used a modified 5-bar linkage mechanism with RCM. Previously they also developed another mechanism with a spherical link mechanism [120]. Another study [121] proposed a two DOF spherical mechanism with RCM. This study mainly addresses the brain biopsy so that the actuated insertion was not required. Another interesting study was presented by Afshar et al. [122], where they presented a retractable spherical mechanism with four stages of unfolding. There are several advantages of spherical mechanisms in neurosurgery. They have an intrinsic spherical workspace with a mechanical RCM. Moreover, they also provide RCM in two DOFs. They can be easily decoupled for the simplification of control. They provide continuous motion, and large precision and accuracy can be achieved through the selection of appropriate actuators. However, the spherical mechanisms have relatively complex architecture. Multiple link mechanisms could have coupled motions that are difficult to control and complicate the system's entire kinematics. In the case of pediatric neuroendoscopy, such structures can also be counter-intuitive for the surgeons. Another favorable type of mechanism is the circular tracking arc. It is the structurally simplest way to have inherited RCM [123]. The basic principle of this mechanism is to move a block along the curvature of the circular track. It provides 1-DOF RCM at the center of the circular track. Another RCM can be achieved by pivoting the circular track with a revolute joint at the base. Probot [124] and UT-NEU [125] used this mechanism for their robotic system. Though this mechanism is very simple in structure, maneuvering the block along a curvilinear track is challenging. However, several mechanisms have been proposed for this actuation such as belt and pulley mechanisms. The MARS robotic system [126] utilizes the same mechanism, and the block was actuated with a gear pinion mechanism. It was as an open-ended circular guide structure. Both the backlash of the gear mechanism and the bending in the arc compromise the system's accuracy. Later on they developed a calibration method to cater to these problems[127]. Another study proposed by Yip et al.[128] using a circular track by guiding the block with a coupled belt actuated mechanism. They used a closed-loop circu-

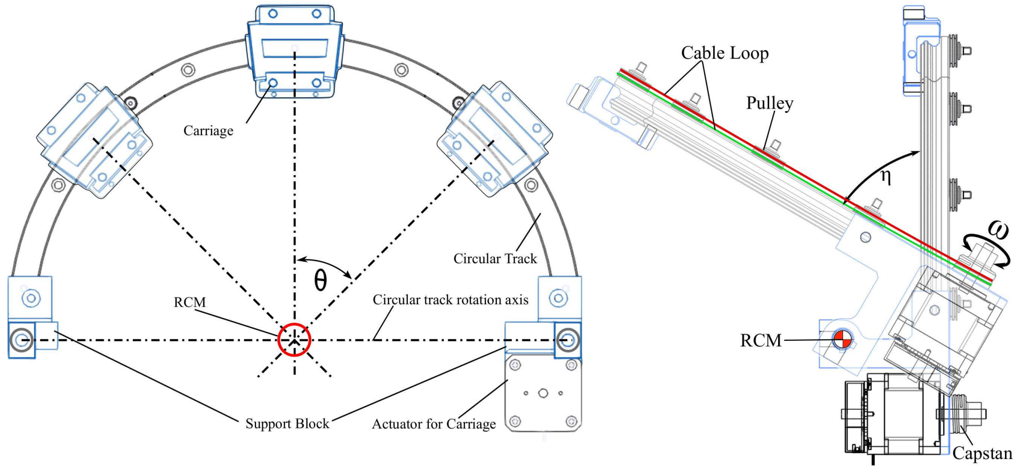


Figure 3.17: Yaw and pitch motion of circular motion system

lar track system. But their major focus is to keep the RCM out of the body as required in gynecological procedures such as uterus positioning.

**Design of circular motion mechanism**

This section presents the design and development of a mechanism for circular motion using a cable pulley mechanism. It provides RCM in two DOFs i.e. pitch and yaw. It is designed specifically for pediatric neuroendoscopy, but it has potential to be used also in other medical and industrial applications.

Fundamentally the mechanism comprises a circular track with a carriage block mounted on it, as shown in figure 3.17. A commercial made-to-order circular guide rail (HCR 15A-60-150R) with a carriage of a radius of 150 mm was selected for our robot. The carriage mounted on the circular guide moves along the curvature ($\theta$). Since the motion is curvilinear, a cable-pulley mechanism is used. The carriage block is equipped with a C-Shape block closed by a plate on the other side of the track. The plate bears an L-shape cable guide bracket with two holes to tie both ends of the cable. Two double groove idle pulleys are mounted on the backside along the curvature of the circular track.

The actuator's motion axis is parallel with the center axis of the circular guide and normal to pitch motion actuator. One end of the cable is tied to the cable guide bracket, and then it is routed towards the capstan of the actuator at the bottom of the track, passing through one groove of the pulley. The cable makes one loop around the capstan and then is routed back to the pulley at the other end, through the second groove. On its way back towards the carriage, the second end of the cable is tied to the second hole on the cable guide bracket.

When the actuator rotates the capstan, friction force from the loop pulls the cable, and as a

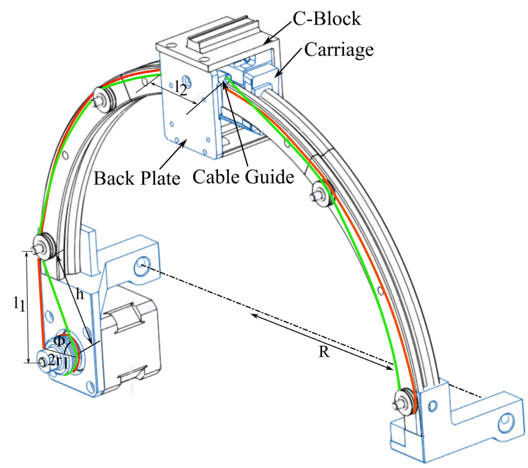


Figure 3.18: Cable routing for circular motion

result, it moves the carriage block. When the carriage block passes through an idle pulley, the cable is disengaged from the pulley because of the cable bracket. Once it has passed through the idle pulley, the cable engages it again because of the tension provided by the actuator. We have used a ST4118M0404 stepper motor with built-in optical encoder to drive the capstan. The stepper is fixed on a custom build block which is also supporting the circular track.

The second DOF of the proposed mechanism was achieved by rotating the circular track around the axis ($\eta$) located at the base shown in figure 3.17. A custom built block was designed to support the circular track on both ends. A high torque brushless DC motor with gearbox is attached to one end of the block, while a braking system is attached to the other end. The motion axis is perpendicular to the axis of the circular track, as shown in figure 3.17.

For our surgical application, the whole mechanism is mounted on the custom built Cartesian coordinate motion system, which supports the system from both ends. Therefore, up to this point, are 5 degrees of freedom to position and orient the endoscope. The final DOF to perform the insertion and retraction of the endoscope into the brain will be described later in this chapter.

The designed carriage is modular and can support a variety of mechanisms mounted on it. For the neurosurgical applications, an endoscope insertion mechanism was designed and mounted on the carriage. That mechanism has a motorized platform to insert the endoscope inside the brain through the burr hole.

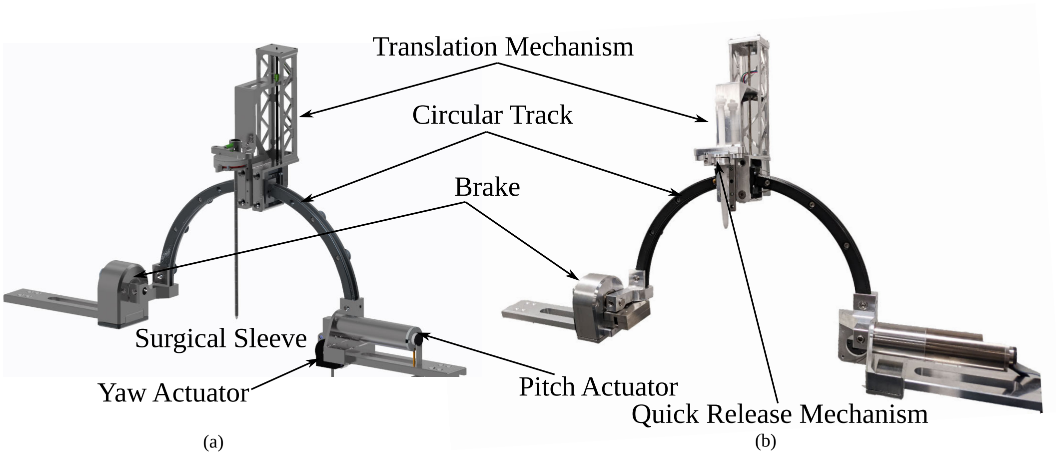

Figure 3.19: (a) CAD Model of circular motion system (b) Actual circular motion mechanism

Table 3.3: Comparison of different mechanism for neuroendoscopy

| **Required Parameters** | **Serial** | **Spherical** | **Cir. Track** |
|---|---|---|---|
| Mechanical RCM | No | Yes | Yes |
| Continuous Motion | Yes | No | Yes |
| Decoupled Motion | No | Yes | Yes |
| Inherited Spherical workspace | No | Yes | Yes |

### 3.2.3 Cable Length

For a cable-driven mechanism, the cable length invariance property is a preferable feature as it can lead to convenience in control, improvement of reliability, and simplicity in actuation [129]. The functionality of the mechanism dictates that the length of the cable has to be constant across the whole motion so the calculation of the cable length is essential. Since the cable is routed in closed loop and passes through the motion axis of the pulley twice, it is not possible to do this calculation using CAD.

Modeling the cable length results in equation 3.1. All the parameters in the equation are constant, so it shows that the cable length will be constant [13].

$$Cablelength = l_1 + 4\pi r_1 + \frac{h}{cos\phi} + 2\pi R - l_2 \tag{3.1}$$

where

$$\phi = tan^{-1}(\frac{l_1}{d_1}) \tag{3.2}$$

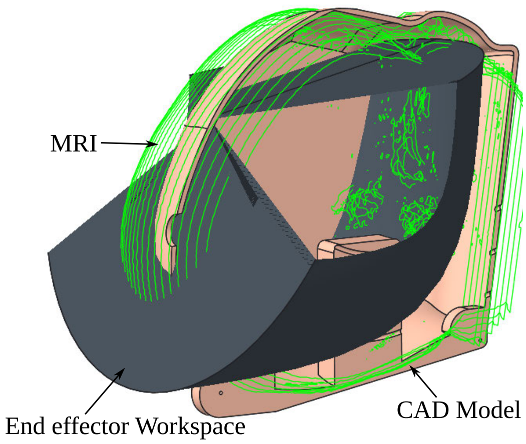


Figure 3.20: Simulation of the robotic system workspace considering the RCM positioned at the incision point.

$l_1$ is the distance between capstan and the consecutive pulley, $r_1$ is radius of the capstan, $\phi$ is the angle between the diameter of the capstan and edge of the consecutive pulley, h is the length of the cable between capstan and edge of the pulley, R is the radius of the circular track, and $_2$ is the distance between two ends of cable guide.

**Remote Center of Motion** Remote center of motion (RCM) is achieved mechanically in two DOFs i.e. pitch and yaw. The mechanism was designed so that the RCM is located at the intersection of the center point of the circular track and the axis of motion of angle $\eta$. Since this is a property of mechanical engineering, the RCM is achieved without any control system effort. RCMs such as this are considered safer for surgical applications. Depending on the application, the RCM is required inside or outside of the body. The proposed mechanism enables this flexibility. The space under the circular track is free, so the RCM can be placed inside, outside, or on the skin of the patient.

### 3.2.4 Workspace of the end effector

It was mentioned in the section 3.1.2 that a real MRI of a baby was converted into CAD surface model as shown in figure 3.20. Later, this model was used to make a hollow 3D model with the exact dimensions to verify the workspace and reach of the end effector. Figure 3.15 indicates that the end effector has a workspace appropriate for the application. It also shows the designed system is also applicable to transnasal procedures.

#### 3.2.4.1 Translation (Insertion)

The final DOF is the insertion of the endoscopic sleeve into the brain. As described in the previous sections, the translation mechanism for the sleeve must be mounted on the carriage of the circular track. Several candidate mechanism to perform this motion were considered. The most straight forward one is to use off-the-shelf linear actuators. But there are several challenges in doing this. First of all, it may occupy too much space under or over the circular track. In general, the size of commercial linear actuators is proportional to their stroke. For our application, the available combinations of the stroke length and the motor size was not optimal. Another issue in using a commercial device would be the likely to the need to customize it.Therefore, It decided to design a custom mechanism to translate the endoscopic sleeve.

The proposed new mechanism is mounted on a C-Block as shown in figure 3.21. The endoscopic sleeve mounts on a Z-shaped strip with a quick-release mechanism (see section 3.2.4.2). The strip is connected to the nut of the lead screw at one end, while the other end is connected to a linear guide. The linear guide constrains the rotation of the strip (under the action of lead screw) and facilitates the translation motion. The lead screw with a small servo motor is rigidly attach to the carriage block through the C-Block as shown in figure 3.21. The Lead screw is also supported from the other end with the help of light weight but rigid carriage.

The proposed mechanism is compact and will not block the surgeons view. Since we are using lead screw mechanism, it is intrinsically safe in case of power failure.

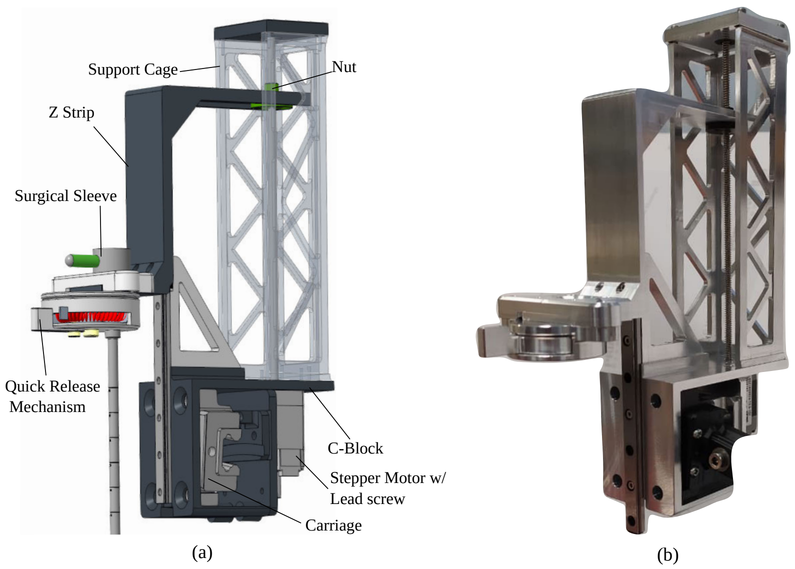


Figure 3.21: Translation mechanism (a) CAD model (b) Actual mechanism

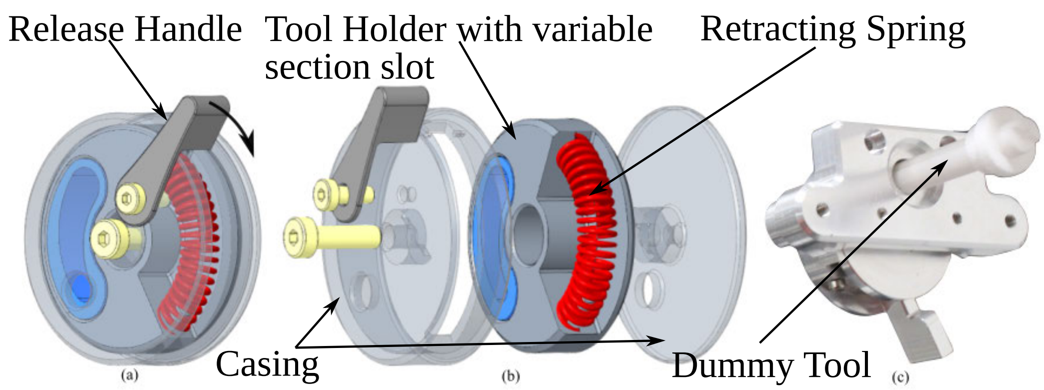


Figure 3.22: (a) CAD model (b) Exploded assembly of quick release mechanism (c) Actual mechanism

#### 3.2.4.2 Quick Release Mechanism

Quick release mechanism is a safety feature widely used in surgical robotics. It is used in case of emergency retrieval of the surgical tool from the body. Here, we designed a spring loaded slot cam mechanism which can hold the endoscopic sleeve and can be released quickly in case of emergency. The slot is designed in shape of cam profile so that it can accommodate any tool of diameter 4 to 7 mm. Figure 3.22 shows the mechanism in detail.

## 3.3 Summation into Complete Robot Design

The complete robotic system is comprised of three major mechanism, as discussed in detail in the previous sections. On combining those mechanism we have a complete robotic system as shown in figure 3.23. The robotic system has six DOF designed to perform several types of surgeries on neo-natal and infants. The robotic system is designed to be directly mounted on surgical bed so that it will not hinder the surgical workflow. The robotic system was designed to save space in OR so it utilize unused space under the operating table. The additional benefit of keeping most of the electrical parts under the bed is that it would not cause interference to the intra-operative neuronavigation. Since it is a safety critical system, four DOFs is designed in a way that it is neutrally stable and doesn't require additional safety feature in case of the failure. The other two DOFs have safety brakes in case of mechanical or electrical failure. A quick release mechanism has also been introduced for the quick retrieval of the surgical tool. A photo realistic rendered image is shown in figure 3.23.

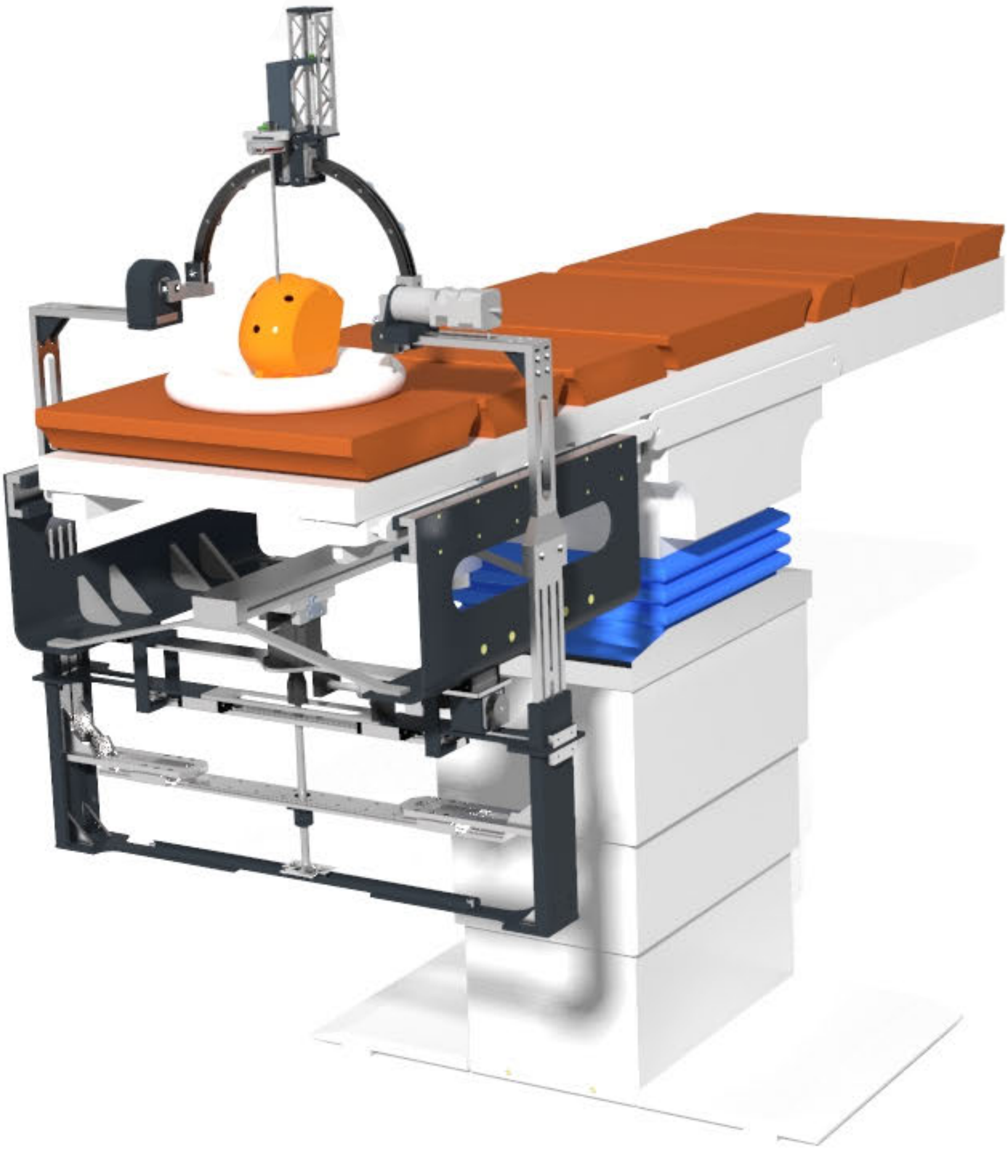

Figure 3.23: Photo realistic image of complete robotic system

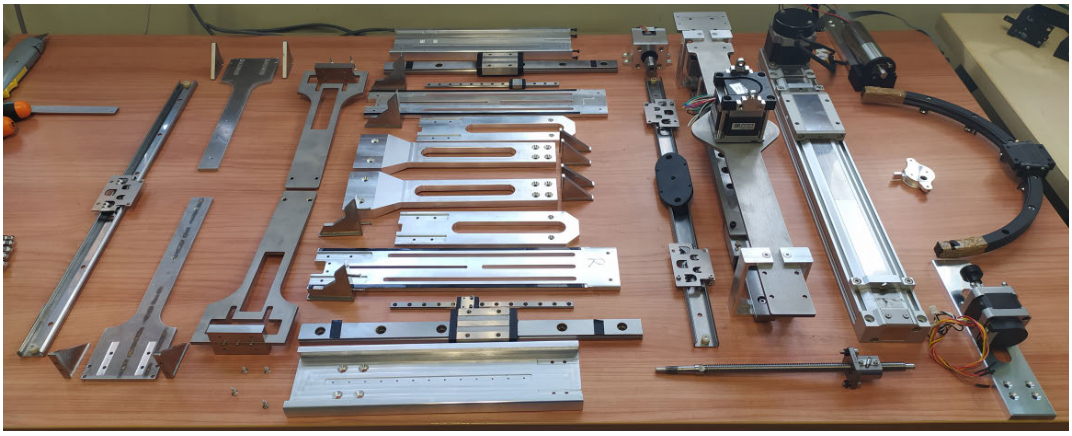

Figure 3.24: Un assembled parts of the robot

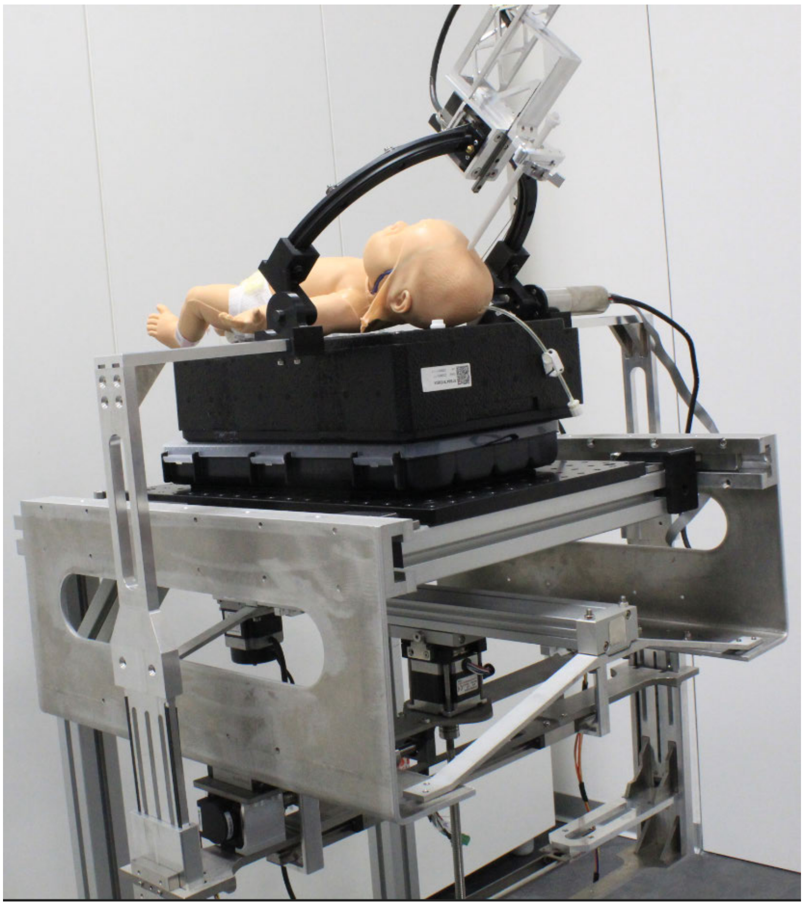

Figure 3.25: Robotic system assembled

*Chapter 4*

# Analysis and Verification

**Summary**
In this chapter, the robotic system is rigorously modelled, simulated, and analyzed using CAE packages. This process started with the kinematic analysis, which verifies that the robotic manipulator was able to achieve the required workspace. Then, the remote center of motion was verified using CAD. Subsequent sections are related to the finite element analysis (FEA) of critical robot components, and analytical and computational verification of required torques.

## 4.1 Kinematic Analysis

In this section, we carry out the kinematic analysis of our six DOF robotic system to verify and ensure the required workspace is achieved. As described in previous chapters, our robotic manipulator has four prismatic and two revolute joints. Its kinematic analysis starts with assigning a reference frame to each link of the kinematic chain using the Denavit-Hartenberg convention, as shown in figure 4.1.

A Denavit-Hartenberg table defined using the reference frame (4.1) is shown in table 4.1. Link 1, 2, and 3 are joined prismatically and are orthogonal to the preceding link. However, link 4 and 5 are joined through a revolute joint. Link 6 is joined prismatically and moves according to link 4 and 5. Joints parameters are also given in table 4.2.

The transformation matrix T gives us the workspace of the end-effector as shown in figure 4.2. The caption of the figure is self explanatory in justifying the required workspace of the system. The workspace has also been verified using the CAD as shown in figure 4.3.

$$T = \begin{bmatrix} \sin(\theta_5) & 0 & \cos(\theta_5) & d_3 + d_6 \cdot \cos(\theta_5) \\ -\cos(\theta_4 - \pi/2) & -\cos(\theta_4) & \cos(\theta_4 - \pi/2) \cdot \sin(\theta_5) & d_2 + d_6 \cdot \sin(\theta_4) \cdot \sin(\theta_5) \\ \cos(\theta_4) \cdot \cos(\theta_5) & -\sin(\theta_4) & -\cos(\theta_4) \cdot \sin(\theta_5) & d_1 - d_6 \cdot \cos(\theta_4) \cdot \sin(\theta_4) \\ 0 & 0 & 0 & 1 \end{bmatrix} \quad (4.1)$$

Table 4.1: D-H parameters.

| link | $\theta$ | $d$ | $a$ | $\alpha$ |
|---|---|---|---|---|
| 1 | 0 | $d_1$ | 0 | $-\pi/2$ |
| 2 | $\pi/2$ | $d_2$ | 0 | $-\pi/2$ |
| 3 | 0 | $d_3$ | 0 | $-\pi/2$ |
| 4 | $\theta_4$ | 0 | 0 | $\pi/2$ |
| 5 | $\theta_5$ | 0 | 0 | $-\pi/2$ |
| 6 | 0 | $d_6$ | 0 | 0 |

Table 4.2: Joints' range of motion.

| Joint | Range [mm] | Joint | Range [rad] |
|---|---|---|---|
| $d_1$ | [0,250] | $\theta_4$ | $[-\pi/3,\pi/3]$ |
| $d_2$ | [0,70] | $\theta_5$ | $[2\pi/18,8\pi/9]$ |
| $d_3$ | [0,150] | | |
| $d_6$ | [0,130] | | |

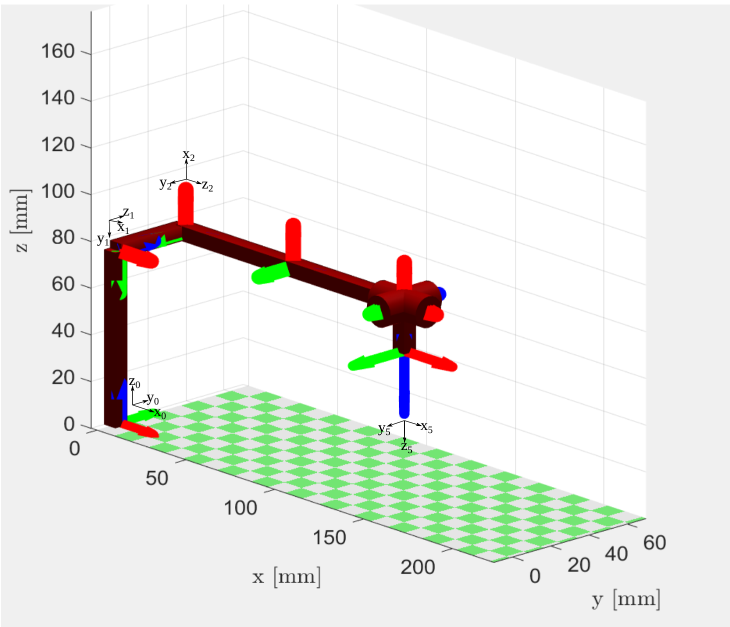


Figure 4.1: Kinematic chain of the robot. A reference frame is attached to each link according to the Denavit-Hartenberg convention. The axes are represented in red (x), green (y), and blue (z). The joints configuration depicted is q=[75 35 125 0 $pi$/2 20]; the joint variables, prismatic and revolute, are expressed in mm and radians, respectively.

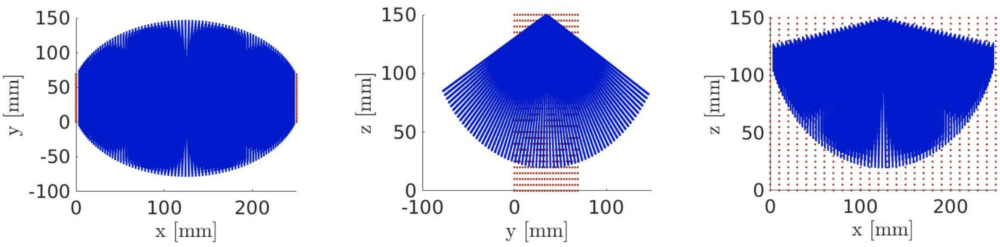


(a) (b) (c)

Figure 4.2: Workspace of the robot. (a) $x-y$ plane (b) $x-z$ plane (c) $y-z$ plane The red dots represent the end effector reachability obtained by spanning the three prismatic joints ($d_1$, $d_2$,$d_3$) within their range. Conversely, the blue region is obtained by setting the three prismatic joints ($d_1$,$d_2$,$d_3$) constant and consequently exploring the working range of the last three joints ($\theta_4$, $\theta_5$,$d_6$). Clearly, it is possible to translate the same motion within the workspace acting on the three prismatic joints ($d_1$,$d_2$,$d_3$).

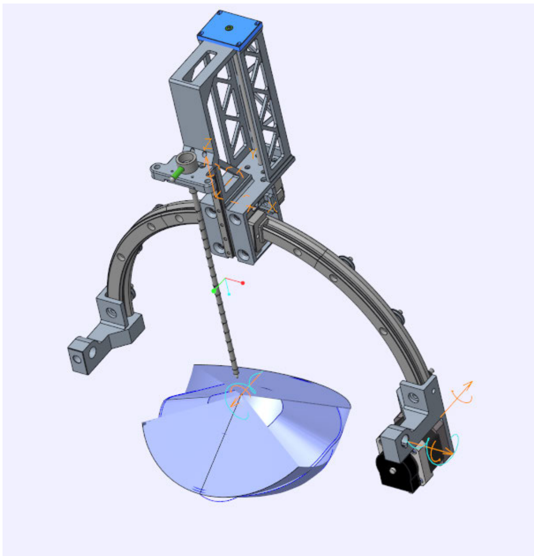

Figure 4.3: Workspace using CAD

## 4.2 Verification of Remote Center of Motion

The Remote center of motion (RCM) is a critical component in most surgical robots. In this research, the RCM of this new robotic system was verified using CAD. This was achieved by assigning data points along the center axis of the surgical sleeve in a regular interval. The points start from the tip of the sleeve and goes all the way to the end. Then the motion of surgical sleeve was simulated in pitch and yaw to the full extents and trace the motion of those points. The drawn curves are shown in the figure 4.4. It is clear from the figure 4.3 that motion of the surgical sleeve become narrower towards the center which shows that it has no movement at the RCM.

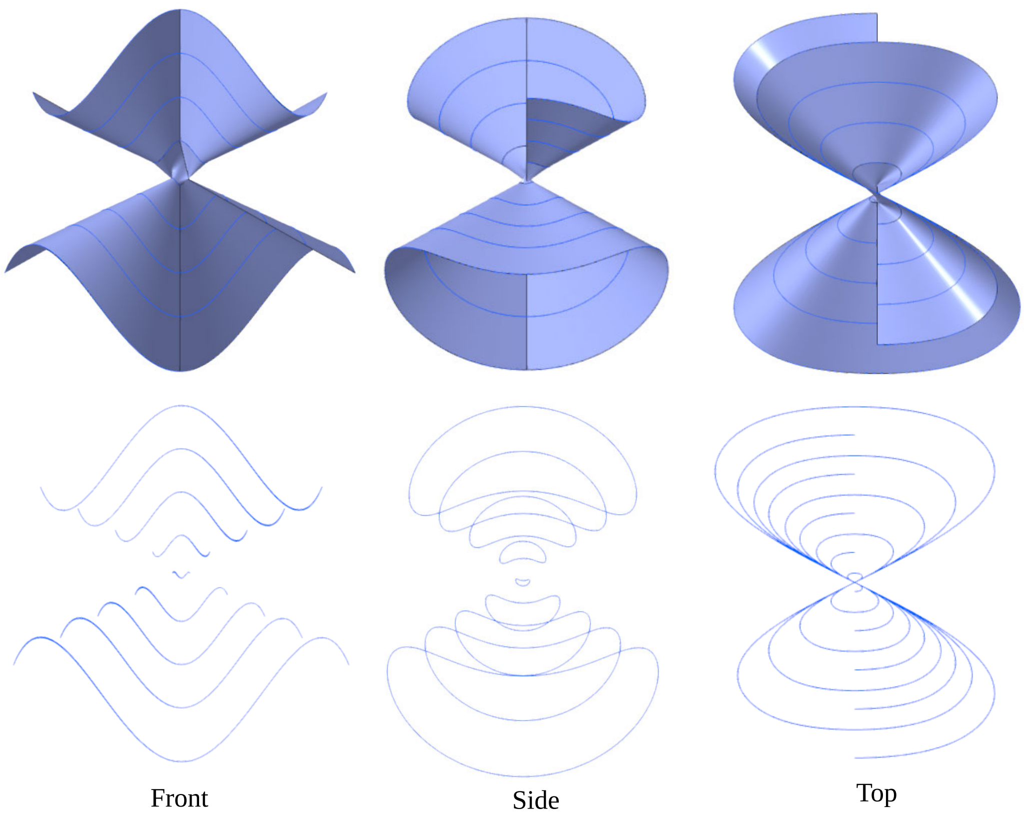


Figure 4.4: Surface and curves for the assigned data points

## 4.3 Verification of Decoupled Motions

Verifying that the individual constituent part of the overall control system are de-coupled is major design characteristic of the overall critical system design. In this section, this verification was carried out using dynamic simulation, performed using Creo Mechanism Dynamic Option. This started with the preparation of the CAD model by applying all mass properties, defining connections, applying motors to the connections, static and dynamic friction, and gravity parameters to make the simulation as close to the real life scenario as possible.

The most straight forward method, was the simulation the motion of one axis, measure the generated displacement of the said axis, and measure the induced motion in other axes. This demonstrated the decoupling of the Cartesian coordinate motion system. A force motor with a varying nominal torque was applied to move the X-axis so that the complete frame moved along with it. The effect of this motion on the Y-axis and Z-axis were then measured respectively. The motion of the X-axis is shown in figure 4.5. However, the effect of this motion was also measured as shown in figure 4.6. It is evident the mean motion generated in Y-axis is less than 1.5 microns. This is not the actual motion. The reason behind is that the lead screw connection of the Y-axis was modeled as slider connection and the minor perturbations caused the model to move in the simulation. It also happened in case of relative motion of Z-Axis as shown in figure 4.7. In this case, the simulation also takes the effect of gravity on Z-Axis. The relative motion of all the cartesian coordinate axes are plotted in figure 4.8. It is clear from the plot that there is virtually no effect of the moving axis on the stationary axes.

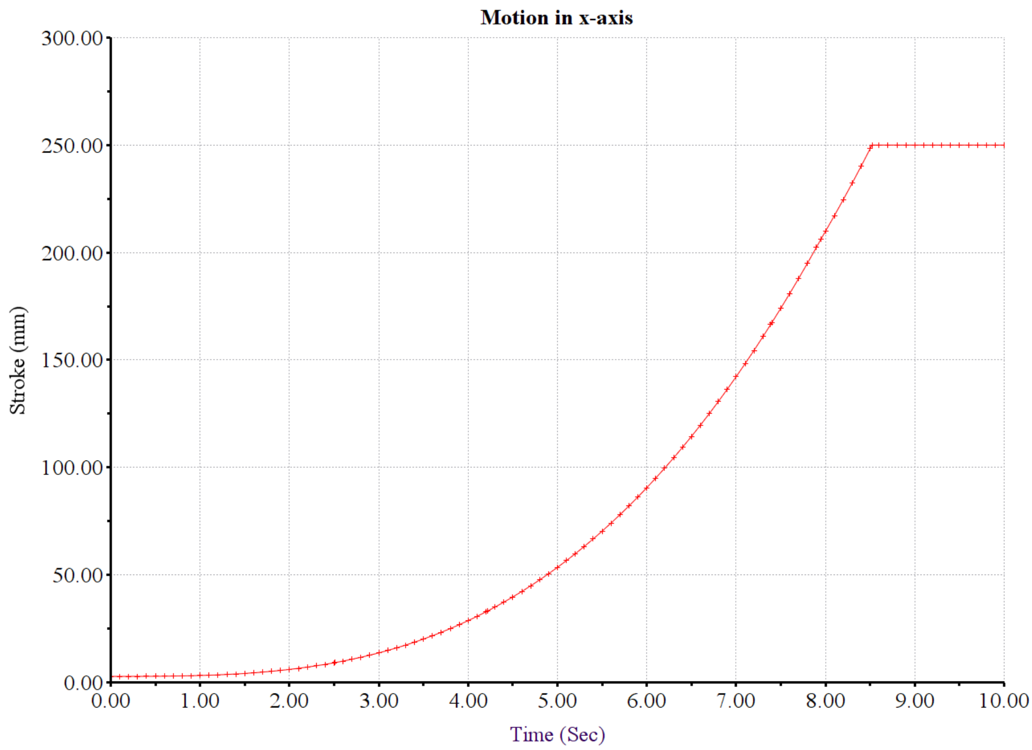


Figure 4.5: Plot of the stroke of X-Axis actuation under the nominal force

## 4.4 Finite Element Analysis of critical parts

After the assembly of the robot, it came to our attention that the application of a force at the circular track, could cause significant bending of the whole frame. This was deemed critical because this situation can happen when the surgeon manipulates the endoscope, producing forces on the circular track. This phenomenon is shown in figure 4.9. It was noticed that this deflection in the structure was caused by the torsion in the clip (shown in 4.9 and 4.10). The clip is the critical part in the robotic system as it bears the load of the whole frame from both sides. The clip is fixed on the top rail and fixation point act as pivot. Therefore, forces at the distal end of the frame magnify the torsion.

We prepare the clip for a finite element analysis as shown in figure 4.10. The clip is fixed with the screws on one end while the uniform load is been applied to the top surface. A

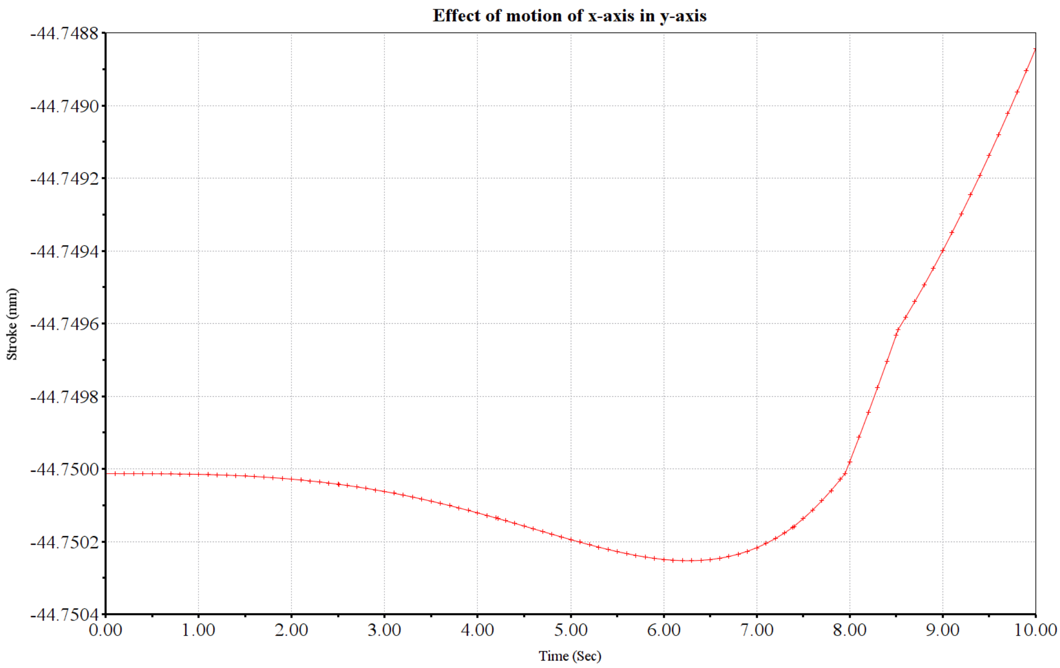


Figure 4.6: Effect of motion of X-Axis in Y-axis

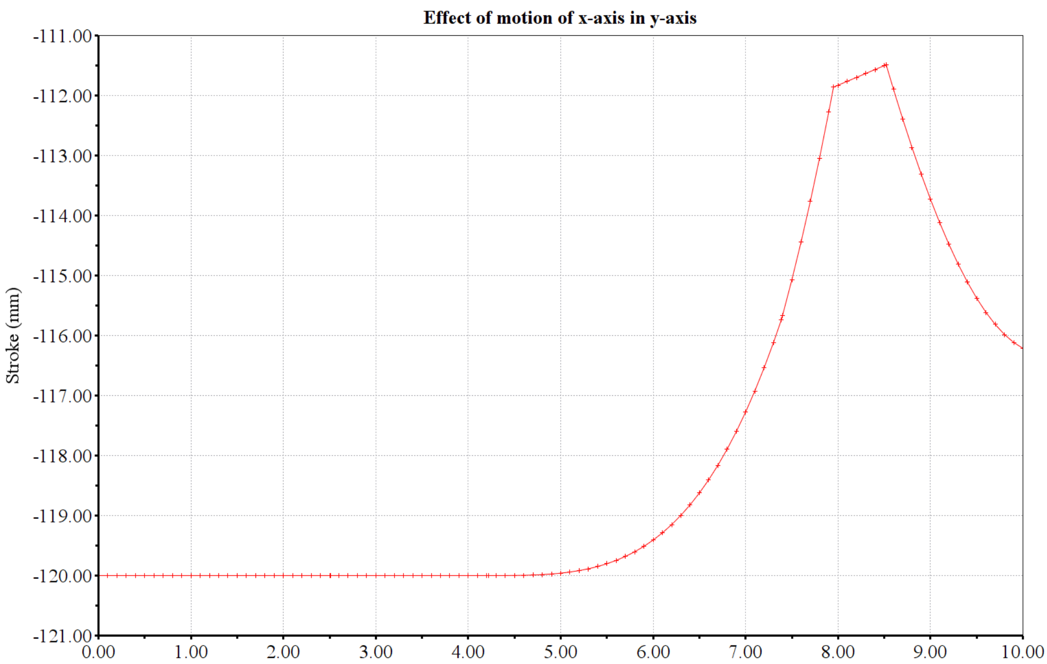


Figure 4.7: Effect of motion of X-axis in Y-axis

bending moment is then applied to right face of the clip to calculate the torsional effects on the clip.

As a result of this analysis, it was observed that the clip was still in the elastic region according to the Von mises failure criteria. But the displacement at the end of the clip was significant, as shown in figure **??**. It can be noticed that the stress concentration was around the slot machined into the clip. Therefore, we ran the same analysis after making the clip slotless. However, this didn't show any significant improvement in the displacement as shown in figure 4.12.

The next solution tested was to increase the thickness of the clip. This thickness could not go beyond a certain limit as there was space constraint in the design at that point. Nonetheless, the issue was tackled using two ribs along the longitude of the clip. A new analysis showed that this new design was successfully able to reduce the undesired displacements by more than 95%, as shown in figure 4.13.

[130, 131]

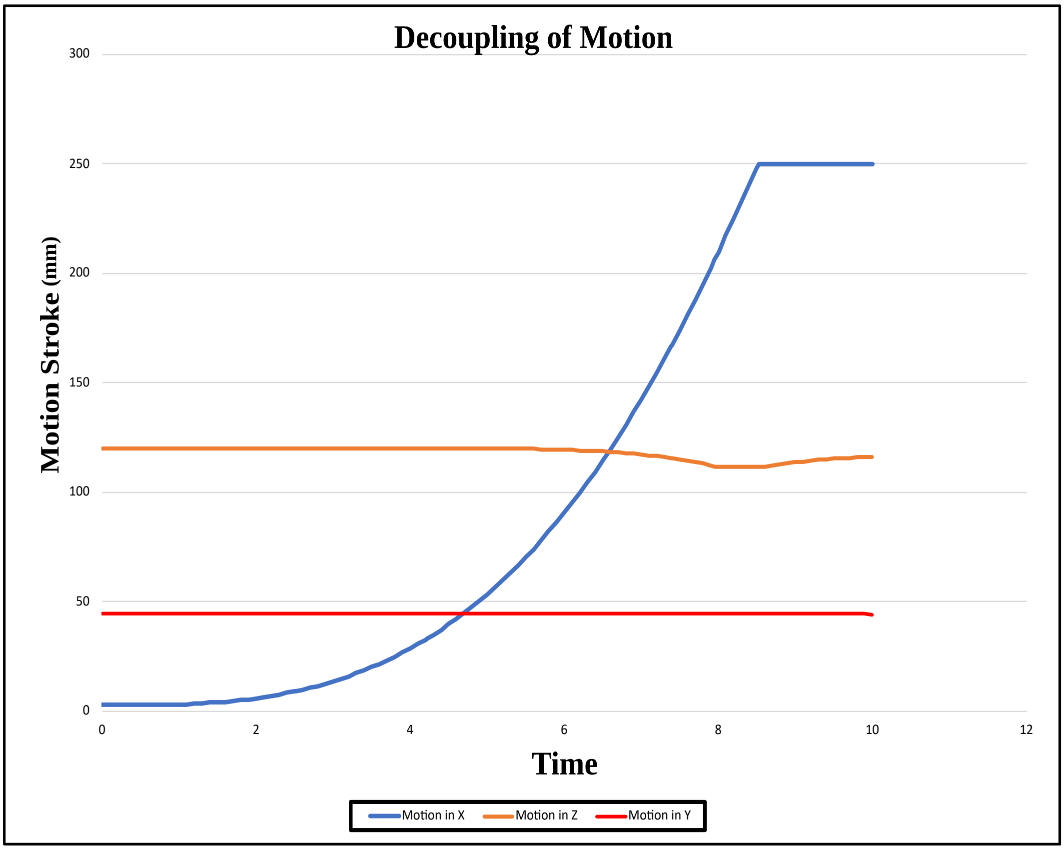


Figure 4.8: Decoupling in cartesian coordinate motion

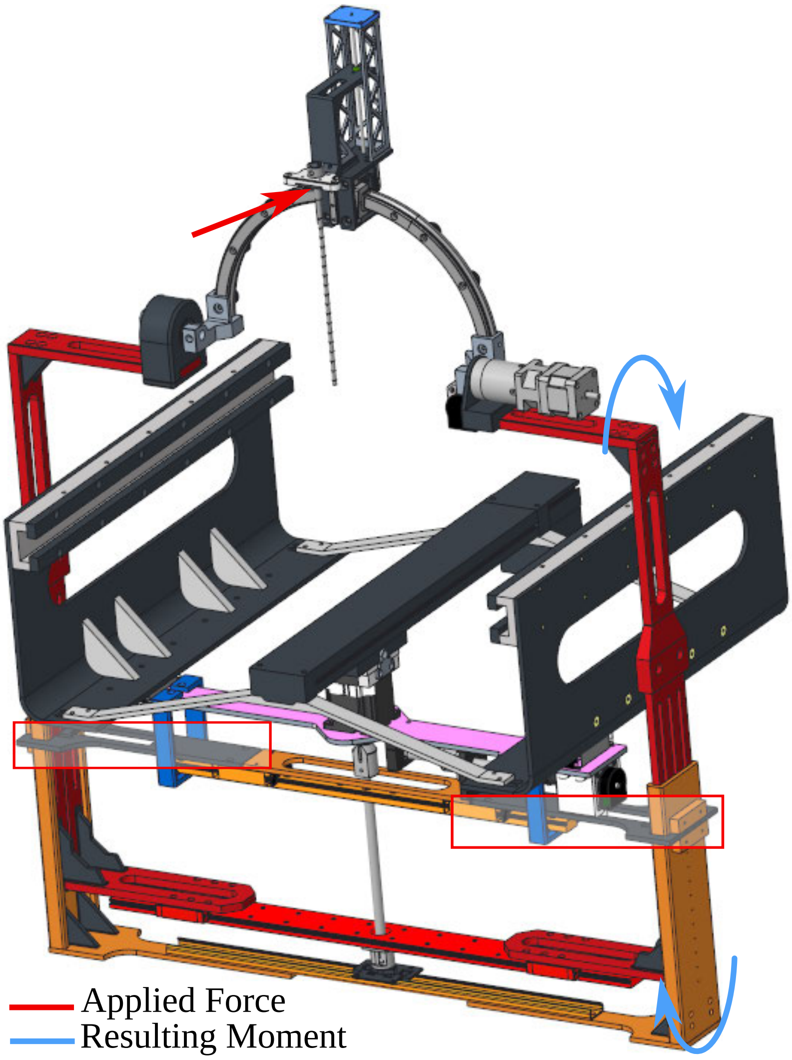


Figure 4.9: Bending moment created due to the applied force.

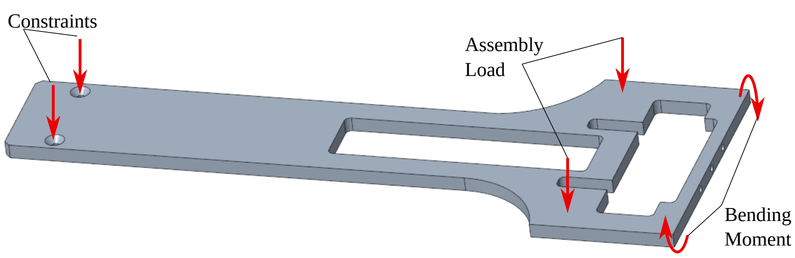


Figure 4.10: Loading conditions applied on the clip to perform the FE analysis

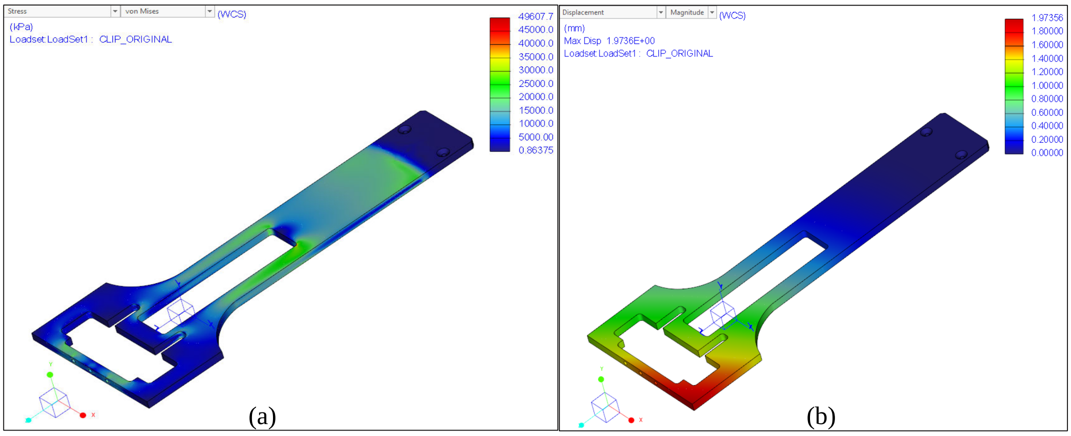


Figure 4.11: (a) Finite element analysis using von mises failure criteria. It is noticeable that the clip is still in the elastic region. (b) Displacement generated due the torsion on the clip.

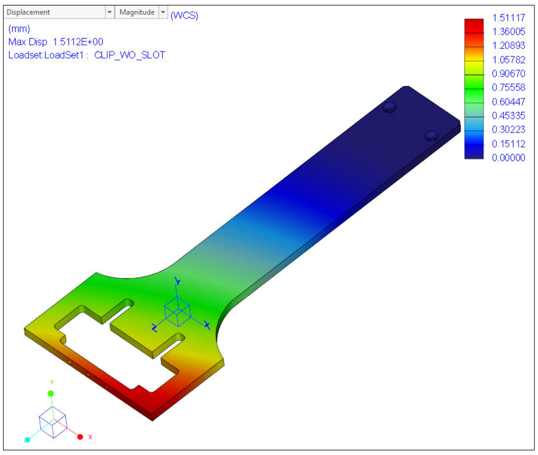


Figure 4.12: FE Analysis of the Clip after the removal of the slot

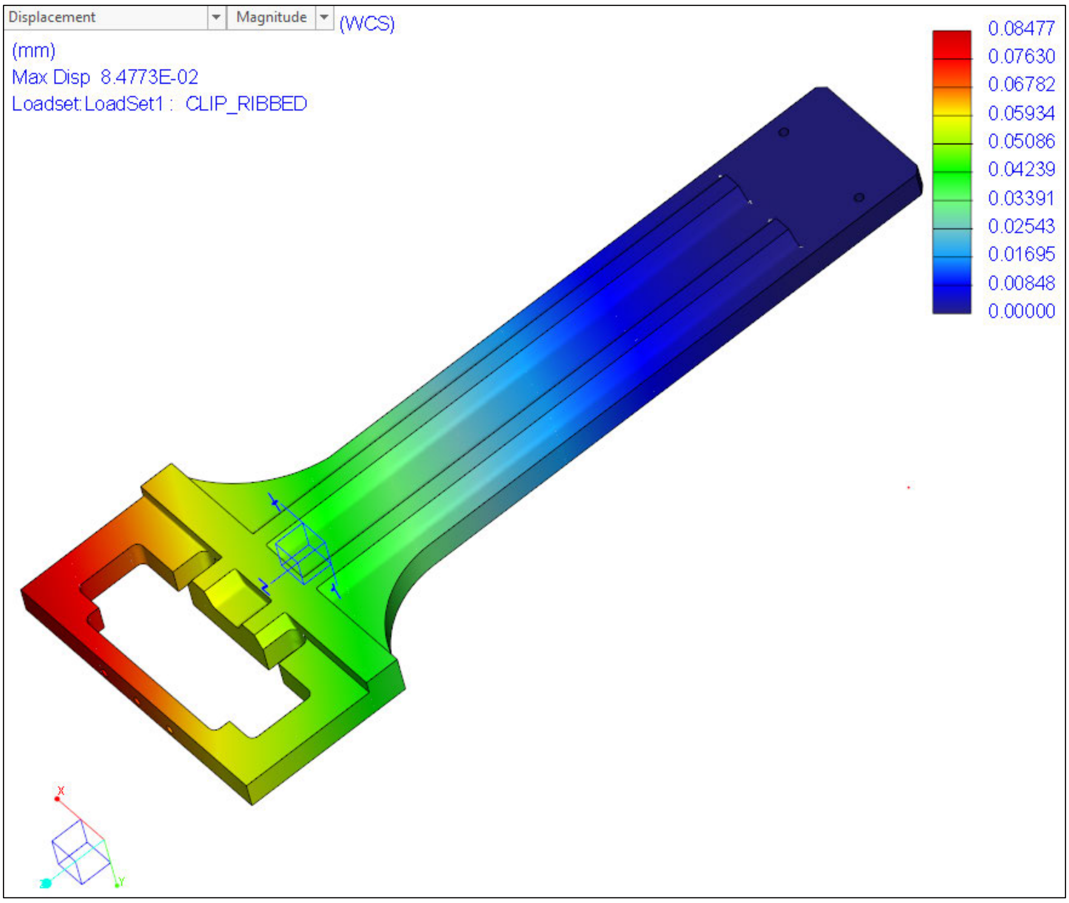


Figure 4.13: FE Analysis of the clip after the addition of the ribs

(a)

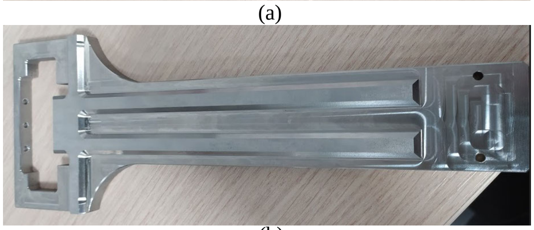

(b)

Figure 4.14: (a) Original Clip with a slot and lesser thickness. (b) Modified Clip with ribs and increased thickness

*Chapter 5*

# Experimental Verification

**Summary**
Experimental verification of any engineering system is crucial to validate the usability of the system. It became even more important in the design of medical systems. In this section, we proposed the experimental verification of the complete robotic system.

## 5.1 Design of Experiment

We determined unidirectional repeatabiltiy, bidirectional repeatability, and Accuracy of our robotic system using International Standard ISO 230-2 (International Organization for Standardization). It was used by other researchers to verify the medical system [132]. It was recommended to take eight target positions for linear axes less than 2000mm and rotational axes more than 90°. However, three target positions are recommended for rotational axis with less than 90°of the rotation. We selected eight target positions ($P_i$) for linear axes (X, Y, Z, and Translation/Insertion) and rotational axis (Yaw). However, three target positions were selected for the rotation axis (Pitch). The target positions ($P_i$) was repeated five times for complete cycle as shown in figure 5.1.

### 5.1.1 Experimental Setup

We used an optical tracking device (Polaris Vega VT) to obtain the spatial data. The optical tracker calculate the position of the marker relative to the previously designated global marker. It is important that the global and local marker should always be in the line of sight of the optical tracker. We chose the top part of the dummy surgical tool to place the marker so that it will be visible in all the motion ranges of all axes. The global marker was placed on the wooden base, simulated as the surgical bed. The experimental setup for the robotic system is shown in figure 5.2

### 5.1.2 Terminology

Since the ISO standard was followed through out the experimentation, it is important to have the understanding about the terminology used in the test results.

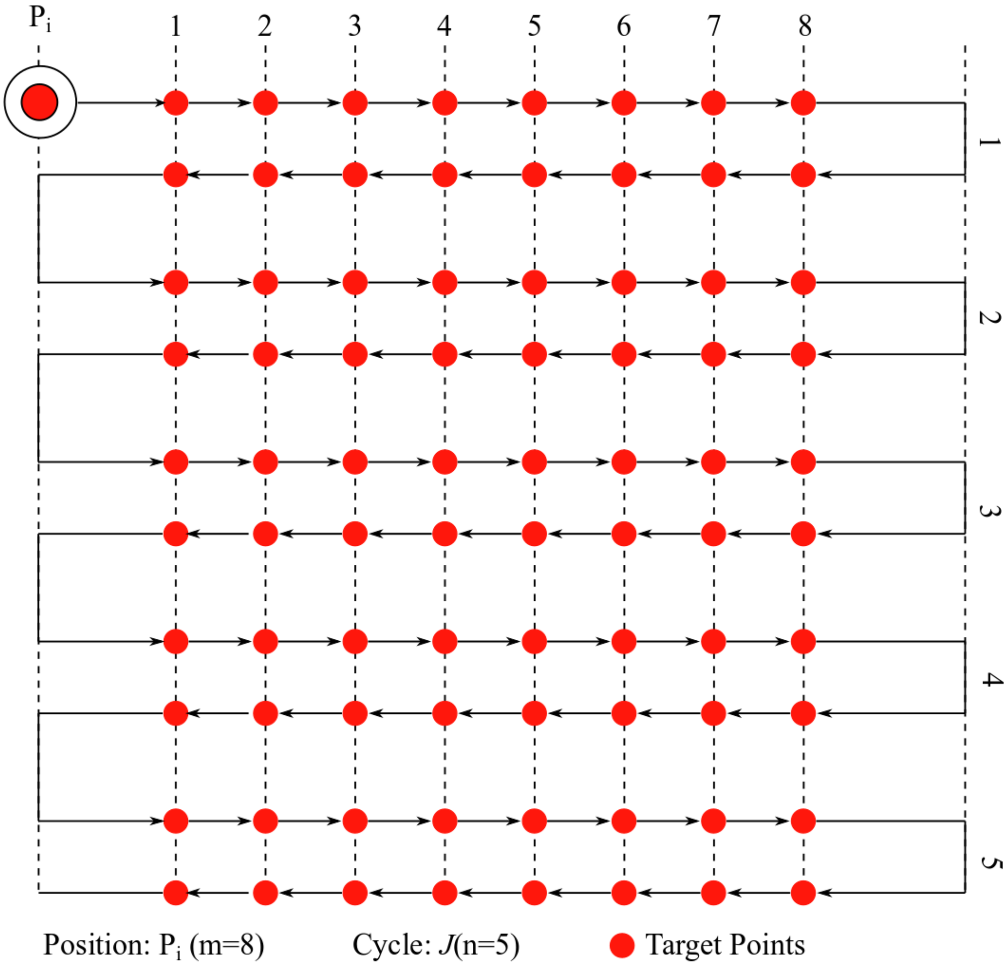


Figure 5.1: Test cycle to carry out the experiment. It indicated the target position and number of cycles.

**Target Position** ($P_i$)

Target position $P_i$ is the predetermined position assigned by the user to the actuator to achieve.

**Actual Position** ($P_{ij}$)

It is the position achieved by the axis and measured by an independent system.

**Positional Deviation** ($x_{ij}$)

It is the difference between the target position assigned by the user and the actual position.()

$$x_{ij} = P_{ij} - P_i \tag{5.1}$$

**Mean Unidirectional Positional Deviation** ($\bar{x}_i \uparrow$ **or** $\bar{x}_i \downarrow$)

It is the arithmetic mean of all the positional deviations in one direction.

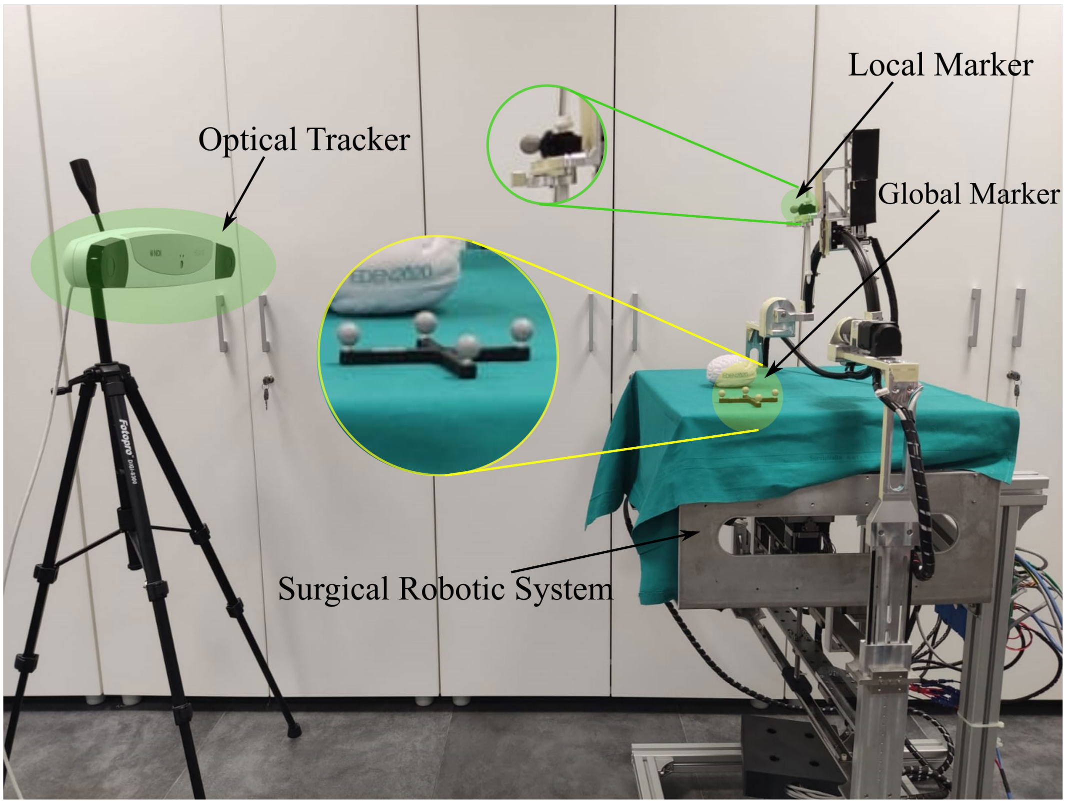

Figure 5.2: Experimental setup for the surgical robotic system

$$\bar{x_i} \uparrow = \frac{1}{n} \sum_{j=1}^{n} x_{ij} \uparrow \tag{5.2}$$

$$\bar{x_i} \downarrow = \frac{1}{n} \sum_{j=1}^{n} x_{ij} \downarrow \tag{5.3}$$

**Mean bi-directional Positional Deviation** ($\bar{x_i}$)
It is the arithmetic mean of the unidirectional means.

$$\bar{x_i} = \frac{\bar{x_i} \uparrow + \bar{x_i} \downarrow}{2} \tag{5.4}$$

**Reversal value at a position** ($B_i$)
Reversal value is difference of two unidirectional means at a specific target position $P_i$.

$$B_i = \bar{x_i} \uparrow - \bar{x_i} \downarrow \tag{5.5}$$

**Reversal value at an axis (B)**

$$B = max\left[\mid B_i \mid\right] \tag{5.6}$$

**Mean reversal value of an axis ($\bar{B}$)**

$$\bar{B} = \frac{1}{m}\sum_{i=1}^{m} B_i \tag{5.7}$$

**Estimator for the unidirectional axis repeatability of positioning at a position** $((s_i \uparrow )or(s_i) \downarrow)$

$$s_i \uparrow = \sqrt{\frac{1}{n-1}\sum_{j=1}^{n}(x_{ij} \uparrow - \bar{x_i} \uparrow)^2} \tag{5.8}$$

$$s_i \downarrow = \sqrt{\frac{1}{n-1}\sum_{j=1}^{n}(x_{ij} \downarrow - \bar{x_i} \downarrow)^2} \tag{5.9}$$

**Unidirectional repeatability of positioning at a position ($R_i \uparrow$ or $R_i \downarrow$)**

$$R_i \uparrow = 4s_i \uparrow \tag{5.10}$$

$$R_i \downarrow = 4s_i \downarrow \tag{5.11}$$

**Bi-directional repeatability of positioning at a position ($R_i$ )**

$$R_i = max[2s_i \uparrow + 2s_i \downarrow + \mid B_i \mid; R_i \uparrow; R_i \downarrow] \tag{5.12}$$

**Unidirectional repeatability of positioning of an axis ($R \uparrow$ or$R \downarrow$)**

$$R \uparrow = max.[R_i \uparrow] \tag{5.13}$$

$$R \downarrow = max.[R_i \downarrow] \tag{5.14}$$

**Bi-directional repeatability of positioning of an axis (R)**

$$R = max\,[R_i] \tag{5.15}$$

**Unidirectional systematic positional deviation of an axis ($E\uparrow$ or $E\downarrow$)**

$$E\uparrow = max.[\overline{x_i}\uparrow] - min[\overline{x_i}\uparrow] \tag{5.16}$$

$$E\downarrow = max.[\overline{x_i}\downarrow] - min[\overline{x_i}\downarrow] \tag{5.17}$$

**Bi-directional systematic positional deviation of an axis (E)**

$$E = max.[\overline{x_i}\uparrow; \overline{x_i}\downarrow] - min.[\overline{x_i}\uparrow; \overline{x_i}\downarrow] \tag{5.18}$$

**Unidirectional accuracy of positioning of an axis ($A\uparrow$ or $A\downarrow$)**

$$A\uparrow = max.[\overline{x_i}\uparrow + 2s_i\uparrow] - min[\overline{x_i}\uparrow - 2s_i\uparrow] \tag{5.19}$$

$$A\downarrow = max.[\overline{x_i}\downarrow + 2s_i\downarrow] - min[\overline{x_i}\downarrow - 2s_i\downarrow] \tag{5.20}$$

$$A = max.[\overline{x_i}\uparrow + 2s_i\uparrow; \overline{x_i}\downarrow - 2s_i\downarrow] - [\overline{x_i}\uparrow + 2s_i\uparrow; \overline{x_i}\downarrow - 2s_i\downarrow] \tag{5.21}$$

## 5.2 Material and Method

The experimental verification of the surgical robotic system involves the rigorous testing of each of its motion axes, according to the guidelines of ISO 230-2. In order to perform the experiments, a dedicated program was written to manually control each axis. This program enables us to give discrete position to move each axis forward and backward. Each linear axis was assigned eight different positions ($P_i$) and measured the actual position using the optical tracker. However, only three target positions were considered for the pitch axis as its rotation is lower than 90 °. The optical tracker records the value at the rate of ten frames per second. The schematic of data acquisition is shown in figure 5.3. The mechanism of detecting the markers are also shown in figure 5.4. The global and local markers are clearly visible through the infrared camera.

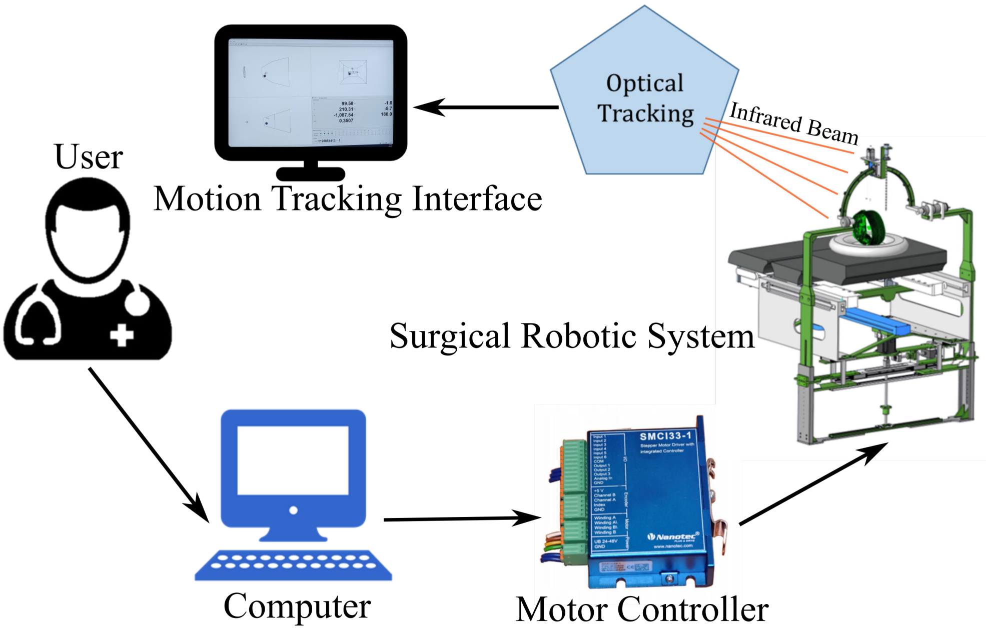


Figure 5.3: Schematic of data acquisition from the surgical robotic system

The data was obtained in comma separated values (CSV) format which was later processed to get values according to the equations from 5.1 to 5.20. Later on, the test results were computed for each axis as shown in tables from 5.1 to 5.6.

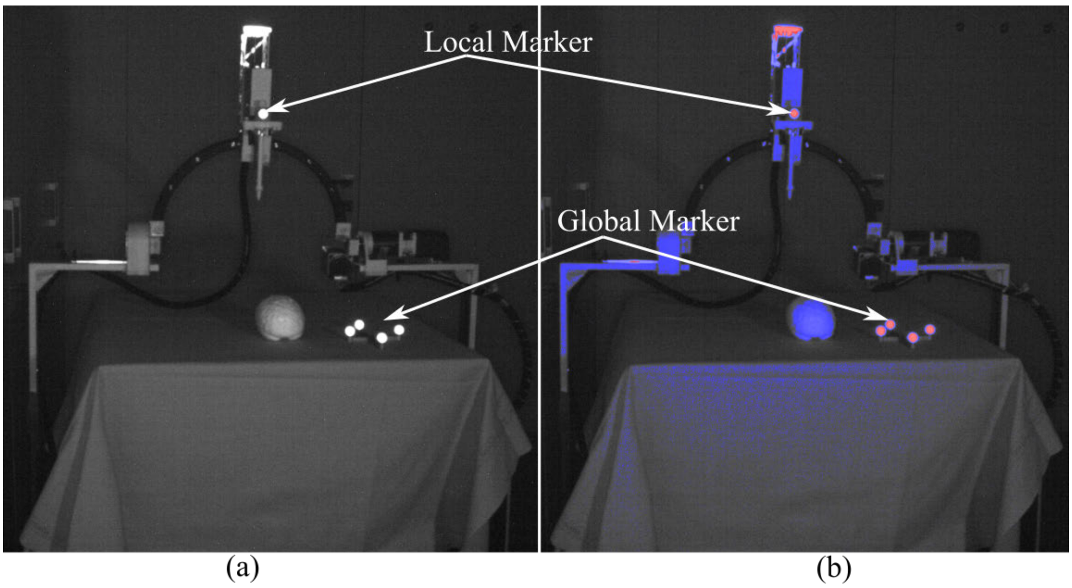


Figure 5.4: (a) Infrared view of the experimental setup. (b) The markers (red) are even more visible, separating the boundaries from other objects in the field of view.

Table 5.1: Test results for X-Axis

| | i | 1 | | 2 | | 3 | | 4 | | 5 | | 6 | | 7 | | 8 | |
|---|---|---|---|---|---|---|---|---|---|---|---|---|---|---|---|---|---|
| **Target Position** (mm) | $P_i$ | -209.108 | | -179.081 | | -149.122 | | -119.116 | | -89.122 | | -59.066 | | -28.992 | | 0.622 | |
| | | $\longrightarrow$ | $\longleftarrow$ | $\longrightarrow$ | $\longleftarrow$ | $\longrightarrow$ | $\longleftarrow$ | $\longrightarrow$ | $\longleftarrow$ | $\longrightarrow$ | $\longleftarrow$ | $\longrightarrow$ | $\longleftarrow$ | $\longrightarrow$ | $\longleftarrow$ | $\longrightarrow$ | $\longleftarrow$ |
| **Positional Deviation (µm)** $X_{ij}$ | $j = 1$ | -228.7 | 187.3 | 28.0 | 209.0 | -86.2 | 47.8 | 11.7 | 123.7 | 39.0 | 175.0 | -43.8 | 291.2 | -5.4 | -574.4 | 317.2 | 317.2 |
| | 2 | -148.7 | 122.3 | 10.0 | 182.0 | 10.8 | 94.8 | 3.7 | 85.7 | -24.0 | 231.0 | 58.2 | 269.2 | -24.4 | 220.6 | 297.2 | 315.2 |
| | 3 | -108.7 | 162.3 | 13.0 | 211.0 | -51.2 | 92.8 | -54.3 | 97.7 | -46.0 | 277.0 | 65.2 | 242.2 | -31.4 | 268.6 | 334.2 | 349.2 |
| | 4 | -38.7 | 129.3 | 11.0 | 226.0 | 21.8 | 100.8 | 6.7 | 115.7 | -37.0 | 171.0 | 31.2 | 224.2 | -3.4 | 177.6 | 323.2 | 338.2 |
| | 5 | -111.7 | 172.3 | 14.0 | 132.0 | -260.2 | 52.8 | -271.3 | 176.7 | -187.0 | 136.0 | -139.8 | -627.8 | -141.4 | 209.6 | 375.2 | 317.2 |
| **Mean positional Deviation (µm)** | | -127.3 | 154.7 | 15.2 | 192.0 | -73.0 | 77.8 | -60.7 | 119.9 | -51.0 | 198.0 | -5.8 | 79.8 | -41.2 | 60.4 | 329.4 | 327.4 |
| **Estimator of standard uncertainty** $S_i$ | | 69.2 | 28.0 | 7.3 | 37.1 | 113.7 | 25.3 | 120.8 | 35.1 | 83.0 | 55.7 | 86.5 | 396.4 | 57.3 | 356.4 | 28.9 | 15.4 |
| **2** $S_i$ | | 138.5 | 55.9 | 14.7 | 74.2 | 227.4 | 50.7 | 241.5 | 70.1 | 166.0 | 111.5 | 172.9 | 792.8 | 114.6 | 712.7 | 57.8 | 30.8 |
| $x_i - 2s_i$ **(µm)** | | -265.8 | 98.8 | 0.5 | 117.8 | -300.4 | 27.1 | -302.2 | 49.8 | -217.0 | 86.5 | -178.8 | -713.0 | -155.7 | -652.3 | 271.5 | 296.6 |
| $x_i + 2s_i$ **(µm)** | | 11.2 | 210.6 | 29.8 | 266.2 | 154.4 | 128.5 | 180.8 | 190.1 | 115.0 | 309.5 | 167.1 | 872.6 | 73.4 | 773.2 | 387.2 | 358.2 |
| **Unidirectional Repeatability** $R_i = 4s_i$ **(µm)** | | 277.0 | 111.8 | 29.3 | 148.4 | 454.8 | 101.4 | 483.0 | 140.3 | 331.9 | 223.0 | 345.9 | 1585.5 | 229.2 | 1425.5 | 115.7 | 61.6 |
| **Reversal Value** $B_i$ **(µm)** | | -27.4 | | -176.8 | | -150.8 | | -180.6 | | -249.0 | | -85.6 | | -101.6 | | 2.0 | |
| **Bidirectional Repeatability** $R_i$ **(µm)** | | 456.4 | | 329.7 | | 428.9 | | 492.3 | | 526.5 | | 1051.3 | | 928.9 | | 90.6 | |
| **Reversal Value** $B$ **(at** $i = 1$**)** | | 0.3 | | | | | | | | | | | | | | | |
| **Mean Reversal Value** | | 195.7 | 0.2 | | | | | | | | | | | | | | |
| **Range Mean Bidir. positional deviation** | | 456.7 | | | | | | | | | | | | | | | |
| **Systematic Positional Deviation** $E$ | | 456.7 | | | | | | | | | | | | | | | |
| **Repeatability of the positioning** $R$ | | 1051.3 | | | | | | | | | | | | | | | |
| **Accuracy** | | 1585.5 | | | | | | | | | | | | | | | |

Table 5.2: Test results for Y-axis

| | i | 1 | | 2 | | 3 | | 4 | | 5 | | 6 | | 7 | | 8 | |
|---|---|---|---|---|---|---|---|---|---|---|---|---|---|---|---|---|---|
| **Target Position** (mm) | $P_i$ | -150.507 | | -160.007 | | -169.307 | | -178.607 | | -187.907 | | -197.207 | | -206.507 | | -215.807 | |
| | | $\longrightarrow$ | $\longleftarrow$ | $\longrightarrow$ | $\longleftarrow$ | $\longrightarrow$ | $\longleftarrow$ | $\longrightarrow$ | $\longleftarrow$ | $\longrightarrow$ | $\longleftarrow$ | $\longrightarrow$ | $\longleftarrow$ | $\longrightarrow$ | $\longleftarrow$ | $\longrightarrow$ | $\longleftarrow$ |
| **Positional Deviation (µm)** $X_{ij}$ | $j = 1$ | -100.0 | -131.0 | 101.0 | -12.0 | 69.0 | -47.0 | 75.0 | -104.0 | 99.0 | -137.0 | 23.0 | -136.0 | 22.0 | -134.0 | 18.0 | -103.0 |
| | 2 | -102.0 | -92.0 | 59.0 | 34.0 | 44.0 | -32.0 | 100.0 | -81.0 | 57.0 | -115.0 | 19.0 | -128.0 | 96.0 | -78.0 | 19.0 | -46.0 |
| | 3 | -72.0 | -72.0 | 98.0 | 37.0 | 65.0 | -22.0 | 23.0 | -86.0 | 13.0 | -72.0 | 22.0 | -104.0 | 87.0 | -96.0 | 9.0 | -43.0 |
| | 4 | -64.0 | -81.0 | 101.0 | 37.0 | 63.0 | -34.0 | 52.0 | -65.0 | 38.0 | -92.0 | 30.0 | -112.0 | 83.0 | -81.0 | -6.0 | -45.0 |
| **Mean positional Deviation (µm)** | | -76.2 | -94.2 | 88.4 | 28.6 | 62.0 | -32.8 | 58.4 | -77.8 | 47.4 | -100.0 | 28.8 | -116.8 | 72.2 | -94.6 | 12.4 | -57.4 |
| **Estimator of standard uncertainity** $S_i$ | | 25.0 | 22.5 | 18.0 | 23.2 | 10.4 | 9.1 | 29.9 | 19.6 | 32.9 | 26.0 | 12.5 | 14.5 | 29.3 | 23.1 | 11.4 | 25.6 |
| **2** $s_i$ | | 50.0 | 45.0 | 36.1 | 46.4 | 20.8 | 18.3 | 59.7 | 39.3 | 65.8 | 51.9 | 25.0 | 29.1 | 58.5 | 46.1 | 22.7 | 51.2 |
| $x_i - 2s_i$ **(µm)** | | -126.2 | -139.2 | 52.3 | -17.8 | 41.2 | -51.1 | -1.3 | -117.1 | -18.4 | -151.9 | 3.8 | -145.9 | 13.7 | -140.7 | -10.3 | -108.6 |
| $x_i + 2s_i$ **(µm)** | | -202.4 | -233.4 | 140.7 | 10.8 | 103.2 | -83.9 | 57.1 | -194.9 | 29.0 | -251.9 | 32.6 | -262.7 | 85.9 | -235.3 | 2.1 | -166.0 |
| **Unidirectional Repeatability** $R_i = 4s_i$ **(µm)** | | 100.0 | 90.0 | 72.2 | 92.9 | 41.6 | 36.6 | 119.5 | 78.6 | 131.6 | 103.9 | 50.1 | 58.1 | 117.0 | 92.2 | 45.5 | 102.5 |
| **Reversal Value** $B_i$ **(µm)** | | 18.0 | | 59.8 | | 94.8 | | 136.2 | | 147.4 | | 145.6 | | 166.8 | | 69.8 | |
| **Bidirectional Repeatability** $R_i$ **(µm)** | | 5.0 | | -10.3 | | 2.5 | | 20.5 | | 13.9 | | -4.0 | | 12.4 | | -28.5 | |
| **Reversal Value** $B$ **(at** $i = 1$**)** | | 166.8 | | | | | | | | | | | | | | | |
| **Mean Reversal Value** | | 104.8 | | | | | | | | | | | | | | | |
| **Range Mean Bidir positional deviation** | | 79.25123 | | | | | | | | | | | | | | | |
| **Systematic Positional Deviation** $E$ | | 205.2 | | | | | | | | | | | | | | | |
| **Repeatability of the positioning** $R$ | | 20.5 | | | | | | | | | | | | | | | |
| **Accuracy** | | 292.6 | | | | | | | | | | | | | | | |

Table 5.3: Test results for Z-axis

| | **i** | **1** | | **2** | | **3** | | **4** | | **5** | | **6** | | **7** | | **8** | |
|---|---|---|---|---|---|---|---|---|---|---|---|---|---|---|---|---|---|
| **Target Position**(mm) | $P_i$ | 274.5229 | | 284.5817 | | 294.4917 | | 304.5014 | | 314.4313 | | 324.2898 | | 334.1214 | | 343.9525 | |
| | | $\longrightarrow$ | $\longleftarrow$ | $\longrightarrow$ | $\longleftarrow$ | $\longrightarrow$ | $\longleftarrow$ | $\longrightarrow$ | $\longleftarrow$ | $\longrightarrow$ | $\longleftarrow$ | $\longrightarrow$ | $\longleftarrow$ | $\longrightarrow$ | $\longleftarrow$ | $\longrightarrow$ | $\longleftarrow$ |
| **Positional Deviation (µm)** $X_{ij}$ | $j = 1$ | 4.10 | -674.90 | -64.70 | -716.70 | 10.30 | -622.70 | 0.60 | -614.40 | 12.70 | -541.30 | 3.20 | -395.80 | -3.40 | -229.40 | -13.50 | -46.50 |
| | 2 | -900.90 | -1536.90 | -973.70 | -1591.70 | -889.70 | -1509.70 | -943.40 | -519.40 | -897.30 | -1458.30 | -759.80 | -1261.80 | -636.40 | -1100.40 | -656.50 | -918.50 |
| | 3 | -1770.90 | -2617.90 | -1889.70 | -2671.70 | -1831.70 | -2585.70 | -1864.40 | -2584.40 | -1810.30 | -2519.30 | -1774.80 | -2345.80 | -1744.40 | -2158.40 | -1768.50 | -1986.50 |
| | 4 | -2829.90 | -3603.90 | -2898.70 | -3661.70 | -2811.70 | -3553.70 | -2832.40 | -3549.40 | -2823.30 | -3487.30 | -2788.80 | -3323.80 | -2729.40 | -3155.40 | -2736.50 | -2982.50 |
| | 5 | -3800.90 | -4316.90 | -3894.70 | -4385.70 | -3815.70 | -4276.70 | -3833.40 | -4278.40 | -3835.30 | -4198.30 | -3748.80 | -4029.80 | -3669.40 | -3838.40 | -3678.50 | -3652.50 |
| **Mean positional Deviation (µm)** | | -1859.70 | -2550.10 | -1944.30 | -2605.50 | -1867.70 | -2509.70 | -1894.60 | -2309.20 | -1870.70 | -2440.90 | -1813.80 | -2271.40 | -1756.60 | -2096.40 | -1770.70 | -1917.30 |
| **Estimator of standard uncertainty** $S_i$ | | 1509.18 | 1481.52 | 1515.99 | 1490.34 | 1514.14 | 1481.45 | 1511.28 | 1700.54 | 1521.96 | 1480.16 | 1509.04 | 1478.36 | 1494.48 | 1469.49 | 1491.78 | 1470.36 |
| **2** $s_i$ | | 3018.36 | 2963.04 | 3031.98 | 2980.67 | 3028.28 | 2962.90 | 3022.56 | 3401.07 | 3043.92 | 2960.33 | 3018.07 | 2956.72 | 2988.95 | 2938.98 | 2983.57 | 2940.72 |
| $x_i - 2s_i$ **(µm)** | | -4878.06 | -5513.14 | -4976.28 | -5586.17 | -4895.98 | -5472.60 | -4917.16 | -5710.27 | -4914.62 | -5401.23 | -4831.87 | -5228.12 | -4745.55 | -5035.38 | -4754.27 | -4858.02 |
| $x_i + 2s_i$ **(µm)** | | 1158.66 | 412.94 | 1087.68 | 375.17 | 1160.58 | 453.20 | 1127.96 | 1091.87 | 1173.22 | 519.43 | 1204.27 | 685.32 | 1232.35 | 842.58 | 1212.87 | 1023.42 |
| **Unidirectional Repeatabilty** $R_i = 4s_i$ **(µm)** | | 6036.71 | 5926.09 | 6063.95 | 5961.35 | 6056.57 | 5925.80 | 6045.13 | 6802.15 | 6087.84 | 5920.65 | 6036.15 | 5913.45 | 5977.91 | 5877.96 | 5967.13 | 5881.45 |
| **Reversal Value** $B_i$**(µm)** | | 690.40 | | 661.20 | | 642.00 | | 414.60 | | 570.20 | | 457.60 | | 339.80 | | 146.60 | |
| **Bidirectional Repeatability** $R_i$ **(µm)** | | 6671.80 | | 6673.85 | | 6633.18 | | 6838.24 | | 6574.45 | | 6432.40 | | 6267.73 | | 6070.89 | |
| **Reversal Value** $B$ **(at** $i = 1$**)** | | 0.69 | | | | | | | | | | | | | | | |
| **Mean Reversal Value** | | 490.30 | 0.49 | | | | | | | | | | | | | | |
| **Range Mean Bidir positional deviation** | | 848.90 | | | | | | | | | | | | | | | |
| **Systematic Positional Deviation** $E$ | | 848.90 | | | | | | | | | | | | | | | |
| **Repeatability of the positioning** $R$ | | 6838.24 | | | | | | | | | | | | | | | |
| **Accuracy** | | 6942.63 | | | | | | | | | | | | | | | |

Table 5.4: Test results for Yaw Axis

| | i | 1 | | 2 | | 3 | | 4 | | 5 | | 6 | | 7 | | 8 | |
|---|---|---|---|---|---|---|---|---|---|---|---|---|---|---|---|---|---|
| **Target Position (degree)** | $P_i$ | 164.545 | | 161.933 | | 160.644 | | 160.441 | | 161.079 | | 162.384 | | 164.187 | | 166.386 | |
| | | $\longrightarrow$ | $\longleftarrow$ | $\longrightarrow$ | $\longleftarrow$ | $\longrightarrow$ | $\longleftarrow$ | $\longrightarrow$ | $\longleftarrow$ | $\longrightarrow$ | $\longleftarrow$ | $\longrightarrow$ | $\longleftarrow$ | $\longrightarrow$ | $\longleftarrow$ | $\longrightarrow$ | $\longleftarrow$ |
| **Positional Deviation (degree)** $X_{ij}$ | $j=1$ | 0.162 | 0.089 | 0.081 | 0.059 | 0.028 | 0.027 | -0.015 | -0.001 | -0.047 | -0.027 | -0.067 | -0.049 | -0.077 | -0.075 | -0.087 | -0.082 |
| | 2 | 0.09 | 0.03 | 0.06 | 0.02 | 0.01 | 0.02 | -0.01 | 0.00 | -0.03 | -0.01 | -0.04 | -0.02 | -0.04 | -0.04 | -0.05 | -0.04 |
| | 3 | 0.04 | -0.03 | 0.01 | -0.01 | 0.00 | 0.00 | -0.01 | 0.01 | -0.01 | 0.01 | -0.01 | 0.01 | 0.00 | 0.00 | 0.00 | 0.00 |
| | 4 | -0.02 | -0.10 | -0.03 | -0.05 | -0.01 | -0.02 | -0.01 | 0.01 | 0.01 | 0.03 | 0.02 | 0.04 | 0.03 | 0.04 | 0.04 | 0.04 |
| | 5 | -0.09 | -0.16 | -0.06 | -0.08 | -0.03 | -0.03 | 0.00 | 0.02 | 0.03 | 0.05 | 0.05 | 0.07 | 0.07 | 0.08 | 0.08 | 0.09 |
| **Mean positional Deviation (degree)** | | 0.03 | -0.03 | 0.01 | -0.01 | 0.00 | 0.00 | -0.01 | 0.01 | -0.01 | 0.01 | -0.01 | 0.01 | 0.00 | 0.00 | 0.00 | 0.00 |
| **Estimator of standard uncertainity** $s_i$ | | 0.10 | 0.10 | 0.06 | 0.06 | 0.02 | 0.02 | 0.01 | 0.01 | 0.03 | 0.03 | 0.05 | 0.05 | 0.06 | 0.06 | 0.07 | 0.07 |
| **2** $s_i$ | | 0.20 | 0.20 | 0.12 | 0.11 | 0.04 | 0.04 | 0.01 | 0.01 | 0.06 | 0.06 | 0.09 | 0.09 | 0.12 | 0.12 | 0.13 | 0.14 |
| $x_i - 2s_i$ **(degree)** | | -0.17 | -0.23 | -0.11 | -0.12 | -0.05 | -0.04 | -0.02 | -0.01 | -0.07 | -0.05 | -0.10 | -0.08 | -0.12 | -0.12 | -0.14 | -0.14 |
| $x_i + 2s_i$ **(degree)** | | 0.23 | 0.16 | 0.13 | 0.10 | 0.04 | 0.04 | 0.01 | 0.02 | 0.05 | 0.07 | 0.09 | 0.10 | 0.12 | 0.13 | 0.13 | 0.14 |
| **Unidirectional Repeatabilty** $R_i = 4s_i$ **(degree)** | | 0.40 | 0.40 | 0.24 | 0.22 | 0.09 | 0.09 | 0.03 | 0.03 | 0.13 | 0.11 | 0.19 | 0.18 | 0.24 | 0.25 | 0.27 | 0.28 |
| **Reversal Value** $B_i$**(degree)** | | 0.07 | | 0.02 | | 0.00 | | -0.02 | | -0.02 | | -0.02 | | -0.01 | | 0.00 | |
| **Bidirectional Repeatability** $R_i$ **(degree)** | | 0.47 | | 0.26 | | 0.09 | | 0.04 | | 0.14 | | 0.20 | | 0.25 | | 0.28 | |
| **Reversal Value** $B$ **(at** $i=1$**)** | | 0.26 | | | | | | | | | | | | | | | |
| **Mean Reversal Value** | | 0.00 | 0.00 | | | | | | | | | | | | | | |
| **Range Mean Bidirectional positional deviation** | | 0.069 | | | | | | | | | | | | | | | |
| **Systematic Positional Deviation** $E$ | | 0.069 | | | | | | | | | | | | | | | |
| **Repeatability of the positioning** $R$ | | 0.47 | | | | | | | | | | | | | | | |
| **Accuracy** | | 0.47 | | | | | | | | | | | | | | | |

Table 5.5: Test results for translation axis

| | i | 1 | | 2 | | 3 | | 4 | | 5 | | 6 | | 7 | | 8 | |
|---|---|---|---|---|---|---|---|---|---|---|---|---|---|---|---|---|---|
| **Target Position** | $P_i$ | **164.545** | | **161.933** | | **160.644** | | **160.441** | | **161.079** | | **162.384** | | **164.187** | | **166.386** | |
| | | $\longrightarrow$ | $\longleftarrow$ | $\longrightarrow$ | $\longleftarrow$ | $\longrightarrow$ | $\longleftarrow$ | $\longrightarrow$ | $\longleftarrow$ | $\longrightarrow$ | $\longleftarrow$ | $\longrightarrow$ | $\longleftarrow$ | $\longrightarrow$ | $\longleftarrow$ | $\longrightarrow$ | $\longleftarrow$ |
| **Positional Deviation (µm)** $X_{ij}$ | $j = 1$ | 3.300 | -74.700 | -2.727 | -42.727 | 1.000 | -38.000 | 1.600 | -415.400 | -3.900 | 1.100 | -7.900 | -73.400 | -1.400 | 20.000 | 5.000 | 20.000 |
| | 2 | -34.700 | -65.700 | 40.273 | -40.727 | -12.000 | -52.000 | -318.400 | -469.400 | -99.900 | -19.900 | 70.100 | -207.400 | -148.400 | -54.000 | 142.000 | -54.000 |
| | 3 | -35.700 | -69.700 | 18.273 | -27.727 | -64.000 | -66.000 | -495.400 | -468.400 | -81.900 | -25.900 | 30.100 | -198.400 | 162.600 | -12.000 | 3.000 | -12.000 |
| | 4 | -34.700 | -91.700 | 18.273 | -27.727 | -58.000 | -71.000 | -461.400 | -440.400 | -0.900 | -44.900 | -23.900 | -209.400 | -97.400 | 0.000 | 8.000 | 0.000 |
| | 5 | -33.700 | -100.700 | -27.727 | -16.727 | -59.000 | -73.000 | -496.400 | -492.400 | -60.900 | -69.900 | -36.900 | -180.400 | -23.400 | -55.000 | -21.000 | -55.000 |
| **Mean Unidirectional positional Deviation (µm)** | | -27.100 | -80.500 | 9.273 | -31.127 | -38.400 | -60.000 | | | -49.500 | -31.900 | 6.300 | -173.800 | -21.600 | -20.200 | 27.400 | -20.200 |
| **Estimator of standard uncertainity** $s_i$ | | 17.009 | 15.023 | 25.671 | 10.691 | 30.468 | 14.782 | | | 45.170 | 26.842 | 43.637 | 57.283 | 118.496 | 33.335 | 65.095 | 33.335 |
| **2** $s_i$ | | 34.018 | 30.047 | 51.342 | 21.382 | 60.936 | 29.563 | | | 90.339 | 53.684 | 87.274 | 114.565 | 236.991 | 66.669 | 130.189 | 66.669 |
| $x_i - 2s_i$ **(µm)** | | -61.118 | -110.547 | -42.069 | -52.510 | -99.336 | -89.563 | | | -139.839 | -85.584 | -80.974 | -288.365 | -258.591 | -86.869 | -102.789 | -86.869 |
| $x_i + 2s_i$ **(µm)** | | 6.918 | -50.453 | 60.615 | -9.745 | 22.536 | -30.437 | | | 40.839 | 21.784 | 93.574 | -59.235 | 215.391 | 46.469 | 157.589 | 46.469 |
| **Unidirectional Repeatabilty** $R_i = 4s_i$ **(degree)** | | 68.035 | 60.093 | 102.684 | 42.764 | 121.872 | 59.127 | | | 180.679 | 107.369 | 174.549 | 229.131 | 473.982 | 133.339 | 260.378 | 133.339 |
| **Reversal Value** $B_i$**(µm)** | | 53.400 | | 40.400 | | 21.600 | | | | -17.600 | | 180.100 | | -1.400 | | 47.600 | |
| **Bidirectional Repeatability** $R_i$ **(µm)** | | 326.064 | | 313.524 | | 241.300 | | | | | | 287.440 | | 405.260 | | 198.858 | |
| **Reversal Value B (at** $i = 1$**)** | | 0.262 | | | | | | | | | | | | | | | |
| **Mean Reversal Value** | | 46.300 | | | | | | | | | | | | | | | |
| **Range Mean Bidirec positional deviation** | | 201.200 | | | | | | | | | | | | | | | |
| **Systematic Positional Deviation** $E$ | | 201.200 | | | | | | | | | | | | | | | |
| **Repeatability of the positioning** $R$ | | 405.260 | | | | | | | | | | | | | | | |
| **Accuracy** | | 503.756 | | | | | | | | | | | | | | | |

Table 5.6: Test results for pitch axis

| | **i** | **1** | | **2** | | **3** | |
|---|---|---|---|---|---|---|---|
| **Target Position(degree)** | $P_i$ | **-41.154** | | **-29.588** | | **-13.905** | |
| | | $\longrightarrow$ | $\longleftarrow$ | $\longrightarrow$ | $\longleftarrow$ | $\longrightarrow$ | $\longleftarrow$ |
| **Positional Deviation (degree)** $X_{ij}$ | $j = 1$ | 0.000 | -0.058 | 0.000 | 0.895 | 0.000 | -0.015 |
| | 2 | 0.013 | 0.023 | 0.060 | 0.860 | -0.037 | 0.047 |
| | 3 | -0.043 | -0.019 | -0.009 | 0.887 | -0.061 | -0.043 |
| | 4 | -0.020 | -0.032 | 0.112 | 0.889 | -0.059 | 0.041 |
| | 5 | 0.008 | -0.037 | 0.143 | 0.867 | 0.047 | 0.062 |
| **Bitmap Mean positionalDeviation (degree)** | | -0.008 | -0.025 | 0.061 | 0.880 | -0.022 | 0.018 |
| **Estimator of standard uncertainity** $s_i$ | | 0.023 | 0.030 | 0.067 | 0.015 | 0.046 | 0.045 |
| **2** $s_i$ | | 0.047 | 0.060 | 0.134 | 0.030 | 0.091 | 0.090 |
| $x_i - 2s_i$ **(degree)** | | -0.055 | -0.085 | -0.072 | 0.849 | -0.113 | -0.072 |
| $x_i + 2s_i$ **(degree)** | | 0.038 | 0.035 | 0.195 | 0.910 | 0.069 | 0.109 |
| **Unidirectional Repeatabilty** $R_i = 4s_i$ **(degree)** | | 0.093 | 0.120 | 0.267 | 0.060 | 0.182 | 0.181 |
| **Reversal Value** $B_i$**(degree)** | | 0.016 | | -0.818 | | -0.040 | |
| **Bidirectional Repeatability** $R_i$ **(degree)** | | 0.123 | | -0.654 | | 0.141 | |
| **Reversal Value B (at** $i = 1$) | | 0.262 | | | | | |
| **Mean Reversal Value** | | -0.281 | 0.000 | | | | |
| **Range Mean Bidirectional positional deviation** | | 0.904 | | | | | |
| **Systematic Positional Deviation** $E$ | | 0.904 | | | | | |
| **Repeatability of the positioning** $R$ | | 0.141 | | | | | |
| **Accuracy** | | 1.023 | | | | | |

## 5.3 Results

The surgical robotic system can be fairly divided into two major parts, namely Cartesian Motion System (CMS) and Spherical Motion System (SMS). CMS can also be described as the pre-surgical setup. The purpose of CMS is to place the RCM on the skull of the patient. However, SMS is use to orient and insert the surgical sleeve inside the cranium or other points of interest such as nasal and mucal cavity. SMS can also be used to perform fine intra-operative adjustments.

### 5.3.1 Cartesian Motion Axes

Cartesian Motion System comprise of three motion axes X, Y, and Z axes. All of these axes are perpendicular and decoupled from each other.
The test results of X-axis are given in detail in table 5.1. X-axis demonstrates the bi-directional repeatability of 1mm and absolute accuracy of 1.5 mm. These values seems higher but if we look at the positional deviation in figure 5.5, X-axis shows high repeatability on both approach and recede. The normal probability density function of X-axis in figure 5.6 shows high repeatability.

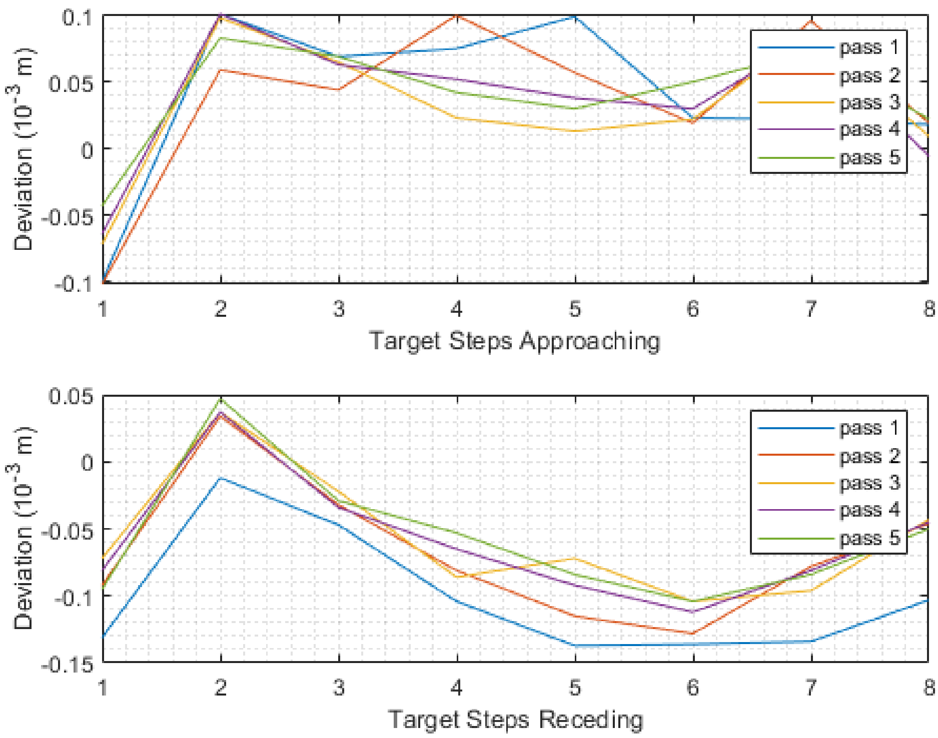


Figure 5.5: Positional deviation of X-axis in approaching and receding

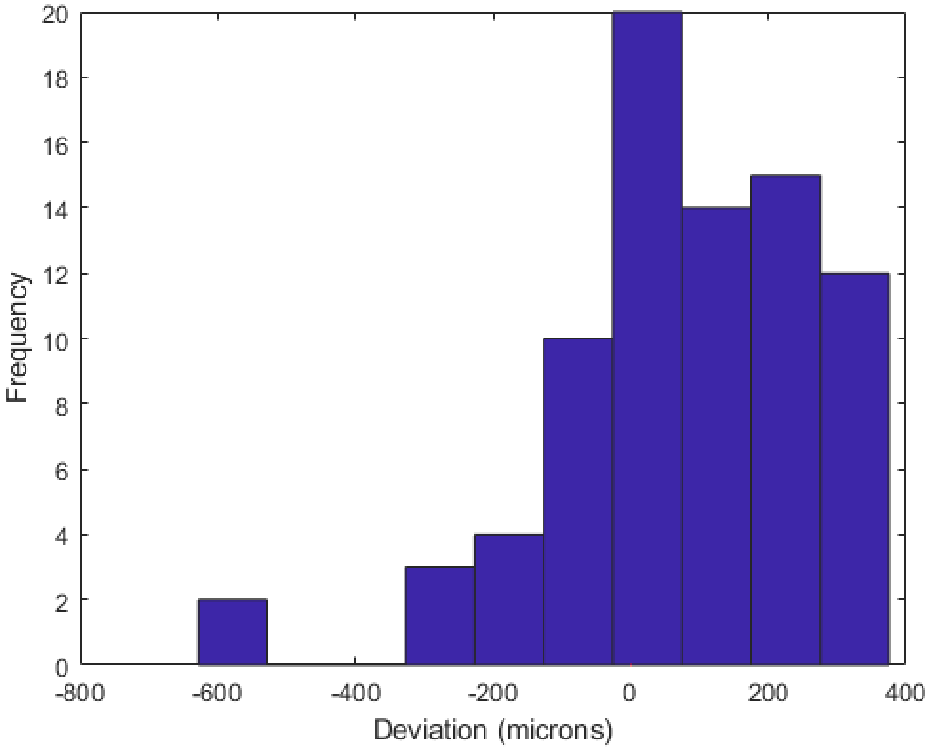


Figure 5.6: Histogram of errors in X-axis

The test results of Y-axis are given in detail in table 5.2. Y-axis demonstrates the bi-directional repeatability of 20 $\mu$m and absolute accuracy of 292 $\mu$m. The reason behind the higher accuracy and repeatability seems to be the intrinsic property of the mechanism. The mechanism for Y-axis is a custom made linear actuator, which gives DOF while designing the control system.The positional deviation of Y-axis is shown in figure 5.7, Y-axis shows high repeatability on both approach and recede. The normal probability density function of Y-axis in figure 5.8 shows high repeatability but not accuracy.

The test results of Z-axis are given in detail in table 5.3. Z-axis demonstrates the bi-directional repeatability of 6.8 mm and absolute accuracy of 6.9 mm. The position deviation plot in figure 5.9 shows that the Z-axis continuously deteriorating in the proceeding passes. Although it follows the same trajectory on the approaching and receding passed but with some negative offset in the target position. Also the plot of normal probability density function in figure 5.10 doesn't show neither accuracy nor repeatability. The Z-axis mechanism is performing under the effect of gravity and all the load of the robotic system is on it. These parameters can be improved with a statically balancing the mass so that center of mass coincide with axis of rotation of pitch and yaw axis.

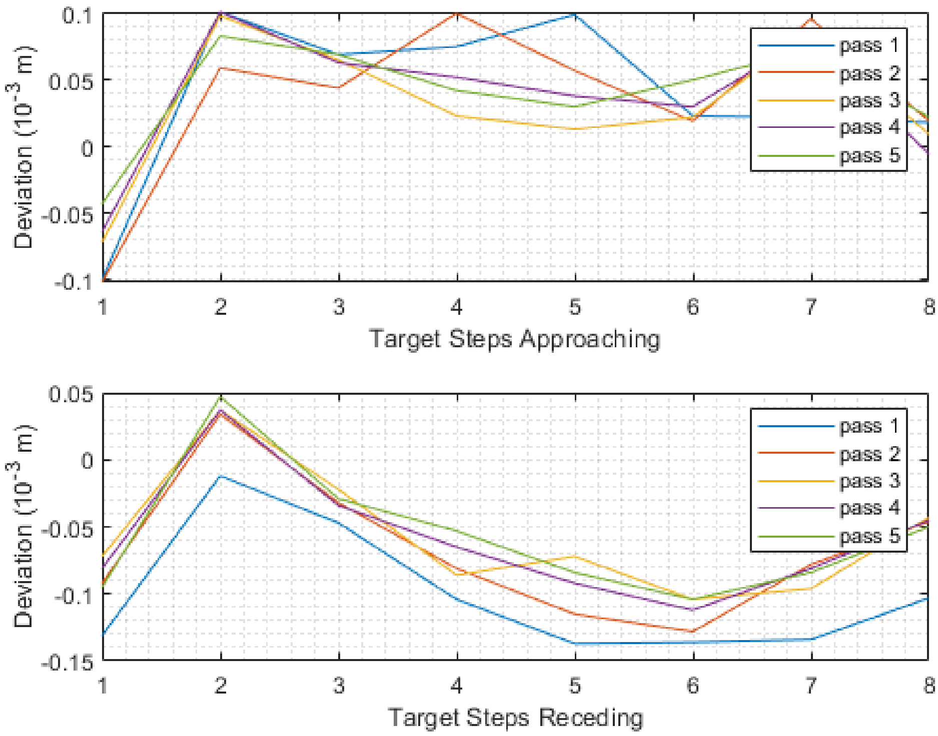


Figure 5.7: Positional deviation of Y-Axis in approaching and receding

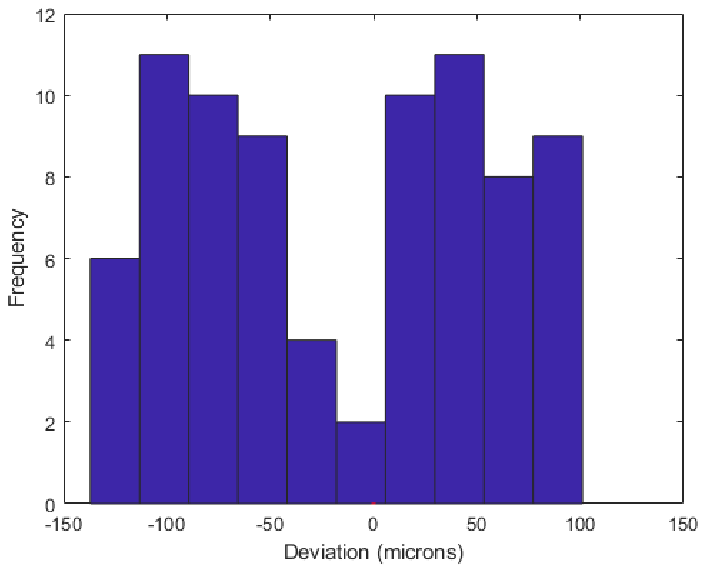


Figure 5.8: Histogram of errors in Y-axis

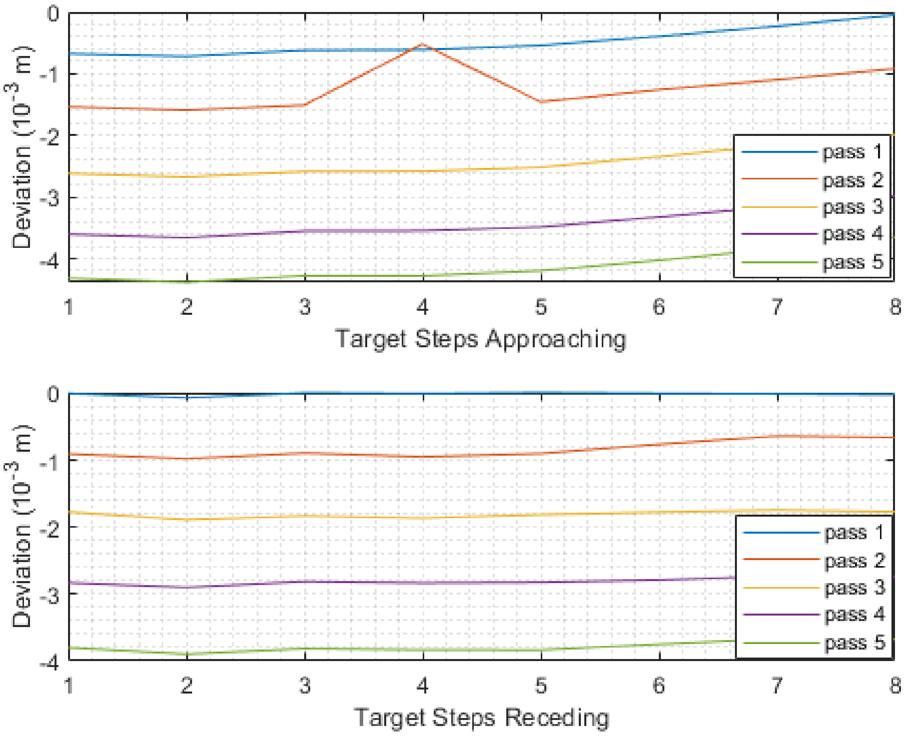


Figure 5.9: Positional deviation of Z-Axis in approaching and receding

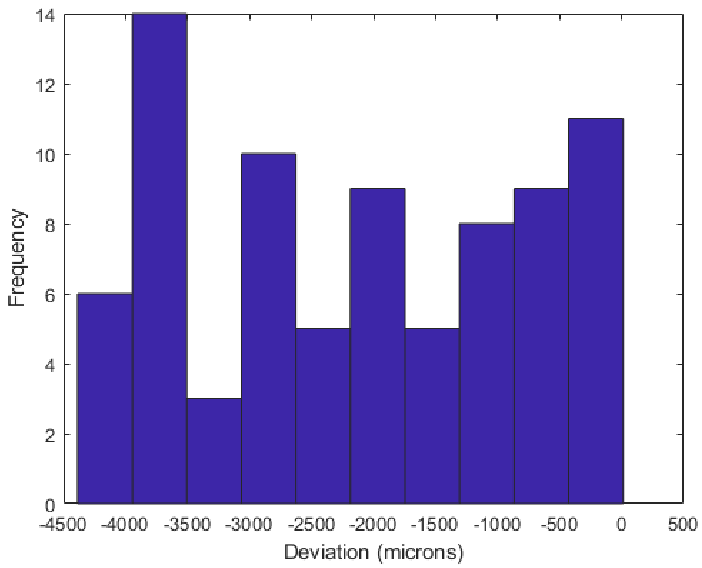


Figure 5.10: Histogram of errors in Z-axis

### 5.3.2 Spherical Motion System

The Spherical Motion System (SMS) comprise of two rotational and one translational axes. The two rotational axes, yaw and pitch, are used to orient the surgical sleeve, while the translation axis insert the endoscope.

The test result of yaw axis are given in table 5.4. The yaw axes depicts the bi-directional repeatability and accuracy of 0.47°. The position deviation plot shown in figure 5.11 shows high repeatability and high accuracy. The normal probability density function shown in figure 5.12 shows that the deviation values are closer to zero.

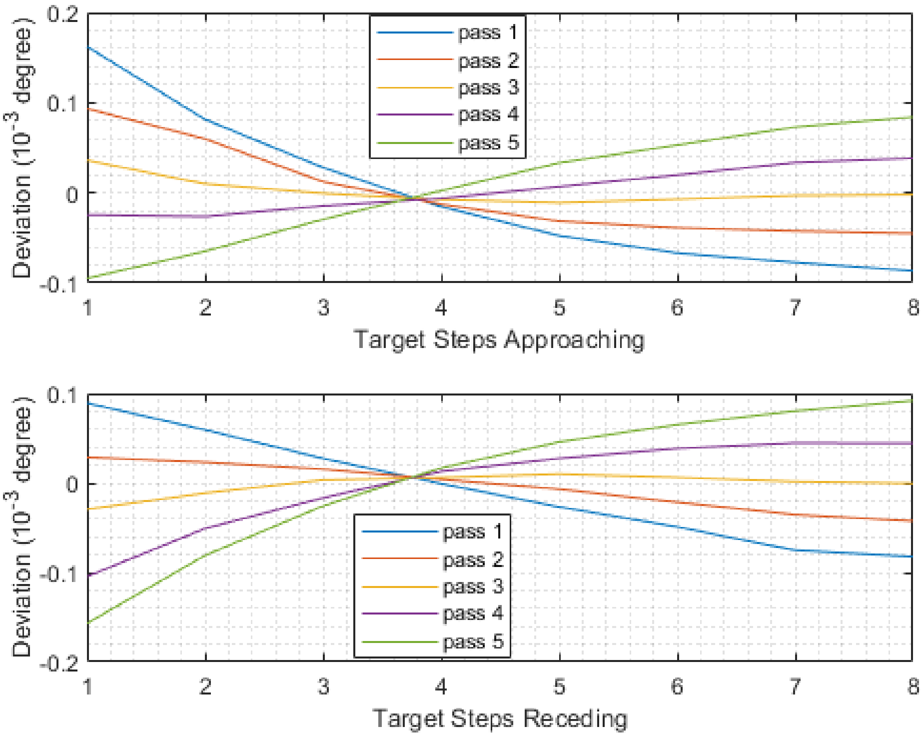


Figure 5.11: Positional deviation of yaw axis in approaching and receding

The test result of pitch axis is shown in detail in table 5.6. The ISO standard 230-2 allows us to take three target position for the axes lesser than 90°. The pitch axis has the bi-directional repeatability of 0.141° and absolute accuracy 1.023°. The position deviation plot in figure 5.13 shows that the approaching cycles are more accurate than receding cycles. It is evident from the plot that the motor is not drawing enough current and losing the repeatability under the effect of gravity. But the normal probability density function in figure 5.14 indicates that deviation is distributed but its is not closer to the mean value.

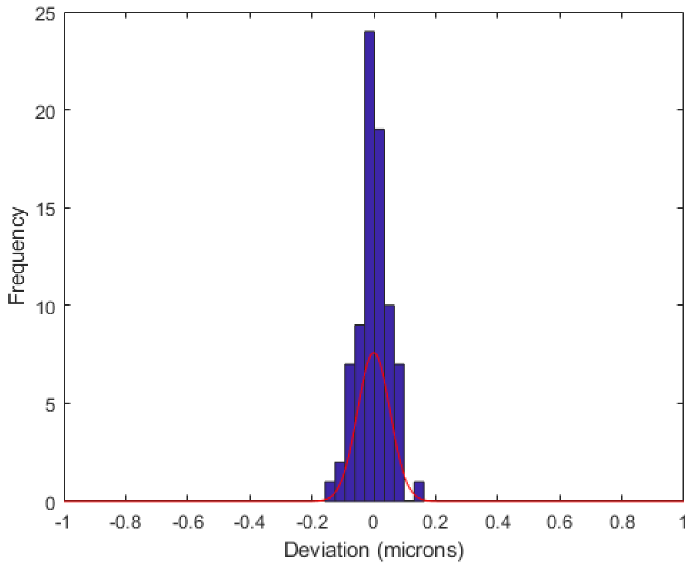


Figure 5.12: Normal probability density function of deviation of yaw axis

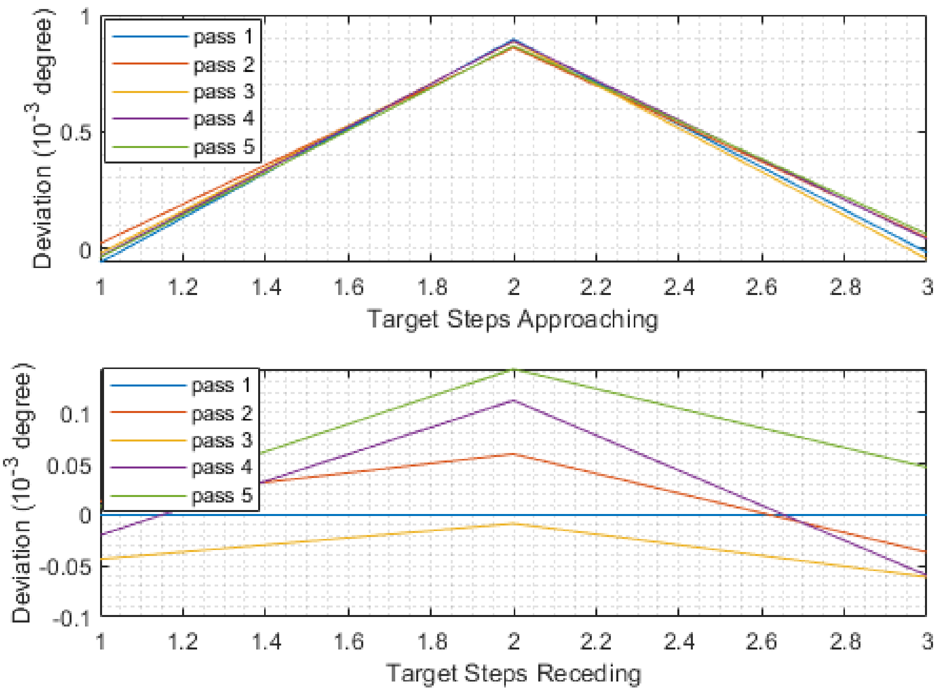


Figure 5.13: Positional deviation of pitch axis in approaching and receding

The test result of translation axis is shown in detail in table 5.5. The translation axis has the bi-directional repeatability of 405$\mu$m and absolute accuracy 503$\mu$m. The position deviation

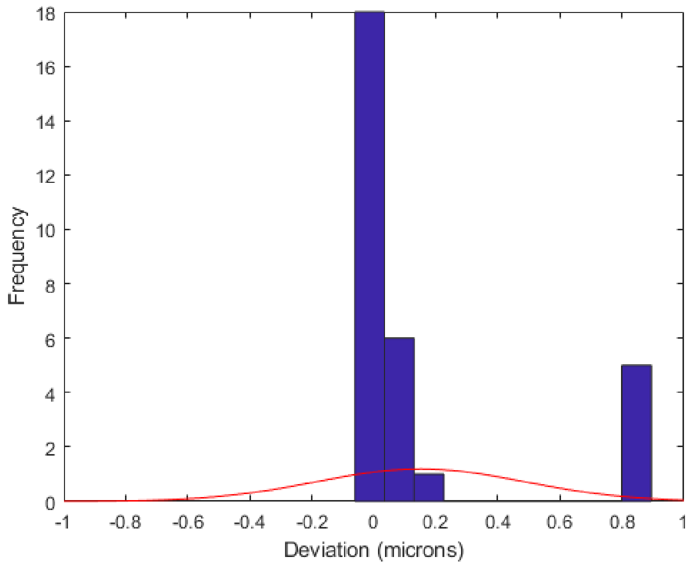


Figure 5.14: Normal probability density function of deviation of pitch axis

plot in figure 5.15 shows that the approaching cycles and receding cycles are following the same trajectory. Also the normal probability density function in figure 5.16 indicates that the values are normally distributed and are closer to zero.

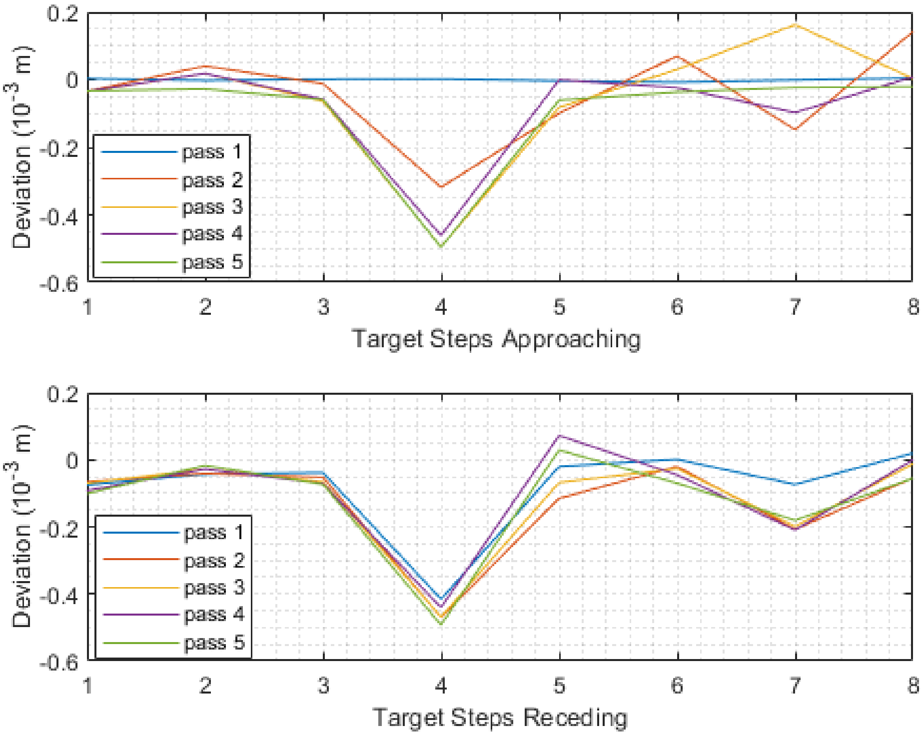


Figure 5.15: Positional deviation of translation axis in approaching and receding

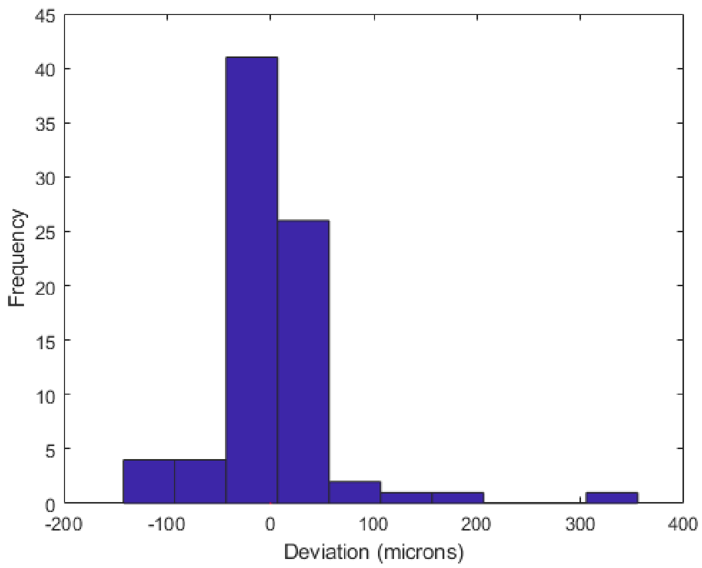


Figure 5.16: Normal probability density function of deviation of translation axis

*Chapter 6*

# Conclusion and Future work

## 6.1 Summary

Surgical robotics has seen its dawn almost 30 years ago. It developed at a slightly lower pace during the better part of the first decade. It seems odd that although the first robotic surgery was a neurological, but the other procedures such as laparoscopy and orthopaedics were relatively quick in embracing the surgical robots. The main reason could be the complex anatomy of the brain as well as the absence of sophisticated illumination and neuronavigation techniques. However the later half of 2000s seen a tremendous growth, when multiple commercial neurosurgical robotic systems were introduced to the market, such as Medtech ROSA, Neuromate, and MARS.There are several features which were lacked by the current robotic systems. One of which is their application to pediatric neurosurgery. These surgical robotic systems do not cater the need of pediatric neurosurgery and neuroendoscopy.

In this study, we identified this gap and tried to address this grave issue to the best of our efforts and knowledge. Once this problem was presented by our medical collaborators we went through the available (both commercial and research) robotic systems. We reviewed the systems that can be utilized in the case of pediatric neuroendoscopy. During the review, multiple features of the robotic systems were identified and analyzed. Consequently, these incapabilities forced the surgeons to perform these delicate surgeries manually. This detailed review is presented in chapter 2.

The challenges involved in manually performing those surgeries are, the requirement of multiple hands in a confined space, very delicate procedure, and inadequate mechanical support. These challenges can only be tackled by a dedicated robotic system. The journey of designing such robotic system started with the identification of requirements and specifications, discussed in detail in section 3.1.1. The detailed requirements and specifications indicate that atleast six DOF are required to carry out these procedures. The DOFs were further divided into two major sub-components i.e cartesian motion mechanism and circular motion mechanism. Several candidate mechanisms were studied for both but none of them can be utilized on "as is basis". So, we designed novel mechanisms for both cartesian coordinate and circular motion, discussed in detail in section 3.2.2.1 and section 3.2.2.2 respectively. The details of the mechanism review can be found in aforementioned sections. Before start-

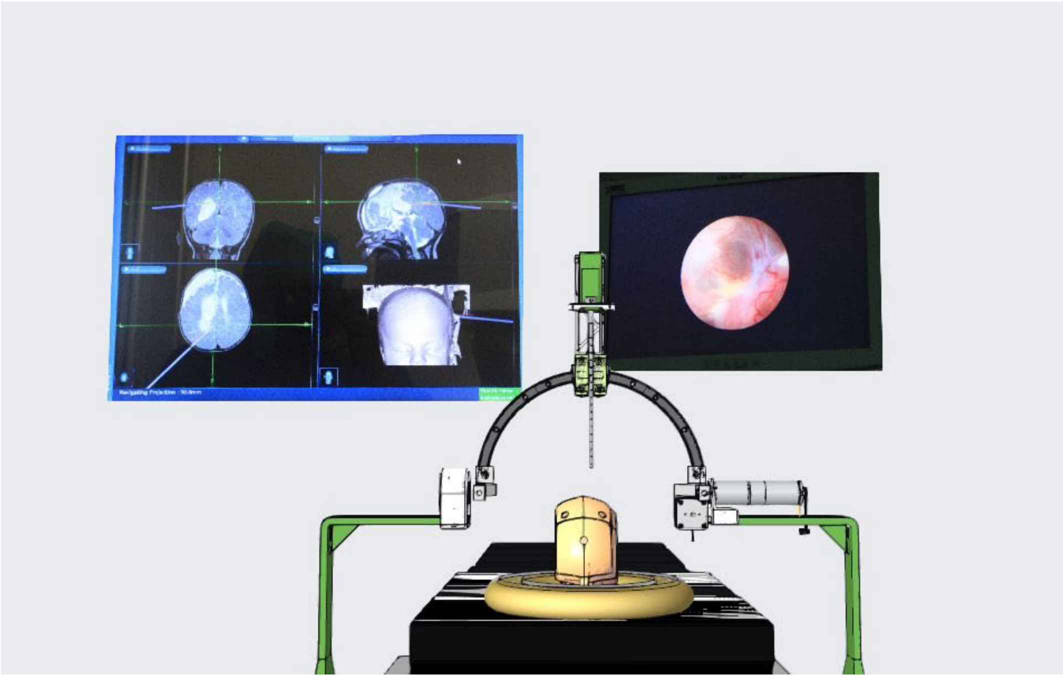

Figure 6.1: Surgeon's vision window: A view from surgeon's perspective which shows that neuronavigation and endocscopic screen is clearly seen along with the patient's head.

ing the manufacturing of the robotic system, a scale down proof-of-concept was developed to verify the relative motion, redundancies, and to have real life experience.

After the 3D modeling, we rigorously analyzed each DOF for their required stroke length, decoupling, and collision with other parts discussed in detail in 4.3. A detailed kinematic was also done to calculate and compare the workspace of the robotic system. We also performed mechanism simulations to verify the RCM of the robotic system. The calculated workspace was later compared with the CAD generated workspace and life size phantom. A detailed report about the analysis can be found in section 4.1 and 4.2.

At this stage, we also ran a crude ergonomic analysis of the robotic system. It has been mentioned earlier that the major problem with the available systems is their huge size. We used a feature of "Vision Window" to see the robotic system through surgeons perspective. Figure 6.1 shows the surgeon's vision window. It indicates that the surgeon vision is cleared and uncluttered.

At this stage, the manufacturing and assembly of the complete robotic system was started. The parts were made in house however several other parts were chosen off-the-shelf to acquire the committed accuracy and time saving. In the end, it is safe to say that we started this robotic system from scratch and able to deliver the first real prototype of complete robotic system. Figure 6.2 shows how the robotic system that can be natively integrated into any operating room.

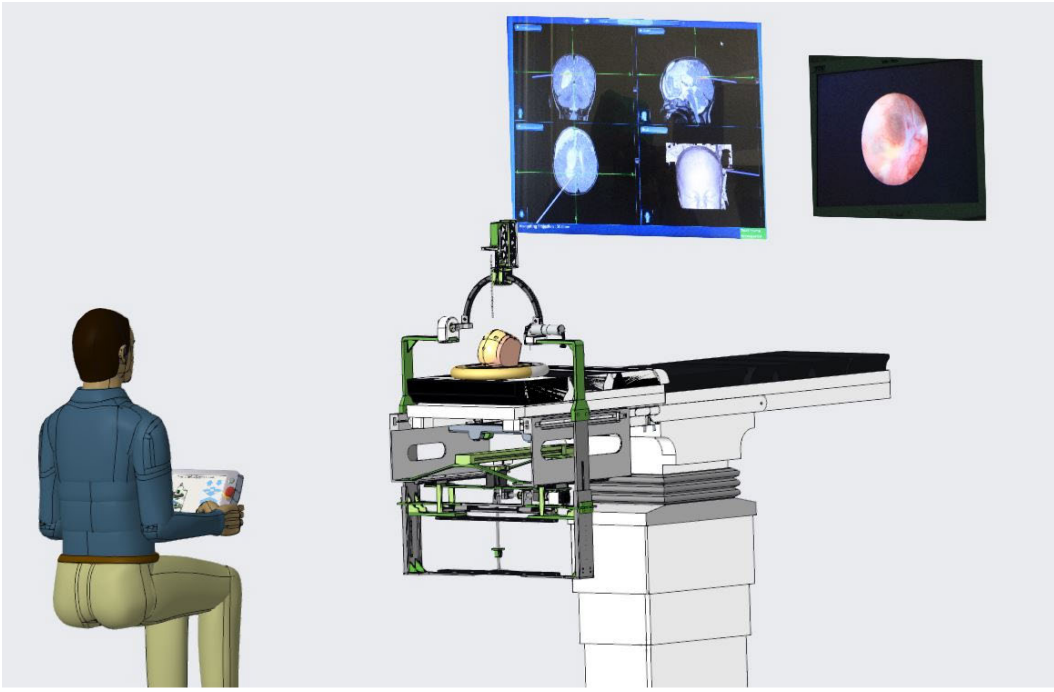

Figure 6.2: Setup of the robotic system in an operating room.

## 6.2 Conclusion

This research aimed to develop a dedicated six DOF robotic manipulator to perform neurosurgery in neonatal and infants. A detailed literature review indicated that there is no such system available in the market today. So we embarked on the journey of developing a robotic system that can answer the challenges in performing neuroendoscopy. We have developed a robotic system that can assist the surgeons to perform these surgeries. The actuated six DOFs of the system replaced the use of multiple hands in the workspace with a rigid support and a fine positioning system. A thorough mechanism review was done before starting the design process. It helped us assess different potential options and create novel mechanisms designed specifically for the pediatric neurosurgery application. Each DOF was carefully designed to ensure the required accuracy, precision, safety. Four out of six DOFs feature inherent safety features, while for the remaining two, additional safety features were added. The new robotic system can orient, insert, and hold the surgical sleeve at any point assigned by the surgeon. This feature helps the surgeon and allow him to focus on the critical part of the surgery. This will reduce the cognitive load on the surgeons.

The robotic system was also designed to work seamlessly with intra-operative neuronavigation as it is required during the surgery. This requirement arises because it is often preferable to avoid the use of clamps on the infant's head. All system requirements have been tested

both through the simulation and experiments. Kinematic analysis proved that our system can cover the required workspace efficiently. It also showed the required reachability of the tool. In addition, the dynamic simulation showed the RCM point and decoupling of all the motion. All of the above mentioned parameters were also validated through experiments with the new robotic system.
Since we have the actual prototype, the robotic system can be explored for transnasal and transmucosal surgeries.

## 6.3 Future work

So far, these were the preliminary steps in the development of the neurosurgical robotic system. There are still a lot of steps required in the further development of a viable surgical robotic system. The necessary future steps required for this project are as under: The next logical step in the development of these systems are the phantom trials. Phantom trials tests the limits of the robotic system and could suggests future improvements in design, if needed.

### 6.3.1 User trials

User trials are necessary to check the usability of the system from the end-user (surgeon's) perspective. It will also suggest the required updates in the later prototypes of the system.

### 6.3.2 Miscellaneous

The miscellaneous future works includes thoroughly checking the compatibility of the electrical systems with the OR, sterility mechanism of direct contact components and overall safety of the system.

### 6.3.3 Future Applications

In future, an advance control system can be designed which can directly coordinate with the MRI image data and surgeon can plan and check the tool trajectory of the robotic system by virtually planning the surgery. In future, the application of the haptic and force feedback of surgical sleeve can also be explored.

# Bibliography


[1] "ROSA® Brain," 2018. [Online]. Available: http://www.medtech.fr/en/rosa-brain

[2] M. Hoeckelmann, I. J. Rudas, P. Fiorini, F. Kirchner, and T. Haidegger, "Current capabilities and development potential in surgical robotics," *International Journal of Advanced Robotic Systems*, vol. 12, 2015.

[3] D. Glauser, P. Flury, and C. W. Burckhardt, "Mechanical concept of the neurosurgical robot 'Minerva'," *Robotica*, vol. 11, no. 6, pp. 567–575, 1993.

[4] T. A. Mattei, A. H. Rodriguez, D. Sambhara, and E. Mendel, "Current state-of-the-art and future perspectives of robotic technology in neurosurgery," *Neurosurgical Review*, vol. 37, no. 3, pp. 357–366, jul 2014. [Online]. Available: http://link.springer.com/10.1007/s10143-014-0540-z

[5] Y. Maddahi, K. Zareinia, N. Sepehri, and G. Sutherland, "Surgical tool motion during conventional freehand and robot-assisted microsurgery conducted using neuroArm," *Advanced Robotics*, vol. 30, no. 9, pp. 621–633, 2016.

[6] G. Deacon, A. Harwood, J. Holdback, D. Maiwand, M. Pearce, I. Reid, M. Street, and J. Taylor, "The pathfinder image-guided surgical robot," *Proceedings of the Institution of Mechanical Engineers, Part H: Journal of Engineering in Medicine*, vol. 224, no. 5, pp. 691–713, 2010.

[7] K. Hongo, S. Kobayashi, Y. Kakizawa, J.-I. Koyama, T. Goto, H. Okudera, K. Kan, M. G. Fujie, H. Iseki, and K. Takakura, "NeuRobot: telecontrolled micromanipulator system for minimally invasive microneurosurgery-preliminary results." *Neurosurgery*, vol. 51, no. 4, pp. 985–8; discussion 988, oct 2002. [Online]. Available: http://www.ncbi.nlm.nih.gov/pubmed/12234407

[8] K. Roessler, K. Ungersboeck, T. Czech, M. Aichholzer, W. Dietrich, H. Goerzer, C. Matula, and W. Koos, "Contour-Guided Brain Tumor Surgery Using a Stereotactic Navigating Microscope," *Stereotactic and Functional Neurosurgery*, vol. 68, no. 1-4, pp. 33–38, 1997.

[9] C. Faria, W. Erlhagen, M. Rito, E. De Momi, G. Ferrigno, and E. Bicho, "Review of robotic technology for stereotactic neurosurgery," *IEEE Reviews in Biomedical Engineering*, vol. 8, pp. 125–137, 2015.

[10] M. D. Comparetti, E. De Momi, A. Vaccarella, M. Riechmann, and G. Ferrigno, "Optically tracked multi-robot system for keyhole neurosurgery," *Proceedings - IEEE International Conference on Robotics and Automation*, pp. 661–666, 2011.

[11] M. Zimmermann, R. Krishnan, A. Raabe, and V. Seifert, "Robot-assisted navigated neuroendoscopy." *Neurosurgery*, vol. 51, no. 6, pp. 1446–51; discussion 1451–2, dec 2002. [Online]. Available: http://www.ncbi.nlm.nih.gov/pubmed/12445350

[12] L. M. Auer, S. Starkie, D. P. Auer, and B. Davies, "Simulating minimally invasive neurosurgical interventions using an active manipulator," *International Congress Series*, vol. 1247, pp. 199–210, dec 2002. [Online]. Available: https://linkinghub.elsevier.com/retrieve/pii/S0531513102010865

[13] S. Behzadipour, "Kinematics and Dynamics of a Self-Stressed Cartesian Cable-Driven Mechanism," *Journal of Mechanical Design*, vol. 131, no. 6, jun 2009. [Online]. Available: https://asmedigitalcollection.asme.org/mechanicaldesign/article/doi/10.1115/1.3125206/466944/Kinematics-and-Dynamics-of-a-SelfStressed

[14] T. P. Tho and N. T. Thinh, "Using a cable-driven parallel robot with applications in 3d concrete printing," *Applied Sciences (Switzerland)*, vol. 11, no. 2, pp. 1–24, 2021.

[15] P.-L. Richard, C. M. Gosselin, and X. Kong, "Kinematic Analysis and Prototyping of a Partially Decoupled 4-DOF 3T1R Parallel Manipulator," *Journal of Mechanical Design*, vol. 129, no. 6, pp. 611–616, jun 2007. [Online]. Available: https://asmedigitalcollection.asme.org/mechanicaldesign/article/129/6/611/451331/Kinematic-Analysis-and-Prototyping-of-a-Partially

[16] P.-L. Yen and C.-C. Lai, "Dynamic modeling and control of a 3-DOF Cartesian parallel manipulator," *Mechatronics*, vol. 19, no. 3, pp. 390–398, apr 2009. [Online]. Available: https://linkinghub.elsevier.com/retrieve/pii/S0957415808001554

[17] P. N. Robinson, "Minimally Invasive Surgery," in *Anesthesia Secrets*. Elsevier, 2011, pp. 511–517. [Online]. Available: https://linkinghub.elsevier.com/retrieve/pii/B9780323065245000751

[18] E. G. Soltesz and D. C. Brooks, "Laparoscopy," in *Encyclopedia of Gastroenterology*. Elsevier, 2004, pp. 487–495. [Online]. Available: https://linkinghub.elsevier.com/retrieve/pii/B0123868602004275

[19] N. M. Shockcor, S. Sultan, J. Alvarez-Casas, P. S. Brazio, M. Phelan, J. C. LaMattina, and R. N. Barth, "Minimally invasive donor nephrectomy: current state of the art," *Langenbeck's Archives of Surgery*, vol. 403, no. 6, pp. 681–691, sep 2018. [Online]. Available: http://link.springer.com/10.1007/s00423-018-1700-3

[20] R. Treuting, “Minimally invasive orthopedic surgery: arthroscopy,” *Ochsner Journal*, vol. 2, no. 3, pp. 158–163, 2000.

[21] A. D. Sihoe, “The evolution of minimally invasive thoracic surgery: implications for the practice of uniportal thoracoscopic surgery,” *Journal of thoracic disease*, vol. 6, no. Suppl 6, p. S604, 2014.

[22] C. Teo, “The concept of minimally invasive neurosurgery,” *Neurosurgery Clinics*, vol. 21, no. 4, pp. 583–584, 2010.

[23] A. Sain, “Laparoscopic cholecystectomy is the current" gold standard" for the treatment of gallstone disease.” *Annals of surgery*, vol. 224, no. 5, p. 689, 1996.

[24] J. C. Ganz, “Principles of Stereotaxy,” in *Gamma Knife Surgery*. Vienna: Springer Vienna, 1997, pp. 7–18. [Online]. Available: http://link.springer.com/10.1007/978-3-7091-6831-8{_}2

[25] R. Mallin and T. A. Rathbun, “A trephined skull from Iran.” *Bulletin of the New York Academy of Medicine*, vol. 52, no. 7, pp. 782–7, sep 1976. [Online]. Available: http://www.ncbi.nlm.nih.gov/pubmed/782613http://www.pubmedcentral.nih.gov/articlerender.fcgi?artid=PMC1807243

[26] Y. Enchev and S. Oi, “Historical trends of neuroendoscopic surgical techniques in the treatment of hydrocephalus,” pp. 249–262, 2008.

[27] P. Grunert, “From the Idea to Its Realization: The Evolution of Minimally Invasive Techniques in Neurosurgery,” *Minimally Invasive Surgery*, vol. 2013, pp. 1–18, 2013. [Online]. Available: http://www.hindawi.com/journals/mis/2013/171369/

[28] R. Abbott, “History of neuroendoscopy,” *Neurosurgery Clinics of North America*, vol. 15, no. 1, pp. 1–7, jan 2004. [Online]. Available: https://linkinghub.elsevier.com/retrieve/pii/S1042368003000652

[29] P. Decq, H. W. Schroeder, M. Fritsch, and P. Cappabianca, “A history of ventricular neuroendoscopy,” pp. S14.e1–S14.e6, 2013. [Online]. Available: http://dx.doi.org/10.1016/j.wneu.2012.02.034

[30] K. Stachura and W. Libionka, “An outline of the history of neuroendoscopy.” *Przeglad lekarski*, vol. 64, no. 2, pp. 118–20, 2007. [Online]. Available: http://www.ncbi.nlm.nih.gov/pubmed/17892045

[31] W. Tirakotai, O. Bozinov, U. Sure, T. Riegel, H. Bertalanffy, and D. Hellwig, “The evolution of stereotactic guidance in neuroendoscopy,” *Child’s Nervous*

*System*, vol. 20, no. 11-12, pp. 790–795, nov 2004. [Online]. Available: http://link.springer.com/10.1007/s00381-004-0932-4

[32] D. Thomas, “Stereotactic Techniques in Clinical Neurosurgery,” *Journal of Neurology, Neurosurgery, and Psychiatry*, vol. 50, no. 2, p. 246, 1987. [Online]. Available: https://www.ncbi.nlm.nih.gov/pmc/articles/PMC1031520/

[33] Robert Levy, “A Short History of Stereotactic Neurosurgery.” [Online]. Available: http://www.neurosurgery.org/cybermuseum/stereotactichall/stereoarticle.html

[34] R. J. Maciunas, R. L. Galloway Jr, and J. W. Latimer, “The application accuracy of stereotactic frames,” *Neurosurgery*, vol. 35, no. 4, pp. 682–695, 1994.

[35] E. Friets, J. Strohbehn, J. Hatch, and D. Roberts, “A frameless stereotaxic operating microscope for neurosurgery,” *IEEE Transactions on Biomedical Engineering*, vol. 36, no. 6, pp. 608–617, jun 1989. [Online]. Available: http://ieeexplore.ieee.org/document/29455/

[36] A. Kato, T. Yoshimine, T. Hayakawa, Y. Tomita, T. Ikeda, M. Mitomo, K. Harada, and H. Mogami, “Computer assisted neurosurgery: development of a frameless and armless navigation system (CNS navigator).” *No shinkei geka. Neurological surgery*, vol. 19, no. 2, pp. 137–42, feb 1991. [Online]. Available: http://www.ncbi.nlm.nih.gov/pubmed/2023669

[37] J. S. Perlmutter and J. W. Mink, “Deep Brain Stimulation,” *Annual Review of Neuroscience*, vol. 29, no. 1, pp. 229–257, jul 2006. [Online]. Available: http://www.annualreviews.org/doi/10.1146/annurev.neuro.29.051605.112824

[38] R. Bartholow, “Experiments on the Functions of the Human Brain,” *British Medical Journal*, vol. 1, no. 700, p. 727, may 1874. [Online]. Available: https://www.ncbi.nlm.nih.gov/pmc/articles/PMC2302912/

[39] M. Rahman, G. J. A. Murad, and J. Mocco, “Early history of the stereotactic apparatus in neurosurgery,” *Neurosurgical Focus*, vol. 27, no. 3, p. E12, sep 2009. [Online]. Available: https://thejns.org/view/journals/neurosurg-focus/27/3/article-pE12.xml

[40] H. Akbari, B. Khalighinejad, J. L. Herrero, A. D. Mehta, and N. Mesgarani, “Towards reconstructing intelligible speech from the human auditory cortex,” *bioRxiv*, p. 350124, oct 2018.

[41] J. A. Gonzalez-Martinez, “The Stereo-Electroencephalography,” *Journal of Clinical Neurophysiology*, 2016.

[42] J. Bancaud and M. B. Dell, “Technics and method of stereotaxic functional

exploration of the brain structures in man (cortex, subcortex, central gray nuclei)." *Revue neurologique*, vol. 101, pp. 213–27, sep 1959. [Online]. Available: http://www.ncbi.nlm.nih.gov/pubmed/13848920

[43] J. Isnard, D. Taussig, F. Bartolomei, P. Bourdillon, H. Catenoix, F. Chassoux, M. Chipaux, S. Clémenceau, S. Colnat-Coulbois, M. Denuelle, S. Derrey, B. Devaux, G. Dorfmüller, V. Gilard, M. Guenot, A.-S. Job-Chapron, E. Landré, A. Lebas, L. Maillard, A. McGonigal, L. Minotti, A. Montavont, V. Navarro, A. Nica, N. Reyns, J. Scholly, J.-C. Sol, W. Szurhaj, A. Trebuchon, L. Tyvaert, M. P. Valenti-Hirsch, L. Valton, J.-P. Vignal, and P. Sauleau, "French guidelines on stereoelectroencephalography (SEEG)," *Neurophysiologie Clinique*, vol. 48, no. 1, pp. 5–13, feb 2018. [Online]. Available: https://linkinghub.elsevier.com/retrieve/pii/S0987705317302873

[44] Y. Yadav, V. Parihar, S. Pande, H. Namdev, and M. Agarwal, "Endoscopic third ventriculostomy," *Journal of Neurosciences in Rural Practice*, vol. 3, no. 2, p. 163, 2012. [Online]. Available: http://www.ruralneuropractice.com/text.asp?2012/3/2/163/98222

[45] M. J. McGirt, A. Zaas, H. E. Fuchs, T. M. George, K. Kaye, and D. J. Sexton, "Risk Factors for Pediatric Ventriculoperitoneal Shunt Infection and Predictors of Infectious Pathogens," *Clinical Infectious Diseases*, vol. 36, no. 7, pp. 858–862, apr 2003. [Online]. Available: https://academic.oup.com/cid/article-lookup/doi/10.1086/368191

[46] A. M. Isaacs, J. Riva-Cambrin, D. Yavin, A. Hockley, T. M. Pringsheim, N. Jette, B. C. Lethebe, M. Lowerison, J. Dronyk, and M. G. Hamilton, "Age-specific global epidemiology of hydrocephalus: Systematic review, metanalysis and global birth surveillance," *PLOS ONE*, vol. 13, no. 10, p. e0204926, oct 2018. [Online]. Available: https://dx.plos.org/10.1371/journal.pone.0204926

[47] H. Association, "20 Powerful facts about Hydrocephalus." [Online]. Available: https://www.hydroassoc.org/

[48] B. J. Dlouhy, N. S. Dahdaleh, and J. D. W. Greenlee, "Emerging technology in intracranial neuroendoscopy: application of the NICO Myriad," *Neurosurgical Focus*, vol. 30, no. 4, p. E6, apr 2011. [Online]. Available: https://thejns.org/view/journals/neurosurg-focus/30/4/2011.2.focus10312.xml

[49] Y. Kwoh, J. Hou, E. Jonckheere, and S. Hayati, "A robot with improved absolute positioning accuracy for CT guided stereotactic brain surgery," *IEEE Transactions*

*on Biomedical Engineering*, vol. 35, no. 2, pp. 153–160, 1988. [Online]. Available: http://ieeexplore.ieee.org/document/1354/

[50] C. S. Karas and E. A. Chiocca, "Neurosurgical robotics: a review of brain and spine applications," *Journal of Robotic Surgery*, vol. 1, no. 1, pp. 39–43, mar 2007. [Online]. Available: http://link.springer.com/10.1007/s11701-006-0006-6

[51] P. Gomes, Ed., *Medical Robotics: Minimally Invasive Surgery*, 1st ed. Woodhead Publishing, 2012. [Online]. Available: https://www.elsevier.com/books/medical-robotics/gomes/978-0-85709-130-7

[52] R. H. Taylor, A. Menciassi, G. Fichtinger, P. Fiorini, and P. Dario, "Medical Robotics and Computer-Integrated Surgery," in *Springer Handbook of Robotics*. Cham: Springer International Publishing, oct 2016, vol. 19, no. 5, pp. 1657–1684. [Online]. Available: http://link.springer.com/10.1007/978-3-319-32552-1{_}63http://ieeexplore.ieee.org/document/1236750/

[53] J.-P. Merlet, "Optimal design of robots," Tech. Rep., 2005. [Online]. Available: https://hal.inria.fr/inria-00000473

[54] R. Alizade, C. Bayram, and E. Gezgin, "Structural synthesis of serial platform manipulators," *Mechanism and Machine Theory*, vol. 42, no. 5, pp. 580–599, 2007.

[55] M. H. Ang and V. D. Tourassis, "Flexible Manufacturing Using Modular Robotic Wrists," in *CAD/CAM Robotics and Factories of the Future*. Berlin, Heidelberg: Springer Berlin Heidelberg, 1989, pp. 166–170. [Online]. Available: http://link.springer.com/10.1007/978-3-662-39962-0{_}29

[56] D. DeMers and K. Kreutz-Delgado, "Inverse Kinematics of Dextrous Manipulators," in *Neural Systems for Robotics*. Elsevier, 1997, pp. 75–116. [Online]. Available: https://linkinghub.elsevier.com/retrieve/pii/B9780080925097500087

[57] A. Kumar and K. J. Waldron, "The Workspaces of a Mechanical Manipulator," *Journal of Mechanical Design*, vol. 103, no. 3, p. 665, 1981. [Online]. Available: http://mechanicaldesign.asmedigitalcollection.asme.org/article.aspx?articleid=1451561

[58] V. D. Tourassis and M. H. Ang, "Identification and Analysis of Robot Manipulator Singularities," *The International Journal of Robotics Research*, vol. 11, no. 3, pp. 248–259, jun 1992. [Online]. Available: http://journals.sagepub.com/doi/10.1177/027836499201100307

[59] J.-P. MERLET, *Parallel Robots*, ser. Solid Mechanics and Its Applications. Berlin/Heidelberg: Springer-Verlag, 2006, vol. 128. [On-

line]. Available: http://link.springer.com/10.1007/978-1-4471-4670-4{_}99http://link.springer.com/10.1007/1-4020-4133-0

[60] Y. D. Patel and P. M. George, "Parallel Manipulators Applications—A Survey," *Modern Mechanical Engineering*, vol. 02, no. 03, pp. 57–64, 2012. [Online]. Available: http://www.scirp.org/journal/doi.aspx?DOI=10.4236/mme.2012.23008

[61] D. Stewart, "A Platform with Six Degrees of Freedom," *Proceedings of the Institution of Mechanical Engineers*, vol. 180, no. 1, pp. 371–386, jun 1965. [Online]. Available: http://journals.sagepub.com/doi/10.1243/PIME{_}PROC{_}1965{_}180{_}029{_}02

[62] Grigore Gogu, *Structural Synthesis of Parallel Robots*, ser. Solid Mechanics and its Applications, G. Gogu, Ed. Dordrecht: Springer Netherlands, 2008, vol. 149. [Online]. Available: http://link.springer.com/10.1007/978-1-4020-5710-6

[63] S. Chen and I. You, "Kinematic and Singularity Analyses of a Six DOF 6-3-3 Parallel Link Machine Tool," *The International Journal of Advanced Manufacturing Technology*, vol. 16, no. 11, pp. 835–842, sep 2000. [Online]. Available: http://link.springer.com/10.1007/s001700070018

[64] Robert L. Williams and Atul R. Joshi, "Planar parallel 3-RPR manipulator," *Proceedings of the Sixth Conference on ...*, no. 740, 1999. [Online]. Available: http://www.quanser.com/english/downloads/toolbox/papers/15Qamr99rpr.pdf

[65] X. Zhao and S. Peng, "Direct displacement analysis of parallel manipulators," *Journal of Robotic Systems*, vol. 17, no. 6, pp. 341–345, jun 2000. [Online]. Available: http://doi.wiley.com/10.1002/{%}28SICI{%}291097-4563{%}28200006{%}2917{%}3A6{%}3C341{%}3A{%}3AAID-ROB4{%
0.CO{%}3B2-N

[66] K. Zhou, D. Mao, and Z. Tao, "Kinematic Analysis and Application Research on a High-Speed Travelling Double Four-Rod Spatial Parallel Mechanism," *The International Journal of Advanced Manufacturing Technology*, vol. 19, no. 12, pp. 873–878, jun 2002. [Online]. Available: http://link.springer.com/10.1007/s001700200099

[67] B. Nahum, F. Badano, E. Roussel, and L. Blondel, "Neurosurgical assistance robot," 2016. [Online]. Available: https://www.google.com/patents/WO2016185140A1?cl=en

[68] J. Gonzalez-Martinez, S. Vadera, J. Mullin, R. Enatsu, A. V. Alexopoulos, R. Patwardhan, W. Bingaman, and I. Najm, "Robot-assisted stereotactic laser

ablation in medically intractable epilepsy: operative technique." *Neurosurgery*, vol. 10 Suppl 2, no. 2, pp. 167–72; discussion 172–3, jun 2014. [Online]. Available: http://www.ncbi.nlm.nih.gov/pubmed/24448180

[69] N. J. Brandmeir and M. D. Sather, "A Technical Report of Robot-Assisted Stereotactic Percutaneous Rhizotomy," *Pain Medicine*, vol. 18, no. 12, pp. 2512–2514, dec 2017. [Online]. Available: https://academic.oup.com/painmedicine/article-lookup/doi/10.1093/pm/pnx110http://academic.oup.com/painmedicine/article/18/12/2512/3798727

[70] A. Fernandes and A. T. Berman, "Introduction to Stereotactic Radiation (Radiosurgery / SRS)," 2018. [Online]. Available: https://www.oncolink.org/cancer-treatment/radiation/types-of-radiation-therapy/introduction-to-stereotactic-radiation-radiosurgery-srs

[71] G. Kurup, "CyberKnife: A new paradigm in radiotherapy," *Journal of Medical Physics*, vol. 35, no. 2, p. 63, 2010. [Online]. Available: http://www.jmp.org.in/text.asp?2010/35/2/63/62194

[72] W. Kilby, J. R. Dooley, G. Kuduvalli, S. Sayeh, and C. R. Maurer, "The CyberKnife® Robotic Radiosurgery System in 2010," *Technology in Cancer Research & Treatment*, vol. 9, no. 5, pp. 433–452, oct 2010. [Online]. Available: http://journals.sagepub.com/doi/10.1177/153303461000900502

[73] K. systems, "Series 2000 : The all-rounders in the high payload range KR 210-2," 2000. [Online]. Available: http://www.kuka-robotics.com/res/sps/6b77eeca-cfe5-42d3-b736-af377562ecaa{_}PF0020{_}KR{_}150-2{_}en.pdf

[74] K. Palenta and A. Babiarz, "KUKA Robot Motion Planning Using the 1742 NI Smart Camera," 2014, pp. 115–122. [Online]. Available: http://link.springer.com/10.1007/978-3-319-02309-0{_}12

[75] A. L. Benabid, P. Cinquin, S. Lavalle, J. F. Le Bas, J. Demongeot, and J. de Rougemont, "Computer-driven robot for stereotactic surgery connected to CT scan and magnetic resonance imaging. Technological design and preliminary results." *Applied neurophysiology*, vol. 50, no. 1-6, pp. 153–4, 1987. [Online]. Available: http://www.ncbi.nlm.nih.gov/pubmed/3329838

[76] T. R. K. Varma and P. Eldridge, "Use of the NeuroMate stereotactic robot in a frameless mode for functional neurosurgery," *The International Journal of Medical Robotics and Computer Assisted Surgery*, vol. 2, no. 2, pp.

107–113, jun 2006. [Online]. Available: http://arxiv.org/abs/1504.07874http://www.ncbi.nlm.nih.gov/pubmed/17520639http://doi.wiley.com/10.1002/rcs.88

[77] Q. H. Li, L. Zamorano, A. Pandya, R. Perez, J. Gong, and F. Diaz, "The application accuracy of the NeuroMate robot?A quantitative comparison with frameless and frame-based surgical localization systems," *Computer Aided Surgery*, vol. 7, no. 2, pp. 90–98, 2002. [Online]. Available: http://doi.wiley.com/10.1002/igs.10035

[78] T. Haidegger, T. Xia, and P. Kazanzides, "Accuracy improvement of a neurosurgical robot system," in *2008 2nd IEEE RAS & EMBS International Conference on Biomedical Robotics and Biomechatronics*. IEEE, oct 2008, pp. 836–841. [Online]. Available: http://ieeexplore.ieee.org/document/4762912/

[79] "Neuro | Mate ® - Key Features," *Technical Data Sheet*, pp. 1–2. [Online]. Available: http://www.renishaw.com/en/neuromate-stereotactic-robot--10712

[80] C. B. Ostertag, "Stereotactic brain surgery." *Deutsche Krankenpflegezeitschrift*, vol. 41, no. 2, pp. 131–4, feb 1988. [Online]. Available: http://ieeexplore.ieee.org/document/391771/http://www.ncbi.nlm.nih.gov/pubmed/3152714

[81] J.-L. Hefti, M. Epitaux, D. Glauser, and H. Fankhauser, "Robotic three-dimensional positioning of a stimulation electrode in the brain," *Computer Aided Surgery*, vol. 3, no. 1, pp. 1–10, 1998. [Online]. Available: http://doi.wiley.com/10.1002/{%}28SICI{%}291097-0150{%}281998{%}293{%}3A1{%}3C1{%}3A{%}3AAID-IGS1{%}3E3.0.CO{%}3B2-3

[82] D. Glauser, H. Fankhauser, M. Epitaux, J.-L. Hefti, and A. Jaccottet, "Neurosurgical Robot Minerva: First Results and Current Developments," *Computer Aided Surgery*, vol. 1, no. 5, pp. 266–272, jan 1995. [Online]. Available: http://www.tandfonline.com/doi/full/10.3109/10929089509106332

[83] Michael J. Lang, A. D. Greer, and G. R. Sutherland, *Intra-operative Robotics: NeuroArm*, ser. Acta Neurochirurgica Supplementum, M. N. Pamir, V. Seifert, and T. Kiris, Eds. Vienna: Springer Vienna, 2011, vol. 109. [Online]. Available: http://link.springer.com/10.1007/978-3-211-99651-5

[84] G. R. Sutherland, I. Latour, A. D. Greer, T. Fielding, G. Feil, and P. Newhook, "AN IMAGE-GUIDED MAGNETIC RESONANCE-COMPATIBLE SURGICAL ROBOT," *Neurosurgery*, vol. 62, no. 2, pp. 286–293, feb 2008. [Online]. Available: https://academic.oup.com/neurosurgery/article/62/2/286/2558431

[85] S. Pandya, J. W. Motkoski, C. Serrano-Almeida, A. D. Greer, I. Latour, and G. R. Sutherland, "Advancing neurosurgery with image-guided robotics." *Journal*

*of neurosurgery*, vol. 111, no. 6, pp. 1141–9, dec 2009. [Online]. Available: http://www.ncbi.nlm.nih.gov/pubmed/19374495

[86] J. Brodie and S. Eljamel, "Evaluation of a neurosurgical robotic system to make accurate burr holes," *The International Journal of Medical Robotics and Computer Assisted Surgery*, vol. 7, no. 1, pp. 101–106, mar 2011. [Online]. Available: http://www.ncbi.nlm.nih.gov/pubmed/17520639http://doi.wiley.com/10.1002/rcs.376

[87] P. S. Morgan, T. Carter, S. Davis, A. Sepehri, J. Punt, P. Byrne, A. Moody, and P. Finlay, "The application accuracy of the Pathfinder neurosurgical robot," *International Congress Series*, vol. 1256, pp. 561–567, jun 2003. [Online]. Available: https://linkinghub.elsevier.com/retrieve/pii/S0531513103004217

[88] M. S. Eljamel, "Robotic neurological surgery applications: Accuracy and consistency or pure fantasy?" *Stereotactic and Functional Neurosurgery*, vol. 87, no. 2, pp. 88–93, 2009.

[89] ——, "Validation of the PathFinder™ neurosurgical robot using a phantom," *The International Journal of Medical Robotics and Computer Assisted Surgery*, vol. 3, no. 4, pp. 372–377, dec 2007. [Online]. Available: http://doi.wiley.com/10.1002/rcs.153

[90] T. Goto, K. Hongo, Y. Kakizawa, H. Muraoka, Y. Miyairi, Y. Tanaka, and S. Kobayashi, "Clinical application of robotic telemanipulation system in neurosurgery: Case report," *Journal of Neurosurgery*, vol. 99, no. 6, pp. 1082–1084, 2003.

[91] T. Goto, T. Miyahara, K. Toyoda, J. Okamoto, Y. Kakizawa, J.-I. Koyama, M. G. Fujie, and K. Hongo, "Telesurgery of Microscopic Micromanipulator System "NeuRobot" in Neurosurgery: Interhospital Preliminary Study," *Journal of brain disease*, vol. 1, p. JCNSD.S2552, 2009.

[92] K. Hongo, T. Goto, T. Miyahara, Y. Kakizawa, J. Koyama, and Y. Tanaka, "Telecontrolled micromanipulator system (NeuRobot) for minimally invasive neurosurgery," in *Medical Technologies in Neurosurgery*. Vienna: Springer Vienna, pp. 63–66. [Online]. Available: http://link.springer.com/10.1007/978-3-211-33303-7{_}9

[93] P. W. Willems, H. J. Noordmans, L. M. Ramos, M. J. Taphoorn, J. W. Berkelbach Van Der Sprenkel, M. A. Viergever, and C. A. Tulleken, "Clinical evaluation of stereotactic brain biopsies with an MKM-mounted instrument holder," *Acta Neurochirurgica*, vol. 145, no. 10, pp. 889–897, 2003.

[94] J. Kaminsky, T. Brinker, A. Samii, G. Arango, P. Vorkapic, and M. Samii, "Technical considerations regarding accuracy of the MKM™ navigation system. An

experimental study on impact factors," *Neurological Research*, vol. 21, no. 4, pp. 420–424, jun 1999. [Online]. Available: https://www.tandfonline.com/doi/full/10.1080/01616412.1999.11740954

[95] P. K. Pillay, "Image-guided stereotactic neurosurgery with the multicoordinate manipulator microscope," *Surgical Neurology*, vol. 47, no. 2, pp. 171–176, 1997.

[96] D. P. Devito, L. Kaplan, R. Dietl, M. Pfeiffer, D. Horne, B. Silberstein, M. Hardenbrook, G. Kiriyanthan, Y. Barzilay, A. Bruskin, D. Sackerer, V. Alexandrovsky, C. Stüer, R. Burger, J. Maeurer, D. G. Gordon, R. Schoenmayr, A. Friedlander, N. Knoller, K. Schmieder, I. Pechlivanis, I.-S. Kim, B. Meyer, and M. Shoham, "Clinical Acceptance and Accuracy Assessment of Spinal Implants Guided With SpineAssist Surgical Robot," *Spine*, vol. 35, no. 24, pp. 2109–2115, nov 2010. [Online]. Available: https://insights.ovid.com/crossref?an=00007632-201011150-00003

[97] L. Joskowicz, M. Shoham, R. Shamir, M. Freiman, E. Zehavi, and Y. Shoshan, "Miniature robot-based precise targeting system for keyhole neurosurgery: Concept and preliminary results," *International Congress Series*, vol. 1281, pp. 618–623, may 2005. [Online]. Available: https://linkinghub.elsevier.com/retrieve/pii/S0531513105006047

[98] M. D. Comparetti, A. Vaccarella, I. Dyagilev, M. Shoham, G. Ferrigno, and E. De Momi, "Accurate multi-robot targeting for keyhole neurosurgery based on external sensor monitoring," *Proceedings of the Institution of Mechanical Engineers, Part H: Journal of Engineering in Medicine*, vol. 226, no. 5, pp. 347–359, may 2012. [Online]. Available: http://journals.sagepub.com/doi/10.1177/0954411912442120

[99] C. Nimsky, J. Rachinger, H. Iro, and R. Fahlbusch, "Adaptation of a Hexapod-Based Robotic System for Extended Endoscope-Assisted Transsphenoidal Skull Base Surgery," *Minimally Invasive Neurosurgery*, vol. 47, no. 1, pp. 41–46, 2004.

[100] A. Radetzky, M. Rudolph, W. Stefanon, S. Starkie, B. Davies, and L. M. Auer, "Simulating Minimally Invasive Neurosurgical Interventions Using an Active Manipulator," in *Medical Image Computing and Computer-Assisted Intervention – MICCAI 2000*, S. L. Delp, A. M. DiGoia, and B. Jaramaz, Eds. Berlin, Heidelberg: Springer Berlin Heidelberg, 2000, pp. 578–587. [Online]. Available: http://link.springer.com/10.1007/978-3-540-40899-4{_}59

[101] A.-L. Benabid, D. Hoffmann, E. Seigneuret, and S. Chabardes, "Robotics in neurosurgery: which tools for what?" in *Medical Technologies in*

*Neurosurgery*. Vienna: Springer Vienna, pp. 43–50. [Online]. Available: http://link.springer.com/10.1007/978-3-211-33303-7{_}7

[102] S. Briot, C. Baradat, S. Guegan, and V. Arakelian, "Contribution to the Mechanical Behavior Improvement of the Robotic Navigation Device Surgiscope," in *Volume 8: 31st Mechanisms and Robotics Conference, Parts A and B*. ASME, 2007, pp. 653–661. [Online]. Available: http://proceedings.asmedigitalcollection.asme.org/proceeding.aspx?articleid=1605258

[103] K. Bekelis, T. A. Radwan, A. Desai, and D. W. Roberts, "Frameless robotically targeted stereotactic brain biopsy: feasibility, diagnostic yield, and safety," *Journal of Neurosurgery*, vol. 116, no. 5, pp. 1002–1006, may 2012. [Online]. Available: https://thejns.org/view/journals/j-neurosurg/116/5/article-p1002.xml

[104] S. S. Lollis and D. W. Roberts, "Robotic placement of a CNS ventricular reservoir for administration of chemotherapy," *British Journal of Neurosurgery*, vol. 23, no. 5, pp. 516–520, jan 2009. [Online]. Available: http://www.tandfonline.com/doi/full/10.1080/02688690902948192

[105] R. Lustig, "Use of Conventional Fractionation Fractionation With Cyber Knife in Children: A Report of 5 Cases," *Journal of Pediatric Hematology/Oncology*, vol. 32, no. 6, p. 441, aug 2010. [Online]. Available: http://journals.lww.com/00043426-201008000-00001

[106] K. R. GMB, "misc." [Online]. Available: https://www.robotskuka.com/app/download/10657871/Manual+Kuka+2000+series+Kr+240.pdf

[107] S. S. Gill, G. McFarland, R. N. Harrison, and P. D. Fielder, "Apparatus for robotic surgery," 2014. [Online]. Available: https://patents.google.com/patent/US20160296293A1/en?q=Neuromate{&}oq=Neuromate

[108] S. Candela, M. I. Vanegas, A. Darling, J. D. Ortigoza-Escobar, M. Alamar, J. Muchart, A. Climent, E. Ferrer, J. Rumià, and B. Pérez-Dueñas, "Frameless robot-assisted pallidal deep brain stimulation surgery in pediatric patients with movement disorders: precision and short-term clinical results," *Journal of Neurosurgery: Pediatrics*, vol. 22, no. 4, pp. 416–425, oct 2018. [Online]. Available: https://thejns.org/view/journals/j-neurosurg-pediatr/22/4/article-p416.xml

[109] M. Robotics, "Surgeons at MCCG Perform First Successful Spine Surgery Using Mazor Robotics Renaissance," 2014. [Online]. Available: https://www.navicenthealth.org/community/single{_}news/surgeons-at-mccg-perform-first-successful-spine-surgery-using-mazor-robotics-renaissance

[110] Cong Bang Pham, Guilin Yang, and Song Huat Yeo, "Dynamic analysis of cable-driven parallel mechanisms," in *Proceedings, 2005 IEEE/ASME International Conference on Advanced Intelligent Mechatronics.* IEEE, pp. 612–617. [Online]. Available: http://ieeexplore.ieee.org/document/1511050/

[111] J. Albus, R. Bostelman, and N. Dagalakis, "The NIST robocrane," *Journal of Robotic Systems*, vol. 10, no. 5, pp. 709–724, jul 1993. [Online]. Available: http://doi.wiley.com/10.1002/rob.4620100509

[112] Y. X. Su, B. Y. Duan, R. D. Nan, and B. Peng, "Development of a large parallel-cable manipulator for the feed-supporting system of a next-generation large radio telescope," *Journal of Robotic Systems*, vol. 18, no. 11, pp. 633–643, nov 2001. [Online]. Available: http://doi.wiley.com/10.1002/rob.8102

[113] J. D. Wentz and G. S. Weldon, *Applicability of a cable driven manipulator system for hazardous environments*, pp. 1–7. [Online]. Available: https://www.icevirtuallibrary.com/doi/abs/10.1680/poticrtfhe.27640.0026

[114] D. Surdilovic and R. Bernhardt, "STRING-MAN: a new wire robot for gait rehabilitation," in *IEEE International Conference on Robotics and Automation, 2004. Proceedings. ICRA '04. 2004.* IEEE, 2004, pp. 2031–2036 Vol.2. [Online]. Available: http://ieeexplore.ieee.org/document/1308122/

[115] D. Mayhew, B. Bachrach, W. Rymer, and R. Beer, "Development of the MACARM - a Novel Cable Robot for Upper Limb Neurorehabilitation," in *9th International Conference on Rehabilitation Robotics, 2005. ICORR 2005.* IEEE, pp. 299–302. [Online]. Available: http://ieeexplore.ieee.org/document/1501106/

[116] M. Métillon, P. Cardou, K. Subrin, C. Charron, and S. Caro, "A Cable-Driven Parallel Robot with Full-Circle End-Effector Rotations," 2021. [Online]. Available: http://arxiv.org/abs/2101.02783

[117] A. Alikhani, S. Behzadipour, S. A. S. Vanini, and A. Alasty, "Workspace Analysis of a Three DOF Cable-Driven Mechanism," *Journal of Mechanisms and Robotics*, vol. 1, no. 4, nov 2009. [Online]. Available: https://asmedigitalcollection.asme.org/mechanismsrobotics/article/doi/10.1115/1.3204255/468269/Workspace-Analysis-of-a-Three-DOF-CableDriven

[118] H. S. Kim and L.-W. Tsai, "Design Optimization of a Cartesian Parallel Manipulator," *Journal of Mechanical Design*, vol. 125, no. 1, pp. 43–51, mar 2003. [Online]. Available: https://asmedigitalcollection.asme.org/mechanicaldesign/article/125/1/43/445728/Design-Optimization-of-a-Cartesian-Parallel

[119] T. Essomba, L. Nguyen Vu, and C.-T. Wu, "Optimization of a Spherical Decoupled Mechanism for Neuro-Endoscopy Based on Experimental Kinematic Data," *Journal of Mechanics*, vol. 36, no. 1, pp. 133–147, feb 2020. [Online]. Available: https://academic.oup.com/jom/article/36/1/133-147/5950369

[120] T. Essomba, Y. Hsu, J. S. Sandoval Arevalo, M. A. Laribi, and S. Zeghloul, "Kinematic Optimization of a Reconfigurable Spherical Parallel Mechanism for Robotic-Assisted Craniotomy," *Journal of Mechanisms and Robotics*, vol. 11, no. 6, dec 2019. [Online]. Available: https://asmedigitalcollection.asme.org/mechanismsrobotics/article/doi/10.1115/1.4044411/956234/Kinematic-Optimization-of-a-Reconfigurable

[121] E. Gezgin, S. Özbek, D. Güzin, O. E. Ağbaş, and E. B. Gezer, "Structural design of a positioning spherical parallel manipulator to be utilized in brain biopsy," *International Journal of Medical Robotics and Computer Assisted Surgery*, vol. 15, no. 5, 2019.

[122] M. Afshar, J. Carriere, T. Meyer, R. Sloboda, S. Husain, N. Usmani, and M. Tavakoli, "Optimal Design of a Novel Spherical Scissor Linkage Remote Center of Motion Mechanism for Medical Robotics," pp. 6459–6465, 2020.

[123] C.-h. Kuo and J. S. Dai, "International Symposium on History of Machines and Mechanisms," *International Symposium on History of Machines and Mechanisms*, pp. 337–354, 2009.

[124] S. Harris, Q. Mei, R. Hibberd, and B. Davies, "Experiences using a special purpose robot for prostate resection," in *1997 8th International Conference on Advanced Robotics. Proceedings. ICAR'97*. IEEE, pp. 161–166. [Online]. Available: http://ieeexplore.ieee.org/document/620177/

[125] K. Masamune, E. Kobayashi, Y. Masutani, M. Suzuki, T. Dohi, H. Iseki, and K. Takakura, "Development of an MRI-compatible needle insertion manipulator for stereotactic neurosurgery," *Journal of Image Guided Surgery*, vol. 1, no. 4, pp. 242–248, 1995. [Online]. Available: https://onlinelibrary.wiley.com/doi/10.1002/(SICI)1522-712X(1995)1:4{%}3C242::AID-IGS7{%}3E3.0.CO;2-A

[126] M. Heinig, M. F. Govela, F. Gasca, C. Dold, U. G. Hofmann, V. Tronnier, A. Schlaefer, and A. Schweikard, "MARS — Motor assisted robotic stereotaxy system," in *2011 5th International IEEE/EMBS Conference on Neural Engineering*. IEEE, apr 2011, pp. 334–337. [Online]. Available: http://ieeexplore.ieee.org/document/5910555/

[127] M. Heinig, U. G. Hofmann, and A. Schlaefer, "Calibration of the motor-assisted robotic stereotaxy system: MARS," *International Journal of Computer Assisted Radiology and Surgery*, vol. 7, no. 6, pp. 911–920, nov 2012. [Online]. Available: http://link.springer.com/10.1007/s11548-012-0676-7

[128] H. M. Yip, P. Li, D. Navarro-Alarcon, Z. Wang, and Y. H. Liu, "A new circular-guided remote center of motion mechanism for assistive surgical robots," *2014 IEEE International Conference on Robotics and Biomimetics, IEEE ROBIO 2014*, pp. 217–222, 2014.

[129] Y. Liu, J. Wang, and P. Ben-Tzvi, "A Cable Length Invariant Robotic Tail Using a Circular Shape Universal Joint Mechanism," *Journal of Mechanisms and Robotics*, vol. 11, no. 5, oct 2019. [Online]. Available: https://asmedigitalcollection.asme.org/mechanismsrobotics/article/doi/10.1115/1.4044067/956020/A-Cable-Length-Invariant-Robotic-Tail-Using-a

[130] A. A. Sharp, A. M. Ortega, D. Restrepo, D. Curran-Everett, and K. Gall, "In vivo penetration mechanics and mechanical properties of mouse brain tissue at micrometer scales." *IEEE transactions on bio-medical engineering*, vol. 56, no. 1, pp. 45–53, jan 2009. [Online]. Available: http://www.ncbi.nlm.nih.gov/pubmed/19224718http://www.pubmedcentral.nih.gov/articlerender.fcgi?artid=PMC2855535

[131] Z. Fekete, A. Németh, G. Márton, I. Ulbert, and A. Pongrácz, "Experimental study on the mechanical interaction between silicon neural microprobes and rat dura mater during insertion," *Journal of Materials Science: Materials in Medicine*, vol. 26, no. 2, p. 70, feb 2015. [Online]. Available: http://link.springer.com/10.1007/s10856-015-5401-y

[132] P. A. York, R. Peña, D. Kent, and R. J. Wood, "Microrobotic laser steering for minimally invasive surgery," *Science Robotics*, vol. 6, no. 50, p. eabd5476, jan 2021. [Online]. Available: https://robotics.sciencemag.org/lookup/doi/10.1126/scirobotics.abd5476

# Appendix A

## 6.4 Theoretical Accuracy

We have mentioned in the section 3.1.1 that the targetted accuracy of the system should be under 100 $\mu$. In order to achieve this target we have to control the accuracy at the very basic level of the system design such as selection of appropriate actuators, lead screws and gearboxes. It has been mentioned and established that all the DOFs are completely decoupled, in the section 4.3, the innate accuracy of any DOF will not effect the other DOFs.
In this section, we will established the theoretical accuracy of each DOF using the the inherent properties of the components of each DOF.

**Cartesian Motion System**

The $x$-axis motion is generated through a linear actuator which uses a stepper motor along with rodless actuation system. Since this system is off-the-shelf, we have to reply on the reported precision. The rated end-to-end precision as $1\mu$, however mid stops have the precision of $100\mu$. But this is at very high acceleration and higher load then we intend to use it for.

The motion along $y$-axis was generated through the custom build actuation system. It comprised of a stepper motor with a step angle of $0.9^0$. The motor is also equipped with a reflective encoder of 4000 Count per Revolution (CPR). The motor is connected to a preloaded ball screw with the zero backlash and the lead of 2mm. All the components have the rigid connected with each other. The rated accuracy $\alpha_y$ of this DOF can calculated through the following relation.

$$\alpha_y = \frac{step - angle}{360} \times lead \tag{6.1}$$

Using the equation 6.1 the rated accuracy of $y$-axis is $5\mu$. We have used the same specification for the $z$-axis as well. It it important to keep in mind that these motors have axial and radial play of 75 $\mu$ and 25 $\mu$ respectively. But with the high resolution encoder, this error can be managed by using +10 or even +50 microsteps.

**Circular motion system**

The motion for pitch required very high torque and high accuracy actuation system, so we used a brushless DC motor with a gearbox, to manage the cyclic load. The gearbox is rigidly connected to the circular track so the rated accuracy of the gearbox dictated the accuracy of this motion axis. This gearbox has the backlash of 0.31 degrees.

It has been mentioned in the section 3.2.2.2, that the yaw motion was carried out through a cable pulley mechanism. We have used the same stepper motor as of the $y$-axis. But in this case, it is also dependent on the diameter of the capstan ($d_c$). The rated accuracy of this motion ($\alpha_{yaw}$) can be carried out through the following relation;

$$\alpha_{yaw} = \frac{\pi \times d_c}{360} \times step\_angle \tag{6.2}$$

if the $d_c$ is 10 $mm$ then the rated accuracy would be 78 $\mu$. If the the diameter of the capstan needed to increase then we can utilize the "+" steps for the stepper motor. The rated accuracy of the insertion/translation mechanism can also be calculated using the 6.1, but the lead of the screw is 1 mm, so the rated accuracy of insertion/translation is 2.5 $\mu$.

# List of Publications Related to the Thesis

- list your publications here